Perceptual decision making, internal state, and neuromodulation in V1

Dissertation

zur Erlangung des Grades
eines Doktors der Naturwissenschaften

der Mathematisch-Naturwissenschaftlichen Fakultät
und der Medizinischen Fakultät
der Eberhard-Karls-Universität Tübingen

vorgelegt von
Katsuhisa Kawaguchi
aus Tokyo, Japan

March, 2019

Tag der mündlichen Prüfung: .....25.03.19.....

Dekan der Math.-Nat. Fakultät: Prof. Dr. W. Rosenstiel

Dekan der Medizinischen Fakultät: Prof. Dr. I. B. Autenrieth

1. Berichterstatter: Prof. Dr. / PD Dr. / Dr. Hendrikje Nienborg

2. Berichterstatter: Prof. Dr. / PD Dr. / Dr. Cornelius Schwarz

Prüfungskommission: Dr. Hendrikje Nienborg

Prof. Dr. Cornelius Schwarz

Prof. Dr. Andreas Nieder

Prof. Dr. Uwe Ilg

Erklärung / Declaration:

Ich erkläre, dass ich die zur Promotion eingereichte Arbeit mit dem Titel

"Perceptual decision making, internal state, and neuromodulation in V1"

selbständig verfasst, nur die angegebenen Quellen und Hilfsmittel benutzt und wörtlich oder inhaltlich übernommene Stellen als solche gekennzeichnet habe. Ich versichere an Eides statt, dass diese Angaben wahr sind und dass ich nichts verschwiegen habe. Mir ist bekannt, dass die falsche Abgabe einer Versicherung an Eides statt mit Freiheitsstrafe bis zu drei Jahren oder mit Geldstrafebestraft wird.

I hereby declare that I have produced the work entitled

"Perceptual decision making, internal state, and neuromodulation in V1"

submitted for the award of a doctorate, on my own (without external help), have used only the sources and aids indicated and have marked passages included from other works, whether verbatim or in content, as such. I swear upon oath that these statements are true and that I have not concealed anything. I am aware that making a false declaration under oath is punishable by a term of imprisonment of up to three years or by a fine.

Tübingen, den 24.01.19 ..... Katsuhisa Kawaguchi .....

Datum / Date Unterschrift / Signature

Table of content

1. Acknowledgement

First and foremost, I appreciate the supervision of Dr. Hendrikje Nienborg. She has been supportive to me and other lab-members and put great emphasis on dialogues, which has ensured that everyone feels safe and supports one another. I learned a tons of things and could not come this far without her.

I appreciate supports from my other co-workers, especially Dr. Lenka Seillier and Katrina Rose Quinn. Lenka always has a clear idea of what to do next and how to improve and organize things. Katrina is the very other doctor student in our lab and always caring, proactive, and enthusiastic.

I would like to mention the exceptional support of the staff of Tübingen's neuroscience graduate school, where I did my master and continued the subsequent doctoral study.

My special thanks go to my advisory board members, Prof. Dr. Cornelius Schwarz and Prof. Dr. Andreas Nieder to give me great feedbacks and cooperate for the timeline of my doctoral study.

Lastly, I have to thank my family and friends in Japan, who understand my transition to Germany and have been supportive to me all the time.

2. Abstract

Perceptual decision making is the process to translate sensory signals into meaningful behaviors yet also affected by internally-generated signals called internal states such as decision confidence, arousal, or mood. The present study aims to get insight into the role of some aspects of internal states during perceptual decision making. To this end we needed trained animals to perform a perceptual decision making task. We refined a traditional monkey-training procedure to facilitate this line of research with precise measurements of eye position. The eye data are important because they contain rich information about animals' internal states. We demonstrated that some aspects of these internal states including their decision confidence during a perceptual decision making task can be inferred from their pupil size. We then used the pupil-inferred confidence to dissect model predictions about how sensory information is used to guide a choice. Finally, we systematically investigated the modulatory role of 5HT, which is linked to decision making and some internal states including mood, in visual processes in the primary visual cortex (V1) of awake macaques by performing extracellular recording with iontophoretic applications of serotonin and pH-matched NaCl. We found that serotonin decreased the gain of visual responses and the functional connectivity in awake macaque V1, suggesting the involvement of serotonin in state-dependent visual processes. Together, these results highlight the importance of studying internal states of trained macaques on a perceptual decision making task and the role of neuromodulators as the substrates of state-dependent visual processes during perceptual decision making.

3. Synopsis.

Animals translate sensory signals into behaviors. This ability is called perceptual decision making and essential for the survival of animals. Consider the situation where a monkey finds a berry which he has never tried. The berry may be tasty, but it could be poisonous. He needs to decide if he eats it or not by exploiting his sensory abilities to get evidence supporting either of the hypotheses. If he notices that the berry is like the one which he has enjoyed eating, he becomes confident that the berry is tasty and decides to eat it. If he is entirely uncertain whether the berry is good or bad, his decision is up to his mood. He may eat it to get at least something today or avoid the risk of the potential stomachache and keep looking for better ones. This illustrates not only the importance of perceptual decision making for animals but the non-negligible influence of animals' internal states such as confidence and mood on their decisions. Although the effect of internal states on perceptual decision making used to be largely ignored for computational tractability of the problem, more and more scientists nowadays are investigating the importance of internal states on perceptual decision making from different perspectives (Najafi & Churchland, 2018).

My doctoral studies used macaque monkeys to get insight into internal states during perceptual decision making from different perspectives. I used macaques because our understanding of perceptual decision making has greatly advanced from non-human primate studies (Shadlen & Kiani, 2013). The macaque is one of the best-established animal models to study visual and decision processes in the brain. Like humans, they have excellent vision and largely rely on visual information to guide behaviors. The common ancestor of humans and macaque monkeys existed 20-30 million years ago,

which is substantially longer after the 80-90 million years ago when our most recent common ancestor with mice existed (Janecka et al., 2007; Mitchell & Leopold, 2015). Therefore, it is expected that a number of brain structures and functions overlap between humans and macaques, especially for the visual system. Indeed, there is some evidence that macaques see things as humans do (Fize et al., 2011; Rajalingham et al., 2015). Like humans, they can also learn a task that even requires complex associative learning (e.g. Kira et al., 2015). Despite the long history of macaque studies, examining the importance of internal states during perceptual decision making with the macaques is still a challenge. Monkeys are non-verbal and generally requires long time of training to learn a decision-making task. In addition, methods to infer monkeys' internal states have not been established.

In the following synopsis, I mention how we can refine the traditional monkey-training procedure to accelerate macaque studies on perceptual decision making tasks with precise measurements of eye position. Obtaining high-quality eye data is important; as the Japanese proverb goes, "Eyes are as eloquent as the tongue". I briefly review studies showing that pupil diameter reflects subjects' internal states. Based on these studies, I explain how we succeeded in inferring animals' internal states such as motivation and confidence during a perceptual decision making task from monkeys' pupil size. Here, I stress the importance of estimating internal states during perceptual decision making tasks by taking an example from our result in which pupil-inferred confidence can differentiate predictions of models about how sensory stimuli are used to guide a choice. Next, I introduce the idea that neuromodulators are well-suited to carry information about internal states and reflect it in the cortical computation (Dayan, 2012)

to highlight the necessity to study neuromodulators to get insight into the modulation of visual/cortical processing by internal states. I also review how the neuromodulators can connect the link between pupil size and internal state. Then I focused on serotonin (5HT), which is believed to regulate some aspects of internal states such as mood and play an important role in decision making faced with uncertainty. Here I stress the fact that even simple computational roles of 5HT on V1 tuning properties had not been systematically examined especially in awake animals. I summarize my third and fourth projects that investigated serotonergic modulations in spikes and local network state of awake macaque V1. Lastly in outlook, I describe the future study that should directly test the role of 5HT in state-dependent visual processes in V1 of macaques performing a spatial attention task.

3.1. Technical refinement for the study of perceptual decision tasks: Head-free training of macaques

Obtaining behavioral and neural data from monkeys is a highly time-consuming process. First of all, naïve monkeys need to get used to a cage in a facility and laboratory members. Afterwards, monkeys need to be trained to get accommodated in a primate chair. Plus, since monkey experiments typically require precise measurements of their eye positions, the surgery to implant a head-post on monkeys' skull is to be performed. This head-post physically connects monkeys' head to a primate chair and limits unwanted head-movements of monkeys during tasks. This surgery is invasive, and it takes usually a few months for the head-post to be stabilized. After the head-post is stabilized on monkeys' skull, monkeys are trained to be connected to a primate chair via the head-post.

It is not until monkeys allow researchers to head-fix them when behavioral training on a task can be initiated.

To facilitate this traditional procedure, we designed a head-free training setup for macaques to be trained without head-posts even on a task requiring precise measurements of eye position. Unlike other head-free setups which require monkeys to be anesthetized during the development of the setup (Amemori et al., 2015; Drucker et al., 2015; Machado & Nelson, 2011; Fairhall et al., 2006; Slater et al., 2016), our setup can be made independently in a workshop without the presence of monkeys. Our setup is relatively easy to install on a standard primate chair and potentially adaptable for multiple monkeys. We trained one naïve monkey on tasks requiring precise measurements of eye position with this head-free setup. The monkey adapted to the setup quickly and learned the tasks. We confirmed that the obtained eye data are comparable to those from head-restricted monkeys with respect to fixation precision, pupil size, and microsaccades. This is my first doctoral project (Kawaguchi et al., "Head-free training of macaques for tasks requiring precise measurements of eye position").

3.2. Internal state during perceptual decision making

Perceptual decisions have been found highly variable even in response to the identical stimuli (e.g. Renart & Machens, 2014; Wyart & Koechlin, 2016). One of the proposed sources of the variability is subjects' internal state (Renart & Machens, 2014), which researchers often ignore for simplicity or computational tractability. Internal state is all sorts of internally-generated signals within subjects, which includes, for example, attention, motivation, confidence, or arousal. The prime reason why internal state tends to

be ignored is that it is literally internal within subjects and thus hardly observable from the outside. In addition, change in internal state often occurs even in the absence of subjects' awareness; it is even unnoticed for the subjects themselves. This covert nature of internal state makes it difficult to study and therefore internal states during perceptual decision making are often ignored for simplicity.

3.2.1. Pupil size to infer internal state

The observation of internal states is difficult from the outside as well as the inside yet possible. Researchers have leveraged the fact that change in internal states including arousal coincides with change in pupil size, vasomotor regulation, and heart rate, likely through the autonomic nervous system (Mitz et al., 2017). Especially, pupil diameter has been one of the most popular measurements to estimate some aspects of internal states because the data can come with the measurements of eye position without additional setups. Human psychophysics with pupillometry have shown that pupil metrics reflect diverse internal states including motivation (Chiew & Braver, 2013; Hopstaken et al., 2015) and confidence (Krishnamurthy et al., 2017; Lampert et al., 2015). Pupil metrics have been also shown to reflect learning (Eldar et al., 2013; Nassar et al., 2012; Van Slooten et al., 2018) and behavioral variability through change in decision bias (Urai et al., 2017; de Gee et al., 2014, 2017).

In my second project, we used monkeys' pupil size to infer some aspects of their internal states while they were performing a perceptual decision making task. Along with the abovementioned human studies, we found that monkeys' pupil size reflects their motivation, confidence, learning, and psychophysical performance (Fig. 3-5: Kawaguchi et al., 2018). Our pupil metric was the pupil size averaged over the last 250 ms of the

total 1500 ms of stimulus presentation period. Notably, our task had much shorter inter-trial intervals (ITIs; median was ~150 ms) than other macaque studies with pupillometry (Rudebeck et al., 2014; Ebitz & Platt, 2015; Suzuki et al., 2016; Mitz et al., 2017). It suggests that long ITIs (> 1000 ms) that have been thought to be necessary to stabilize the pupillary light reflex on a trial-by-trial basis (Mitz et al., 2017) may not always be necessary at least when monochromatic stimuli are used like in our task.

3.2.2. Internal state to constrain models of perceptual decision making

Being able to infer internal states such as the decision confidence of animals during perceptual decision making has potentials to explain observations that have puzzled scientists. One such observation is so-called early psychophysical weighting. In a sequential-sampling perceptual decision making task where stimuli are sequentially presented for a fixed duration, the optimal strategy to maximize the percent correct is to integrate all the presented stimuli and make a choice. However, subjects typically rely more strongly on stimuli presented early rather than late within a trial. In other words, subjects tend to ignore stimuli presented towards the end of a trial. This early psychophysical weighting is a sub-optimal strategy from the perspective of maximizing sensory information, yet has been found in many (especially macaque) studies (e.g. Kiani et al., 2008; Neri and Levi, 2008; Nienborg and Cumming, 2009; Yates et al., 2017).

Three classes of computational models predict the early psychophysical weighting: the integration-to-bound model (e.g. Radcliff & McKaan, 2008; Smith & Ratcliff 2004), models with attractor dynamics either within the decision area or due to feedback to sensory areas including the neural sampling-based probabilistic inference model (Haefner et al., 2016), and early sensory weighting model (Yates et al., 2017).

Although they all predict the early psychophysical weighting, they have completely different perspectives. The integration-to-bound model assumes decision bounds, which terminate evidence-integration processes even when the stimulus presentation is not finished. Therefore, on average across trials, the stimuli presented early are used more than the stimuli presented late to guide a choice. The neural sampling-based probabilistic inference model is one of attractor models and assumes top-down feedback mechanisms such that sensory neurons represent less and less sensory information towards the end of trials, thereby sensory weights are decreasing over time within trials. The early sensory weighting model is in contrast a strictly feedforward account, which predicts the early psychophysical weighting simply by inheriting the decay of sensory responses due to sensory adaptation within trials.

In the second project, we leveraged the idea that confidence can be statistically defined in a perceptual decision making task (Hangya et al., 2016) and implemented decision confidence into all the three models. We found that it can differentiate model predictions about the early psychophysical weighting. To test it empirically, we split trials based on the pupil-inferred confidence and separately performed psychophysical reverse correlation analysis (Nienborg & Cumming, 2009) to estimate monkeys' temporal weighting of the stimuli to guide a choice. Our model fitting as well as extensive parameter search showed that the integration-to-bound model accounted for the data the best (Fig. 7-8: Kawaguchi et al., 2018). Note that our results do not deny the validity of the alternative models. These alternative models can account for dynamics beyond the early psychophysical weighting such as the activity of sensory neurons. But 'hard' decision bounds that terminate evidence accumulation processes seem necessary to

explain our data. This work exemplifies the importance of accessing internal states in non-human primate studies combined with computational modelling, which have greatly advanced our understanding of perceptual decision making (Shadlen & Kiani, 2013). This work was published in the Journal of neuroscience (Kawaguchi et al., 2018. "Differentiating between models of perceptual decision-making using pupil-size inferred confidence").

3.3. Internal state and neuromodulators

Internal states affect perceptual decision making. How internal states are mechanistically implemented in the brain is a critical question to get insight into the information processing in the brain. For example, if an animal encounters its predator, a neural circuit that detects fear has to send the information right away to all the relevant brain regions including sensory and decision areas so that the animal can prioritize its behavior to deal with the life-threatening situation. If there was a problem in the communication between brain regions, it would soon be eaten. To achieve such a communication, a neural circuit detecting change in internal states should have at least following three capacities (Dayan, 2012). First, it should have wide-range connections to the cortex including sensory and decision areas so that information can be rapidly distributed. Second, the signals from this neural circuit should be "tagged", or at least unique enough for cortical neurons to be able to distinguish it from ongoing sensory inputs. Third, signals from this neural circuit should be able to alter ongoing computations in the cortex over flexible time-scales. The neuromodulatory systems, including acetylcholine (ACh), noradrenaline (NA), dopamine (DA), and serotonin

(5HT), appear to be an ideal candidate for such computational roles in the brain (Dayan, 2012). These systems are based on distinct regions mainly in the brainstem and project to a wide range of the cortical areas. Furthermore, cortical neurons express specific receptors for neuromodulators, which makes the "tagging" possible because those receptors are stimulated when change in internal states occurs. Lastly, receptor-expression patterns are different among neuronal types across brain regions. This suggests that a uniform input regarding change in internal states can be processed differently depending on computational roles of each neural circuit and brain region over flexible time-scales. Altogether, neuromodulators appear to be well-suited to perform the information processing about internal states in the brain.

3.3.1. Neuromodulators to connect internal state with pupil size

In the section 3.2.1, I mentioned that pupil size reflects a variety of internal states. Given that the neuromodulatory systems are believed to control internal state (Dayan, 2012), pupil size may be also controlled by neuromodulators. Although identifying causal influence of neuromodulators on pupil size is not straightforward, the idea that neuromodulators mechanically connect pupil size with internal states seems likely (Larsen & Waters, 2018). The activities of neurons (both spikes and LFPs) in the locus coeruleus (LC) were shown to reflect change in pupil diameter (Joshi et al., 2016). The same study showed that electrical microstimulation in the LC increases pupil diameter. The LC is the primary source of noradrenergic projections to cortex, therefore pupil-linked modulations are often interpreted as actions of the noradrenergic activity in the brain (Aston-Jones & Cohen, 2005). However, DA (Colizoli et al., 2018) and ACh (Polack et al., 2013; Reimer et al., 2016) are also suggested to be involved in change in

pupil size. 5HT is not an exception; agonists of the 5HT1A receptor were shown to change pupil size in rodents, monkeys, and humans in a dose-dependent manner (Fanciullacci et al., 1995; Kotani et al., 2017; Szabadi, 2018; Yu et al., 2004). These results suggest that pupil size reflects activities of multiple neuromodulatory systems in the brain.

Understanding how each neuromodulator contributes to change in pupil size is difficult because activities of these neuromodulators in the brain are correlated with one another. The involvement of the cholinergic activity in change in pupil size is relatively clear thanks to the existence of a direct pathway. The iris sphincter muscle, which controls the pupillary muscle, is controlled by cholinergic motoneurons in the Edinger-Westphal (E-W) nucleus (Beatty & Lucero-Wagoner, 2000). As for NA, the correlation between the LC activity and pupil size has been observed across species (de Gee et al., 2017; Joshi et al., 2016; Reimer et al., 2016). Whether there is a direct pathway between the noradrenergic system in the brain and pupil size is controversial, but indirect pathways seem to play an important role. For example, the LC projects to the basal forebrain (Jones, 2004), which is the primary source of cholinergic projections to cortex, such that the noradrenergic activity drives the cholinergic activity. The LC also projects to the superior colliculus, which projects to the E-W nucleus controlling pupil size (Wang & Munoz, 2015). The correlation between 5HT and pupil size is also likely to be mediated by an indirect pathway through the noradrenergic system because the activation of 5HT1A receptors triggers the release of NA, likely from the LC (Yu et al., 2004). These results support the idea that change in pupil size is influenced by the activity of neuromodulators especially ACh and NA, but likely also 5HT in the brain.

3.3.2. Importance of serotonin in the brain and decision making

5HT has diverse affective functions such as mood control, perception, and memory (Berger et al., 2009). The variety of serotonergic functions stem from the diverse serotonergic receptors. Currently 14 different 5HT receptors in 7 families have been found. Among the 7 families, the 5HT3 receptor is a ligand-gated ion channel and others are G-protein coupled receptors. The effect of each receptor type differs; the 5HT1 and 5 receptors are inhibitory, and all the others are excitatory. These receptors have spatial preference of expression patterns with respect to both brain regions and synaptic localizations (Celada et al., 2013). In addition to the diverse receptor types, the serotonergic projections from the dorsal raphe nucleus (DRN) cover nearly the entire cortex. Interestingly, the serotonergic projections are more pronounced to the macaque primary visual and auditory cortices than those of DA and NA (Jacobs & Nienborg, 2018). These findings suggest that 5HT in the brain is one of the cellular mechanisms underlying change in variety of internal states and state-dependent sensory processes in primary sensory areas. More recently, stimulating the DRN during behavioral tasks has revealed causal roles of serotonergic modulations in learning and decision making. These studies found functional roles of 5HT on trade-offs between immediate small reward and delayed large rewards (Correia et al., 2017; Fonseca et al., 2015; Miyazaki et al., 2014, 2018; Xu et al., 2017), cognitive flexibility (Matias et al., 2017), and reinforcement learning (Iigaya et al., 2018).

3.3.2.1. Serotonergic modulation of spiking activity in V1

Although the serotonergic modulation linked to neurological disorders or decision making faced with uncertainty have been extensively studied, the basic role of 5HT on tuning properties in sensory areas was surprisingly little known especially in awake animals. The V1 of humans and non-human primates is a region where 5HT receptors are preferentially expressed (Watakabe et al., 2008; Shukla et al., 2014). Therefore, 5HT should have a modulatory function there. In the olfactory cortex of mice, 5HT decreases spontaneous activity but has no effect on sensory responses (Lottem et al., 2016). Are such serotonergic modulations also the case with the primate V1?

To explore the role of 5HT on visual processes in primate V1, we performed extracellular recordings on V1 neurons of awake macaque monkeys on a standard fixation task while iontophoretically applying 5HT or pH-matched NaCl. We found that 5HT predominantly decreased the gain of the visual responses. This uniform effect of serotonin is surprising given the diversity of its receptor types. The decrease in gain of visual responses were observed across all the tested stimulus dimensions (orientation, contrast, size, and spatial frequency). This effect was explained by a simple model with a linear shift in membrane potential or spiking threshold. We argued that 5HT affects state-dependent visual processes by controlling the response gain of V1 neurons. This work was published in the Journal of neuroscience (Seillier*, Lorenz*, Kawaguchi et al., 2018. "Serotonin decreases the gain of visual responses in awake macaque V1").

3.3.2.2. Serotonergic modulation of local network state in V1

The state-dependent visual process is not only signified by change in spiking activity but also accompanied by change in local network state inferred by the local field potential (LFP). For example, spatial attention decreases the LFP power especially in low-frequency range in macaque V1 (Chalk et al., 2010; Das & Ray, 2018; Spyropoulos et al., 2018). Stimulation of the basal forebrain, the primary source of cholinergic inputs to cortex, has been also shown to decrease the low-frequency LFP power in mouse V1 (De Luna et al., 2017; Goard & Dan, 2009; Pinto et al., 2013). Although whether change in LFP power in V1 is meaningful for sensory coding or epiphenomenal of spiking activity is under debate, one hypothesis tells that desynchronized state, which is typically accompanied by decrease in low-frequency LFP power, favors reliable sensory representation, whereas synchronized state, which is typically accompanied by increase in low-frequency LFP power, is suited for reactivation of previous experience for learning and memory (Lee & Dan, 2012). Although 5HT was shown to decrease low-frequency LFP power in the prefrontal cortex of rodents (Kjaerby et al., 2016; Puig et al., 2010), whether 5HT favors which cortical state in macaque V1 had not been demonstrated.

To examine the role of 5HT on local network state in awake macaque V1, I used the same dataset from the third project and analyzed LFPs as well as spikes. Consistent with the rodent studies, I found that 5HT decreased the low-frequency LFP power in macaque V1. Next, I computed the spike-triggered average LFP (stLFP) to capture the spike-LFP relationship (Ray, 2015) and found that 5HT decreased the amplitude of the stLFP. The stLFP represents cross-correlation between the response of a single neuron

and the mean synaptic activity of the population (Okun et al., 2010) and can be used to estimate the functional connectivity of a neuron with the local population (Nauhaus et al., 2009; Okun et al., 2015). Hence the decrease in the amplitude of the stLFP by 5HT suggests that 5HT decreases the functional connectivity in V1. These results resemble previously reported effects of spatial attention in V1 (Chalk et al., 2010; Das & Ray, 2018), which raises the possibility that 5HT is involved in the attentional modulation in visual processes in macaque V1.

Based on our finding that 5HT decreases low-frequency LFP power in V1, I aimed to test the hypothesis that 5HT and ACh are two independent sources of the decrease in low-frequency rhythmic activity in cortex (Vanderwolf & Baker, 1986). Since ACh and 5HT were both suggested to desynchronize cortical state at least in rodents (Lee & Dan, 2012), asking whether activities of ACh and 5HT in visual areas of macaques are linked or not is important to elucidate the role of these neuromodulators in primate visual processes. To this end I leveraged the finding that pupil size reflects the cholinergic and noradrenergic activities in the brain (Reimer et al., 2016) and asked whether effects of 5HT and pupil metrics on low-frequency LFP power were independent. Note that although 5HT is thought to be one of the neuromodulators linked to change in pupil size (Yu et al., 2004), our manipulation of the serotonergic system was confined to V1 and not directly involved in any pathways suggested to changes in pupil size. I used generalized linear regression model to explain trial-by-trial low-frequency LFP power by linear combinations of pupil size (proxy of ACh; Reimer et al., 2016), pupil derivative (proxy of NA; Reimer et al., 2016), drug (0: baseline, 1: 5HT), and their interactions. I observed significant contributions of pupil size and drug to explain low-

frequency LFP power. Along with the hypothesis, I found no significant contributions of interaction terms (Fig. 4 in the manuscript "Serotoninergic modulation of functional connectivity in awake macaque V1"). This result suggests that 5HT and ACh independently decreases low-frequency LFP power in awake macaque V1. This work is to be submitted (Kawaguchi*, Seillier* et al., 2018. "Serotoninergic modulation of functional connectivity in awake macaque V1").

3.4. Summary and conclusion

Perceptual decision making is not only influenced by sensory inputs but internal states such as motivation, confidence, and mood. To understand how the brain combines external sensory information with internal states to form a decision is a major goal in systems neuroscience. Although studies with macaque monkeys have greatly advanced our understanding of perceptual decision making, it has been difficult to use macaques to study internal states during perceptual decision making. First, it takes generally long time of training until monkeys understand the task structure. Second, methods to estimate monkeys' internal states have not been established.

The first project refined a traditional monkey-training procedure by designing a head-free training setup. This setup allows researchers to train monkeys even before the head-post implantation surgery and during a few months of the recovery period after it, thereby facilitating the monkey-training procedure. We trained a naïve monkey without the head-post in this setup. We showed that this head-free monkey can be trained on tasks requiring precise measurements of eye position. Importantly, the obtained eye data from this head-free monkey were comparable to head-fixed monkeys with respect to fixation

precision, pupil size, and microsaccades. This is important because eye data especially pupil size contain rich information about monkeys' internal states.

My second project overcame the difficulty to estimate some aspects of internal states of monkeys by using pupil size. Change in pupil size is believed to reflect activities of multiple neuromodulators in the brain and some aspects of internal states such as arousal. Human psychophysics with pupillometry revealed that pupil size reflects diverse behaviorally relevant internal states. Along with these studies, we succeeded in inferring monkeys' internal states such as motivation and decision confidence by using monkeys' pupil size during a perceptual decision making task. This project demonstrated the importance to estimate such forms of internal states of animals during perceptual decision making by showing that pupil-linked confidence can differentiate predictions of models about how sensory information is temporally weighted to guide a choice.

Finally, we investigated the role of 5HT, which is one of the important neuromodulators linked to some aspects of internal states and decision making, in visual processes in V1. Primate V1 is one of the regions where serotonergic receptors are preferentially expressed. Given the ample evidence linking 5HT to internal states, 5HT is expected to play a role in state-dependent visual processes. However, even simple computational roles of 5HT in visual processes in V1 of awake animals were largely unknown. The third and fourth projects systematically investigated the serotonergic modulation of both spikes and LFPs in awake macaque V1. Our results showed that 5HT decreased the gain of V1 responses, the low-frequency LFP power, and functional connectivity in V1. These observations suggest that 5HT contributes to state-dependent visual processes in awake macaque V1.

Together, these four projects contribute to getting insight into internal states during perceptual decision making from different perspectives. The first and second projects overcame difficulties of studying internal states of macaque monkeys performing perceptual decision making tasks. The second project highlighted the importance of inferring internal states of macaque monkeys during a perceptual decision making task. The third and fourth projects showed that 5HT, a neuromodulator that is believed to be a substrate for some aspects of internal states and influence decisions, altered visual processing in awake macaque V1.

3.5. Outlook

With these results in mind, a future study may directly address the role of 5HT in a spatial attention task. Spatial attention is typically accompanied by the increase in firing rate (Thiele & Bellgrove, 2018), which is opposite to the decrease in firing rate by 5HT (project 3). Spatial attention typically decreases low-frequency LFP power and the stLFP (Chalk et al., 2010), which is similar to the serotonergic modulation in LFPs (project 4). When comparing to the effect of spatial attention, 5HT modulates spikes and LFPs in opposite directions. This discrepancy in serotonergic modulations between spikes and LFPs can be clarified using macaque monkeys performing a spatial attention task while recording spikes and LFPs in V1 with the iontophoretic application of 5HT or pH-matched NaCl. To this end I am currently training a monkey on a spatial attention task. In the spatial attention task, we instruct monkeys to pay attention covertly to one location and discriminate the presented stimulus. First of all, we should establish the well-known attentional modulations in V1 in the baseline condition without drugs: the increase in

firing rate and the decrease in low-frequency LFP power when the attend-in condition (attention locus is on the receptive field) is compared against the attend-out condition (attention locus is out of the receptive field). We should also control the effect of eye movements such as fixation precision and microsaccades (project 1) on those attentional modulations. Especially we may want to use the best-available technique to correctly detect microsaccades (e.g. Bellet et al., 2018) so that we can properly estimate their effects because a substantial involvement of microsaccades on attentional modulations was reported (Lowet et al., 2018). We should monitor pupil size of the animals during the task because it sensitively reflects animals' internal states (project 2) and activities of neuromodulators especially ACh and NA (Reimer et al., 2016; Larsen & Waters, 2018).

In this setup we can directly ask how 5HT contributes to the attentional modulations in macaque V1 with respect to spikes and LFPs. A previous study reported that ACh enhanced the attentional modulation of firing rate in macaque V1 (Herrero et al., 2008). Given that 5HT decreases the gain of visual responses (project 3), the hypothesis is that 5HT decreases the attentional modulation of firing rate, as opposed to ACh. How the serotonergic modulation in LFPs interacts with the attentional modulation in LFPs remains to be seen. Our analysis using the same dataset as project 4 showed that pupil size and 5HT significantly affects low-frequency LFP power in V1, but these effects are independent of each other. This supports the hypothesis that ACh and 5HT are two independent sources to desynchronize cortical state (Vanderwolf & Baker, 1986; Harris & Thiele, 2011). If the attentional modulation in LFPs are also mediated by ACh, we expect that 5HT decreases low-frequency LFP power independently on top of the attentional modulation in LFPs. In addition, we can ask how change in pupil size, which

reflects internal states such as motivation and decision confidence during perceptual decision making (project 2), interacts with the effect of 5HT on the attentional modulations in macaque V1. This future project will advance our understanding of how external sensory information, internal states, and neuromodulators shape visual processes in V1 and influence perceptual decisions by exploring the link among pupil-inferred internal states, effects of 5HT on attentional modulations in V1, and perceptual decisions.

3.6. Reference

Amemori, S., Amemori, K. I., Cantor, M. L., & Graybiel, A. M. (2015). A non-invasive head-holding device for chronic neural recordings in awake behaving monkeys. *Journal of Neuroscience Methods*, *240*, 154-160.

Aston-Jones, G., & Cohen, J. D. (2005). An integrative theory of locus coeruleus-norepinephrine function: adaptive gain and optimal performance. *Annu. Rev. Neurosci.*, *28*, 403-450.

Beatty, J., & Lucero-Wagoner, B. (2000). The pupillary system. *Handbook of Psychophysiology*, *2*(142-162).

Bellet, M. E., Bellet, J., Nienborg, H., Hafed, Z. M., & Berens, P. (2018). Human-level saccade detection performance using deep neural networks. *Journal of Neurophysiology*.

Berger, M., Gray, J. A., & Roth, B. L. (2009). The expanded biology of serotonin. *Annual Review of Medicine*, *60*, 355-366.

Celada, P., Puig, M., & Artigas, F. (2013). Serotonin modulation of cortical neurons and networks. *Frontiers in Integrative Neuroscience*, *7*, 25.

Chalk, M., Herrero, J. L., Gieselmann, M. A., Delicato, L. S., Gotthardt, S., & Thiele, A. (2010). Attention reduces stimulus-driven gamma frequency oscillations and spike field coherence in V1. *Neuron*, *66*(1), 114-125.

Colizoli, O., de Gee, J. W., Urai, A. E., & Donner, T. H. (2018). Task-evoked pupil responses reflect internal belief states. *Scientific Reports*, *8*(1), 15904.

Correia, P. A., Lottem, E., Banerjee, D., Machado, A. S., Carey, M. R., & Mainen, Z. F. (2017). Transient inhibition and long-term facilitation of locomotion by phasic optogenetic activation of serotonin neurons. *Elife*, *6*, e20975.

Chiew, K. S., & Braver, T. S. (2013). Temporal dynamics of motivation-cognitive control interactions revealed by high-resolution pupillometry. *Frontiers in Psychology*, *4*, 15.

Das, A., & Ray, S. (2018). Effect of stimulus contrast and visual attention on spike-gamma phase relationship in macaque primary visual cortex. *Frontiers in Computational Neuroscience*, *12*.

Dayan, P. (2012). Twenty-five lessons from computational neuromodulation. *Neuron*, *76*(1), 240-256.

de Gee, J. W., Knapen, T., & Donner, T. H. (2014). Decision-related pupil dilation reflects upcoming choice and individual bias. *Proceedings of the National Academy of Sciences*, *111*(5), E618-E625.

de Gee, J. W., Colizoli, O., Kloosterman, N. A., Knapen, T., Nieuwenhuis, S., & Donner, T. H. (2017). Dynamic modulation of decision biases by brainstem arousal systems. *Elife*, *6*, e23232.

De Luna, P., Veit, J., & Rainer, G. (2017). Basal forebrain activation enhances between-trial reliability of low-frequency local field potentials (LFP) and spiking activity in tree shrew primary visual cortex (V1). *Brain Structure and Function*, *222*(9), 4239-4252.

Drucker, C. B., Carlson, M. L., Toda, K., DeWind, N. K., & Platt, M. L. (2015). Non-invasive primate head restraint using thermoplastic masks. *Journal of Neuroscience Methods*, *253*, 90-100.

Ebitz, R. B., & Platt, M. L. (2015). Neuronal activity in primate dorsal anterior cingulate cortex signals task conflict and predicts adjustments in pupil-linked arousal. *Neuron*, *85*(3), 628-640.

Eldar, E., Cohen, J. D., & Niv, Y. (2013). The effects of neural gain on attention and learning. *Nature Neuroscience*, *16*(8), 1146.

Fanciullacci, M., Sicuteri, R., Alessandri, M., & Geppetti, P. (1995). Buspirone, but not sumatriptan, induces miosis in humans: relevance for a serotoninergic pupil control. *Clinical Pharmacology & Therapeutics*, *57*(3), 349-355.

Fairhall, S. J., Dickson, C. A., Scott, L., & Pearce, P. C. (2006). A non- invasive method for studying an index of pupil diameter and visual performance in the rhesus monkey. *Journal of Medical Primatology*, *35*(2), 67-77.

Fize, D., Cauchoix, M., & Fabre-Thorpe, M. (2011). Humans and monkeys share visual representations. *Proceedings of the National Academy of Sciences*, 108(18), 7635–7640.

Fonseca, M. S., Murakami, M., & Mainen, Z. F. (2015). Activation of dorsal raphe serotonergic neurons promotes waiting but is not reinforcing. *Current Biology*, *25*(3), 306-315.

Fries, P., Reynolds, J. H., Rorie, A. E., & Desimone, R. (2001). Modulation of oscillatory neuronal synchronization by selective visual attention. *Science*, *291*(5508), 1560-1563.

Goard, M., & Dan, Y. (2009). Basal forebrain activation enhances cortical coding of natural scenes. *Nature Neuroscience*, *12*(11), 1444.

Hangya, B., Sanders, J. I., & Kepecs, A. (2016). A mathematical framework for statistical decision confidence. *Neural Computation*, *28*(9), 1840-1858.

Harris, K. D., & Thiele, A. (2011). Cortical state and attention. *Nature Reviews Neuroscience*, *12*(9), 509.

Haefner, R. M., Berkes, P., & Fiser, J. (2016). Perceptual decision-making as probabilistic inference by neural sampling. *Neuron*, *90*(3), 649-660.

Herrero, J. L., Roberts, M. J., Delicato, L. S., Gieselmann, M. A., Dayan, P., & Thiele, A. (2008). Acetylcholine contributes through muscarinic receptors to attentional modulation in V1. *Nature*, *454*(7208), 1110.

Hopstaken, J. F., Van Der Linden, D., Bakker, A. B., & Kompier, M. A. (2015). A multifaceted investigation of the link between mental fatigue and task disengagement. *Psychophysiology*, *52*(3), 305-315.

Iigaya, K., Fonseca, M. S., Murakami, M., Mainen, Z. F., & Dayan, P. (2018). An effect of serotonergic stimulation on learning rates for rewards apparent after long intertrial intervals. *Nature Communications*, *9*(1), 2477.

Jacob, S., & Nienborg, H. (2018). Monoaminergic neuromodulation of sensory processing. *Frontiers in Neural Circuits*, *12*, 51.

Janečka, J. E., Miller, W., Pringle, T. H., Wiens, F., Zitzmann, A., Helgen, K. M., ... & Murphy, W. J. (2007). Molecular and genomic data identify the closest living relative of primates. *Science*, *318*(5851), 792-794.

Jones, B. E. (2004). Activity, modulation and role of basal forebrain cholinergic neurons innervating the cerebral cortex. *Progress in Brain Research*, *145*, 157-169.

Joshi, S., Li, Y., Kalwani, R. M., & Gold, J. I. (2016). Relationships between pupil diameter and neuronal activity in the locus coeruleus, colliculi, and cingulate cortex. *Neuron*, *89*(1), 221-234.

Kawaguchi, K., Clery, S., Pourriahi, P., Seillier, L., Haefner, R. M., & Nienborg, H. (2018). Differentiating between models of perceptual decision making using pupil size inferred confidence. *Journal of Neuroscience*, *38*(41), 8874-8888.

Kiani, R., Hanks, T. D., & Shadlen, M. N. (2008). Bounded integration in parietal cortex underlies decisions even when viewing duration is dictated by the environment. *Journal of Neuroscience*, *28*(12), 3017-3029.

Kira, S., Yang, T., & Shadlen, M. N. (2015). A neural implementation of Wald's sequential probability ratio test. *Neuron*, *85*(4), 861-873.

Kjaerby, C., Athilingam, J., Robinson, S. E., Iafrati, J., & Sohal, V. S. (2016). Serotonin 1B receptors regulate prefrontal function by gating callosal and hippocampal inputs. *Cell Reports*, *17*(11), 2882-2890.

Kotani, M., Urushino, N., Natsutani, I., Ogi, Y., & Ikeda, K. (2017). Effects of the 5-HT1A receptor agonists buspirone and 8-OH-DPAT on pupil size in common marmosets. *Behavioural Pharmacology*, *28*(4), 313-317.

Krishnamurthy, K., Nassar, M. R., Sarode, S., & Gold, J. I. (2017). Arousal-related adjustments of perceptual biases optimize perception in dynamic environments. *Nature Human Behaviour*, *1*(6), 0107.

Larsen, R. S., & Waters, J. (2018). Neuromodulatory Correlates of Pupil Dilation. *Frontiers in Neural Circuits*, *12*, 21.

Lempert, K. M., Chen, Y. L., & Fleming, S. M. (2015). Relating pupil dilation and metacognitive confidence during auditory decision-making. *PLoS One*, *10*(5), e0126588.

Lee, S. H., & Dan, Y. (2012). Neuromodulation of brain states. *Neuron*, *76*(1), 209-222.

Lowet, E., Gomes, B., Srinivasan, K., Zhou, H., Schafer, R. J., & Desimone, R. (2018). Enhanced Neural Processing by Covert Attention only during Microsaccades Directed toward the Attended Stimulus. *Neuron*, 1–8

Lottem, E., Lörincz, M. L., & Mainen, Z. F. (2016). Optogenetic activation of dorsal raphe serotonin neurons rapidly inhibits spontaneous but not odor-evoked activity in olfactory cortex. *Journal of Neuroscience*, *36*(1), 7-18.

Machado, C. J., & Nelson, E. E. (2011). Eye- tracking with nonhuman primates is now more accessible than ever before. *American Journal of Primatology*, *73*(6), 562-569.

Matias, S., Lottem, E., Dugue, G. P., & Mainen, Z. F. (2017). Activity patterns of serotonin neurons underlying cognitive flexibility. *Elife*, *6*, e20552.

McCorry, L. K. (2007). Physiology of the autonomic nervous system. *American Journal of Pharmaceutical Education*, *71*(4), 78.

Mitchell, J. F., & Leopold, D. A. (2015). The marmoset monkey as a model for visual neuroscience. *Neuroscience Research*, *93*, 20-46.

Mitz, A. R., Chacko, R. V., Putnam, P. T., Rudebeck, P. H., & Murray, E. A. (2017). Using pupil size and heart rate to infer affective states during behavioral neurophysiology and neuropsychology experiments. *Journal of Neuroscience Methods*, *279*, 1-12.

Miyazaki, K. W., Miyazaki, K., Tanaka, K. F., Yamanaka, A., Takahashi, A., Tabuchi, S., & Doya, K. (2014). Optogenetic activation of dorsal raphe serotonin neurons enhances patience for future rewards. *Current Biology*, *24*(17), 2033-2040.

Miyazaki, K., Miyazaki, K. W., Yamanaka, A., Tokuda, T., Tanaka, K. F., & Doya, K. (2018). Reward probability and timing uncertainty alter the effect of dorsal raphe serotonin neurons on patience. *Nature Communications*, *9*(1), 2048.

Nassar, M. R., Rumsey, K. M., Wilson, R. C., Parikh, K., Heasly, B., & Gold, J. I. (2012). Rational regulation of learning dynamics by pupil-linked arousal systems. *Nature Neuroscience*, *15*(7), 1040.

Nauhaus, I., Busse, L., Carandini, M., & Ringach, D. L. (2009). Stimulus contrast modulates functional connectivity in visual cortex. *Nature Neuroscience*, *12*(1), 70.

Najafi, F., & Churchland, A. K. (2018). Perceptual Decision-Making: A Field in the Midst of a Transformation. *Neuron*, *100*(2), 453-462.

Neri, P., & Levi, D. (2008). Temporal dynamics of directional selectivity in human vision. *Journal of Vision*, *8*(1), 22-22.

Nienborg, H., & Cumming, B. G. (2009). Decision-related activity in sensory neurons reflects more than a neuron's causal effect. *Nature*, *459*(7243), 89.

Okun, M., Naim, A., & Lampl, I. (2010). The subthreshold relation between cortical local field potential and neuronal firing unveiled by intracellular recordings in awake rats. *Journal of Neuroscience*, *30*(12), 4440-4448.

Okun, M., Steinmetz, N. A., Cossell, L., Iacaruso, M. F., Ko, H., Barthó, P., ... & Harris, K. D. (2015). Diverse coupling of neurons to populations in sensory cortex. *Nature*, *521*(7553), 511.

Pinto, L., Goard, M. J., Estandian, D., Xu, M., Kwan, A. C., Lee, S. H., ... & Dan, Y. (2013). Fast modulation of visual perception by basal forebrain cholinergic neurons. *Nature Neuroscience*, *16*(12), 1857.

Polack, P. O., Friedman, J., & Golshani, P. (2013). Cellular mechanisms of brain state–dependent gain modulation in visual cortex. *Nature Neuroscience*, *16*(9), 1331.

Puig, M. V., Watakabe, A., Ushimaru, M., Yamamori, T., & Kawaguchi, Y. (2010). Serotonin modulates fast-spiking interneuron and synchronous activity in the rat prefrontal cortex through 5-HT1A and 5-HT2A receptors. *Journal of Neuroscience*, *30*(6), 2211-2222.

Rajalingham, R., Schmidt, K., & DiCarlo, J. J. (2015). Comparison of object recognition behavior in human and monkey. *Journal of Neuroscience*, *35*(35), 12127-12136.

Ratcliff, R., & McKoon, G. (2008). The diffusion decision model: theory and data for two-choice decision tasks. *Neural Computation*, *20*(4), 873-922.

Ray, S. (2015). Challenges in the quantification and interpretation of spike-LFP relationships. *Current Opinion in Neurobiology*, *31*, 111-118.

Renart, A., & Machens, C. K. (2014). Variability in neural activity and behavior. *Current Opinion in Neurobiology*, *25*, 211-220.

Reimer, J., McGinley, M. J., Liu, Y., Rodenkirch, C., Wang, Q., McCormick, D. A., & Tolias, A. S. (2016). Pupil fluctuations track rapid changes in adrenergic and cholinergic activity in cortex. *Nature Communications*, *7*, 13289.

Rudebeck, P. H., Putnam, P. T., Daniels, T. E., Yang, T., Mitz, A. R., Rhodes, S. E., & Murray, E. A. (2014). A role for primate subgenual cingulate cortex in sustaining autonomic arousal. *Proceedings of the National Academy of Sciences*, *111*(14), 5391-5396.

Seillier, L., Lorenz, C., Kawaguchi, K., Ott, T., Nieder, A., Pourriahi, P., & Nienborg, H. (2017). Serotonin decreases the gain of visual responses in awake macaque V1. *Journal of Neuroscience*, 1339-17.

Shukla, R., Watakabe, A., & Yamamori, T. (2014). mRNA expression profile of serotonin receptor subtypes and distribution of serotonergic terminations in marmoset brain. *Frontiers in Neural Circuits*, *8*, 52.

Shadlen, M. N., & Kiani, R. (2013). Decision making as a window on cognition. *Neuron*, *80*(3), 791-806.

Slater, H., Milne, A. E., Wilson, B., Muers, R. S., Balezeau, F., Hunter, D., ... & Petkov, C. I. (2016). Individually customisable non-invasive head immobilisation system for non-human primates with an option for voluntary engagement. *Journal of Neuroscience Methods*, *269*, 46-60.

Spyropoulos, G., Bosman, C. A., & Fries, P. (2018). A theta rhythm in macaque visual cortex and its attentional modulation. *Proceedings of the National Academy of Sciences*, 115(24), E5614–E5623.

Szabadi, E. (2018). Functional Organization of the Sympathetic Control of the Pupil. *Frontiers in Neurology*, *9*, 1069.

Thiele, A., & Bellgrove, M. A. (2018). Neuromodulation of attention. *Neuron*, *97*(4), 769-785.

Suzuki, T. W., Kunimatsu, J., & Tanaka, M. (2016). Correlation between pupil size and subjective passage of time in non-human primates. *Journal of Neuroscience, 36*(44), 11331-11337.

Urai, A. E., Braun, A., & Donner, T. H. (2017). Pupil-linked arousal is driven by decision uncertainty and alters serial choice bias. *Nature Communications, 8*, 14637.

Vanderwolf, C. H., & Baker, G. B. (1986). Evidence that serotonin mediates non-cholinergic neocortical low voltage fast activity, non-cholinergic hippocampal rhythmical slow activity and contributes to intelligent behavior. *Brain Research, 374*(2), 342-356.

Van Slooten, J. C., Jahfari, S., Knapen, T., & Theeuwes, J. (2018). How pupil responses track value-based decision-making during and after reinforcement learning. *PLoS Computational Biology, 14*(11), e1006632.

Wang, C. A., & Munoz, D. P. (2015). A circuit for pupil orienting responses: implications for cognitive modulation of pupil size. *Current Opinion in Neurobiology, 33*, 134-140.

Watakabe, A., Komatsu, Y., Sadakane, O., Shimegi, S., Takahata, T., Higo, N., ... & Sakamoto, H. (2008). Enriched expression of serotonin 1B and 2A receptor genes in macaque visual cortex and their bidirectional modulatory effects on neuronal responses. *Cerebral Cortex, 19*(8), 1915-1928.

Wyart, V., & Koechlin, E. (2016). Choice variability and suboptimality in uncertain environments. *Current Opinion in Behavioral Sciences, 11*, 109-115.

Xu, S., Das, G., Hueske, E., & Tonegawa, S. (2017). Dorsal Raphe Serotonergic Neurons Control Intertemporal Choice under Trade-off. *Current Biology, 27*(20), 3111-3119.

Yates, J. L., Park, I. M., Katz, L. N., Pillow, J. W., & Huk, A. C. (2017). Functional dissection of signal and noise in MT and LIP during decision-making. *Nature Neuroscience, 20*(9), 1285.

Yu, Y., Ramage, A. G., & Koss, M. C. (2004). Pharmacological studies of 8-OH-DPAT-induced pupillary dilation in anesthetized rats. *European Journal of Pharmacology, 489*(3), 207-213.

4. List of appended papers and statement of contribution.

Project 1. **Head-free training of macaques for tasks requiring precise measurements of eye position**. Kawaguchi, K., Seillier, L., Pourruahi, P., Clery, S., & Nienborg, H. (to be submitted).

I trained one animal, collected the data, performed all the data analysis, and wrote the first draft. Pourriahi P and Nienborg H designed the setup. Seillier L and Clery, S contributed to the data collection. Seillier L and Nienborg H modified the draft.

Project 2. **Differentiating between models of perceptual decision-making using pupil-size inferred confidence**. Kawaguchi, K., Clery, S., Pourriahi, P., Seillier, L., Haefner, R., & Nienborg, H. (2018). The Journal of Neuroscience, 38(41), 0735-18. https://doi.org/10.1523/JNEUROSCI.0735-18.2018

I performed all the analysis and computational modeling, generated the figures, and wrote the first draft of this paper. Clery S, Pourriahi P, and Seillier L collected the data. Haefner R and Nienborg H designed research and modified the draft.

Project 3. **Serotonin decreases the gain of visual responses in awake macaque V1**. Seillier, L., Lorenz, C., Kawaguchi, K., Ott, T., Nieder, A., Pourriahi, P., & Nienborg, H. (2017). *The Journal of Neuroscience*, *37*(47), 1339–17. https://doi.org/10.1523/JNEUROSCI.1339-17.2017

I trained one of the animals and contributed to the data collection. I performed the data analysis for the revision of the paper and generated Figure 3, 8, and 9. Seillier L and Nienborg H designed the study. Seillier L, Pourriahi P, and Nienborg H collected the rest

of the data. Ott T and Nieder A contributed unpublished reagents/analytic tools. Lorenz C analyzed the original data. Seillier L, Lorenz C, and Nienborg H wrote the paper.

Project 4. **Serotoninergic modulation of functional connectivity in awake macaque**

V1. Kawaguchi, K., Seillier, L., & Nienborg, H. (to be submitted).

This study used the same dataset as our previous serotonin study. I trained one of the animals and contributed to the data collection. I performed all the data analysis, generated figures, and wrote the first draft. Seillier L and Nienborg H designed the original study. Seillier L, and Nienborg H collected the rest of the data. Seillier L and Nienborg H modified the draft.

Head-free training of macaques for tasks requiring precise measurements of eye position

Katsuhisa Kawaguchi[1,2], Lenka Seillier[2], Paria Pourriahi[2], Stephane Clery[2], Hendrikje Nienborg[2,*]

[1] Graduate School of Neural and Behavioural Sciences, International Max Planck Research School, 72074 Tuebingen, Germany
[2] University of Tuebingen, Werner Reichardt Centre for Integrative Neuroscience, 72076 Tuebingen, Germany

[*]correspondence should be addressed to: hendrikje.nienborg@cin.uni-tuebingen.de

Highlights

- We developed a head-free setup with measurements of eye position to train macaques without head-fixation
- A monkey could move its head freely in the setup but needs to return its head in a stable position whenever it was seeking reward
- Behaviors and eye data from the head-free monkey are comparable to head-fixed monkeys in a visual fixation and discrimination task.
- This method may facilitate a non-human primate research requiring extensive training on animals with precise measurements of eye position

Keywords:

Head-free training

Non-invasive

Macaque monkey

Eye tracking

Fixation precision

Abstract

Background: Our understanding of the brain benefits from extensively trained macaques on tasks requiring precise measurements of eye position. Monkeys are typically trained with their heads fixed via surgically implanted head-posts to minimize noise of eye-data derived from head movements. Therefore, training cannot be initiated until the head-posts are stabilized on animals' skull.

New Method: To train monkeys without head-fixation, we used a reward spout mounted inside a horizontally tilted cup opening towards a monkey's mouth. This setup can be built independently in a workshop, and easily connected to a standard primate chair. The animal in the setup can move its head freely, but the cup ensures that its head returns to a similar position whenever it is seeking reward so that a video eye-tracker can measure its eye position and pupil size.

Results: A male monkey who was naïve to any behavioral training but being seated in a primate chair was trained with the head-free setup in a standard fixation task (46 sessions) and discrimination task (16 sessions). He adapted quickly to the head-free setup, and we were able to gradually increase the fixation duration per trial and decrease the fixation window with measurements of eye position.

Comparison with Existing Method(s): The animal showed behaviors and eye data comparable to head-fixed animals. We also evaluated the head-free setup against the comprehensive criteria for non-invasive head-immobilization systems (Slater et al., 2016).

Conclusions: The head-free setup enables researchers to train macaques without head-fixation on tasks requiring precise measurements of eye position.

1. Introduction

Neuroscience studies with trained awake macaque monkeys have greatly advanced our understanding of the brain. Animals in such studies are trained extensively prior to data acquisition, and many tasks require tight control of the animals' eye movements. For precise measurements of eye position the animals' heads are typically fixed mechanically to a primate chair using surgically implanted head-posts mounted to the animal's skull (Adams et al., 2007; Betelak et al., 2001; Mountcastle et al., 1975). The head-post implantation surgery is invasive yet widely considered to be necessary for neural recordings as well as measurements of eye position. It takes normally a few months for the head-posts to be stabilized on the animals' skull. Until this recovery period is over, training animals cannot be initiated.

A head-free training of macaques without head-fixation is therefore highly desired because not only it is non-invasive, but monkeys can be trained on tasks even before the head-post surgery. Such an option can accelerate research requiring extensive training of animals. Although it is challenging to limit animals' head-movement adequately for eye data without head-fixation, several studies succeeded to develop non-invasive head-immobilization systems with measurements of eye position (Amemori et al., 2015; Drucker et al., 2015; Machado & Nelson, 2011; Fairhall et al., 2006; Slater et al., 2016). To limit animals' head-movement, a two-piece plastic head mold and a bar clamp holder (Amemori et al., 2015) or masks or helmets covering the entire face or head of animals (Drucker et al., 2015; Machado & Nelson, 2011; Fairhall et al., 2006; Slater et al., 2016) were employed, and showed noteworthy results in tandem with other techniques (neural recordings; Amemori et al., 2015; Drucker et al., 2015, transcranial magnetic stimulation; Drucker et al., 2015, eye tracking; Amemori et al., 2015; Druker et al., 2015; Fairhall et al., 2006; Slater et al., 2016; magnetic resonance imaging; Slater et al., 2016). Some studies computed the cost of their systems and showed that labs could benefit from installing such non-invasive head-immobilization systems (Drucker et al., 2015; Slater et al., 2016). Although these studies should be encouraged considering ethical perspectives (e.g. The 3Rs; Russell & Burch, 1959), these systems may be still too complex to be widely used (e.g. requiring sedation during making head-immobilization systems; Amemori et al., 2015; Drucker et al., 2015; Machado & Nelson, 2011; Fairhall et al., 2006; Slater et al., 2016).

To contribute to these lines of studies and accelerate procedures of neuroscience research using awake macaque monkeys, we developed a simple non-invasive setup for precise measurements of eye position in a head-free animal. We used a reward spout mounted inside a

horizontally tilted cup opening towards the animal's mouth. Although the animal could move its head freely, the cup ensured that the animal's head returned to a similar position whenever it was seeking rewards, reducing variability in its head position. Presumably due to the component of voluntary engagement, habituation took only 4 sessions. We monitored the animal's eye position using a video eye-tracker (Eyelink 1000, SR Research Ltd.) and trained the animal on a standard visual fixation task (46 sessions) and orientation discrimination task (16 sessions). Whereas studies with non-invasive head-immobilization often report results only from an example session, we reported results of key experimental parameters, behaviors, and eye data from all the 62 sessions to highlight that head-free animals can be trained on tasks requiring precise measurements of eye position. The setup can be built independently in a workshop without the presence of animals. Since it can be easily combined with existing standard primate chairs and potentially shared by different animals, its installation is relatively easy and can be widely used.

2. Methods

2.1. *Subject*

This study was approved by the local authority (Regierungspraesidium Tübingen), and all the procedures were in accordance with its guideline for animal experiments. We collected data from one head-free male rhesus monkey (*Macaca mulatta*; 12kg) performing a standard visual fixation task and a discrimination task. This monkey did not have an implanted head post and was naïve to any behavioral training in a laboratory setup but being seated in a standard primate chair. After the animal was trained with the head-free setup on the tasks, the head-post implantation surgery was performed under general anesthesia. Fixation precision (see *2.6.2*) was compared in the same animal with or without head-fixation.

2.2. *Head-free setup*

We trained a rhesus monkey without the head-fixation on a visual fixation and a discrimination task. The animal was positioned in a primate chair and viewed the monitor located in a fixed distance. We used a reward spout mounted inside a horizontally tilted cup opening (Fig. 1a). On the base of the cup, there is a small hole from which the metal reward tube, supplying fluid

reward, comes out by approximately 1cm towards the inner space of the spout. The cup facing down the ground is largely open to remove the remaining fluid reward such that the animal could not get remaining reward in following incomplete trials. Whenever the animal was seeking reward, he needed to poke his mouth inside the cup. That reinforced the animal to return his head in a stable position in the primate chair. Whenever the animal wanted to abort a trial, he was able to move his head around freely. Before each day's experiment, the head-free system was mounted in front of the animal's mouth by using the bar-clamp holders connecting the system and the primate chair (Fig. 1c). Since the video-based eye-tracker was positioned between the monitor and the animal, we positioned the cup such that the animal's pupil was successfully detected by the infrared camera when the animal viewed the monitor. We also ensured that the connection between the head-free system and the primate chair was tight enough such that the animal could not move the cup around by using his mouth. The cup was made of hard plastic and not breakable by the animal's bites. We used an operant conditioning for the animal to get used to the setup until he learned to get a reward by poking into the cup. It took only 4 sessions before starting the fixation task, suggesting that the animal quickly adapted himself to this head-free setup.

2.3. *Behavioral tasks*

After the monkey was habituated to the head-free setup, we started to train him on a standard visual fixation task. We then trained him to make a saccade to the target dot when the fixation dot was off (4 sessions). Thereafter we trained him on an orientation discrimination task. We report results from the 46 consecutive sessions for the visual fixation task and the 16 consecutive sessions for the orientation discrimination task. In the both cases, the first session was the first day for the monkey to experience the task.

2.3.1 *Visual fixation task*

We trained the monkey to fixate at a dot in the center of the monitor. The monkey was rewarded (with water or juice) after maintaining fixation for certain fixation duration within a small fixation window around the dot. Once the monitored eye position was out of the fixation window, the trial was aborted. We increased the fixation duration up to 2 sec per trial and decreased the fixation window over the course of training. In our head-free condition, the monkey reached the 2000ms fixation at session 6. This was much earlier than our other two monkeys with head-fixation (took

13 and 28 sessions each), suggesting that the head-free setup might facilitate the animals' task engagement. We started to present a visual stimulus peripherally after session 7. The stimuli were circular drifting sinusoidal luminance gratings similar to (Seillier et al., 2017). We were able to use the fixation window smaller than 1.7^{o} x 1.7^{o} after session 8.

2.3.2. *Orientation discrimination task*

After the monkey learned to maintain a stable fixation, we trained the animal on a two-alternate forced-choice (2AFC) visual discrimination task in which the monkey discriminated orientation of the visual stimuli and indicated his choice via saccade. Trials started upon fixation. The dynamic visual stimuli, in which the Gabor grating changed its orientation frame-by-frame, were presented peripherally for a fixed duration (1.5 sec in 2 sessions and 2 sec in 14 sessions). When the stimulus duration was 1.5 sec, the pre-stimulus duration of 0.5 sec was preceded such that the total fixation duration per trial was 2 sec. Two targets were also presented above and below the fixation dot simultaneously during the stimulus presentation period. One target contained Gabor grating with 100% of horizontal orientation, and the other contained Gabor grating with 100% of vertical orientation. The monkey was required to maintain fixation at the center dot of the monitor during the stimulus presentation period and make a saccade to one of the targets whose orientation was closer to that of the presented stimulus once the fixation dot was off. The target positions for the two types of the targets were randomized across trials to disentangle saccade direction and choice. For correct choices, the monkey got a fluid reward (water or juice). To discourage the animals from guessing in the discrimination task, the available reward size was increased based on their task performance. After three consecutive trials with correct choices, the available reward size was doubled compared to the original reward size. After four consecutive trials with correct choices, the available reward size was again doubled (quadruple compared to the original size) and remained at this size until the next error. After every error trial, the available reward size was reset to the original. For the analyses in Fig. 5b "large available reward" trials refer to both intermediate and large available reward trials collapsed to approximately equalize the number of trials to the small available reward trials.

2.4. *Visual stimuli*

Visual stimuli (luminance linearized) were back-projected on a screen by two projection design projectors (F21 DLP; 60Hz; 1920 x 1080 pixel resolution, 225 cd/m^2 mean luminance) with the

viewing distance of 149 cm. Stimuli were generated with a custom written software using MATLAB (Mathworks, USA) based psychophysics toolbox (Brainard, 1997; Kleiner et al., 2007; Pelli, 1997).

In the visual fixation task, we used sets of stimuli in our previous study (Seillier et al., 2017). The stimuli were circular drifting sinusoidal luminance gratings presented for 450 ms (temporal frequency typically 7 Hz). The direction (16 equally spaced values), the spatial frequency (8 logarithmically spaced values from 0.125 to 16 cycles per degree), the contrast (typically seven logarithmically spaced values from 1.56 to 100%), or the size (typically 12 logarithmically spaced values from 0.3 to 8°) of the grating was pseudorandomly varied, randomly interleaved by blank stimuli, with all other parameters constant.

In the orientation discrimination task, the stimuli were circular drifting sinusoidal luminance gratings. The orientation of the stimuli was changed randomly on each video-frame according to the probability mass distribution set for the stimulus. For the 0% signal stimulus the orientation was drawn from a uniform distribution (8 equally-spaced values between 22.5^{o} and 180^{o}). The monkeys were rewarded randomly on half of the trials on the 0% signal trials. These 0% signal trials were randomly interleaved with horizontal or vertical orientation signal trials. To introduce orientation signal in those trials, the probability of either horizontal or vertical orientation on each video frame during the stimulus presentation was increased. The range of signal strengths was adjusted between sessions to manipulate task difficulty and encourage performance at psychophysical threshold. Typical added signal values were 25%, 50% and 100%.

2.5. *Behavioral analysis*

We performed a survival analysis to summarize the effect of training on the animals' fixating behavior. For the orientation discrimination task, we quantified the animals' psychometric performance as a psychophysical threshold. All the fittings were performed using the Matlab *fminsearch* function.

2.5.1 *Training effect*

We used two statistical tests to examine whether there was an effect of training on a behavior. First, we computed the Spearman's rank correlation between values in the behavior and the session numbers. Second, we split sessions into the first and second half and used the Wilcoxon rank sum test to quantify the difference in the behavior between the two periods.

2.5.2. *Survival analysis on aborting trials*

To quantify the effect of training on the animal's aborting trials by fixation breaks, survival analysis was performed using data of fixation durations from all the trials in each session. First, the maximum fixation duration in each session was split into 11 time bins with a uniform width. The survivor function was generated as the probability *p* that the animal kept fixation at the time bin *t*. The survivor function was fit with 1 - cumulative Weibull distribution by the least squared error:

$$\mathrm{P}(\text{fixating at time bin } t) = e^{-(t/a)^b}$$

where a is the scale parameter and b is the shape parameter, which extend the exponential distribution in that there is no assumption of a constant hazard rate over time. To quantify a distribution of the animal's fixation duration, we computed the median of the fitted Weibull distribution by$a(ln2)^{1/b}$.

2.5.3. *Psychometric threshold*

The animals' choice-behaviors in the discrimination task were summarized as a psychometric function by plotting the probability of 'vertical' choices as a function of the signed signal strength *x* and then fitted with a cumulative Gaussian function by maximum likelihood estimation:

$$\mathrm{P}(\text{choose vertical target}) = \frac{1}{2}[1 + \mathrm{erf}\left(\frac{x - \mu}{\sigma\sqrt{2}}\right)]$$

where *erf* denotes the error function, and μ and σ are mean and standard deviation of the fitted cumulative Gaussian distribution, respectively. The standard deviation σ was defined as the psychophysical threshold, which corresponds to the 84% correct level.

2.6. *Eye-data*

During the experiments, the animals' eye position and pupil size were monocularly measured at 500Hz using an infrared video-based eye tracker (Eyelink 1000, SR Research Ltd, Canada) with the pupil-CR (corneal-reflex) mode in head-referenced coordinates (HREF mode), and digitized and stored for the subsequent offline analysis using Matlab or Python3. The eye tracker was mounted in a fixed position on the primate chair to minimize variability in pupil size measurements between sessions. For each day's experiment, we calibrated the video-based eye-tracker by applying a linear transformation to the raw eye-position signal. This calibration

procedure required the animal to fixate at 5 fixation dots sequentially appearing in different positions (selected from center, left top, right top, left bottom, or right bottom in a 3x3 grid) on the monitor. We applied a linear gain and offset adjustments to the analog output of the Host PC to transform the raw eye-position in the given arbitrary voltage values into pixels (deg; degree visual angle). Our eye-data analysis focused on the period of animals' fixation in which the gaze angles were constant. The background of the display was at mid-gray levels throughout resulting in considerable illumination of the darkened experimental booths.

2.6.1. *Preprocessing of eye traces*

We transformed the eye position *x* to velocity *v*, which represented a moving average of velocities over 5 data samples (Engbert & Kliegel, 2003):

$$\mathrm{v_n} = \frac{\mathrm{x_{n+2}} + \mathrm{x_{n+1}} - \mathrm{x_{n-1}} - \mathrm{x_{n-2}}}{6\,\Delta\,\mathrm{t}}$$

where $\Delta\,\mathrm{t}$ is an inverse of sampling rate. Eye position values were reconstructed using the velocity values to suppress noise (Engbert & Mergenthaler, 2006):

$$x_n = x_0 + \Delta t \sum_{i=1}^{n} v_n$$

We used the reconstructed eye position for the following analysis.

2.6.2. *Fixation precision*

To quantify fixation quality of the head-free monkey, we computed variance of horizontal and vertical eye positions separately. In addition, we computed fixation precision in each session by means of fixation span: area around the mean eye-position during fixation, where the line of sight is found with a desired probability *p* (Cherici et al, 2012). We included completed trials where the animal fixated successfully for a fixed duration (typically 2 sec) in our analysis. In each trial, the eye-position during fixation was subtracted from its mean value to correct the possible calibration offset from the fixation dot. We then pooled the measured eye-position across all the completed trials in each session and estimated the 2D probability density function by making 2D histograms on a grid covering the entire area of fixation using the Matlab *ndhist*

function with the bin size of 1.2. Based on this probability density function, we found the region corresponding to the p^{th} percentile of the distribution. In other words, we computed an area in which p% of the line of sight was found. The probability p was set to 0.75 along with the original study (Cherici et al, 2012). We used this fixation span as the animals' fixation precision. The smaller value of the fixation precision indicates smaller variance of the distribution of the eye position, meaning more precise fixation.

2.6.3. *Pupil size*

Pupil size measured by the Eyelink was given as arbitrary voltage values with a particular dynamic range. We regarded values of pupil size beyond ±4.8 as the timing of blinks and replaced values 100ms before and after the timing with nans. Thereafter all the nans in the pupil size were linearly interpolated. Next, we applied the 2nd order band-pass Butterworth filter with the cutoff frequencies of 0.1 and 10 Hz (same as Urai et al., 2017). To compare pupil size across sessions, the band-passed pupil size was z-scored using the mean and standard deviation (SD) of the pupil size during the stimulus presentation period across all completed trials within each session. On average the pupil size time-course showed a sharp constriction after the stimulus onset followed by a slow dilation towards the stimulus offset (example in Fig. 5a). Since the pupillary dynamic is relatively slow, the pupil size time-course was strongly affected by the stimulus duration. To compare the pupil dynamics across sessions with different stimulus durations (1.5 or 2 sec), we computed the pupil response from the averaged time-series of pupil size: the maximum value during the dilation towards the stimulus offset – the minimum value during the constriction after the stimulus onset (Fig. 5a). To compare the difference in the pupil response between large and small available reward trials, we restricted our analysis to the 0% signal trials to exclude a potential effect of signal strength on pupil dynamics (Kawaguchi et al., 2018).

2.6.4. *Microsaccade detection*

We used a recently developed microsaccade detection algorithm using a convolutional neural network (U'n'Eye; https://github.com/berenslab/uneye; Bellet et al., 2018). We used pretrained weights obtained in the original study based on multiple datasets and detected microsaccades of the head-free animal during the stimulus presentation period. We examined whether detected microsaccades obeyed the "main sequence": a linear relationship between saccadic peak velocity and amplitude (Zuber & Stark, 1965).

3. Results

3.1 Head-free setup for macaques with measurements of eye position

In a typical cognitive neuroscience research using macaques with measures of eye position, monkeys' heads are typically mounted to primate chairs via head-posts surgically implanted on animals' skull. The surgery for head-post implantation is invasive yet considered to be necessary to limit animals' head movements for high quality eye data. One apparent downside with this procedure apart from its invasive aspect is that it takes normally a few months for head-posts to be stabilized on monkeys' skulls and therefore training monkeys cannot be initiated until this stabilization period is over (Fig. 1a, gray line). Training macaques without head-fixation would accelerate such a procedure because animals can be trained before the head-post implant surgery as well as during the head-post stabilization period (Fig. 1a, red line). For some studies without neural recordings it may be possible to complete data collection without the invasive head-post implantation.

To train macaques without head-fixation, we used a reward spout mounted inside a horizontally tilted cup opening towards the animal's mouth (Fig. 1b). We used a naïve male animal without a head-post and any prior trainings but being seated in a standard primate chair. The animal was seated in a primate chair and trained via operant conditioning to stabilize his head in a fixed position to receive fluid rewards (Fig. 1c, left). The cup-like shape of the reward delivery system reduced variability in the head position. Although the animal could move his head freely, the system ensured that the animal's head returned to a similar position whenever he was seeking rewards (Fig. 1c, right). Presumably due to the option for voluntary engagement, the animal adapted himself quickly to this setup. After 4 sessions of habituation to this setup we were able to start monitoring the animal's eye position using a video eye-tracker (Eyelink 1000, SR Research Ltd.) during a standard visual fixation task. We used the pupil-CR (corneal-reflex) mode in head-referenced coordinates (HREF mode). Example measured eye traces and pupil size are shown in Fig. 1d.

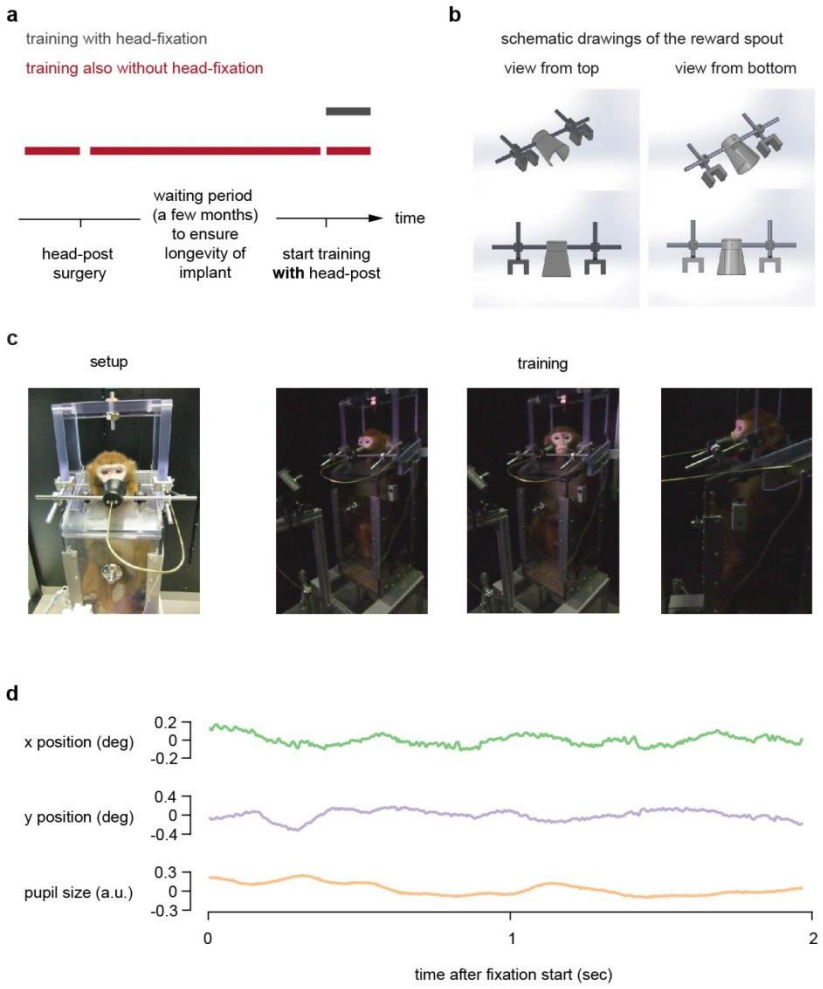

352

353 Fig. 1. Head-free setup for macaques. a) Benefit of a head-free training. Monkeys are typically
354 trained only after head-posts are surgically implanted and stabilized on animals' skulls (gray) to
355 limit animals' head-movements for precise measurements of eye position. Training without
356 head-fixation (red) can accelerate research. b) Schematic drawings of the 'cup'. A reward spout
357 is mounted inside the cup to provide animals with fluid reward. c) Photos showing the head-free
358 setup with a monkey (left) and example scenes of training (right). Note that an animal can move
359 its head freely, yet the cup ensures that the animal returns his head to a stable position
360 whenever he is seeking reward. d) Eye (top: x; horizontal position, middle: y; vertical position)
361 and pupil size (bottom) traces of the head-free animal in an example trial with 2-sec fixation.
362 Eye data were obtained by a video-based eye-tracker with the pupil-CR (corneal-reflex) mode in
363 head-referenced coordinates (HREF mode).

364

3.2. Training on a standard visual fixation task

We trained the head-free animal on a standard visual fixation task (46 sessions; Fig. 2a). Initially we did not present any stimuli except for a fixation dot on the center of the screen. Based on the animal's fixating behavior, we sought to increase fixation duration per trial required to get reward and decrease fixation window session-by-session (Fig. 2b, c). Within 6 sessions the animal was able to fixate for 2 sec per trial, which were substantially earlier than our other two monkeys with head-fixation via head-posts (13 and 28 sessions each). Presumably the option for voluntary engagement helped him to quickly learn the task. We presented visual stimuli that the animal was required to ignore on a peripheral location after session 7. In the head-free setup, the animal could abort a trial whenever he wanted by breaking fixation. That led to relatively high proportion of fixation breaks across sessions (Fig. 2d). We did not observe a systematic effect of training on the proportion of fixation breaks (Spearman's rank correlation: $r = -0.09$, $p = 0.53$; Wilcoxson rank sum test: $p = 0.38$), presumably because we changed sets of experimental parameters across sessions: fixation duration per trial, fixation window, and new sets of visual stimuli. We observed the animal worked longer over the course of training especially in the early training period (Fig. 2e). We hypothesized that the animal fixated longer even within fixation-break trials in later sessions. To test this hypothesis, we performed a survival analysis on fixation duration in all the trials including ones with fixation breaks in each session. The survivor function decreased as a function of time, as expected (examples in Fig. 2f left). Over the course of training across sessions, the median from fitted Weibull survivor functions tended to be on increase (Spearman's rank correlation: $r = 0.2$, $p = 0.18$; Wilcoxson rank sum test: $p < 0.05$), suggesting that the animal tended to fixate longer in later sessions over the course of training (Fig. 2f right).

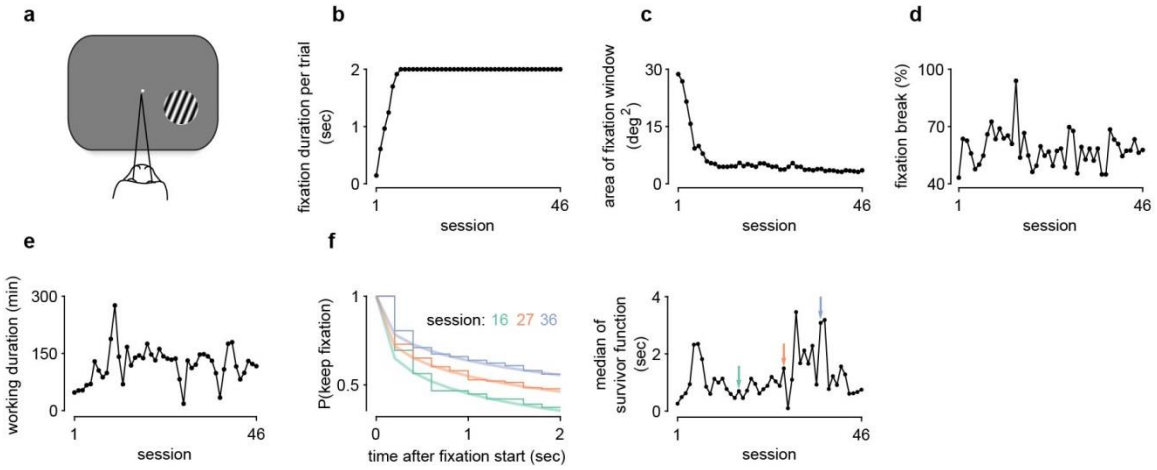

Fig. 2. Experimental parameters and the head-free animal's behaviors on a visual fixation task. a) Fixation task. The head-free animal maintained fixation on the fixation dot. Visual stimuli were presented periphery after session 7. b) Fixation duration per trial required to get reward set by experimenters. It took the head-free animal 6 sessions to reach 2 sec of fixation duration per trial. c) Same as b) but for area of fixation window. d) Proportion of trials with fixation break. e) Working duration of the animal per session (min). f) (Left) Survivor functions and their fits for fixation breaks in the three example sessions. (Right) The median of the survivor function. Overall the animal fixated longer in later sessions.

Importantly for this head-free setup, we observed that the quality of the head-free animal's visual fixation quantified as variance of eye position (Fig. 3a) and fixation span (Cherici et al., 2012; Fig. 3b) improved over the course of training (Spearman's rank correlation: $r = -0.59$, $p < 10^{-4}$; Wilcoxson rank sum test: $p < 10^{-2}$; Fig. 3b). We did not observe statistically significant difference in variance between horizontal (x) and vertical (y) eye position ($p = 0.26$, $t = 1.13$; paired t-test), suggesting that the animal's pupil margin was not systematically occluded (Choe et al., 2016). The head-free animal's fixation precision went steadily under 0.7 (deg^2) after 13 sessions. The median fixation precision from all the sessions in the fixation task was 0.33 (deg^2). This was comparable to the median fixation precision (0.28 deg^2) from the same animal but with head-fixation in later sessions (the first 46 sessions with head-fixation via the head-post). This suggests that animals can be trained to yield high quality eye data with this head-free setup.

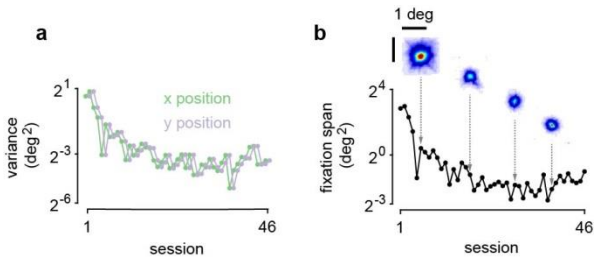

Fig. 3. Quality of fixation during the fixation task. a) Variance of x (horizontal; green) and y (vertical; purple) position of the eye. Data points are horizontally jittered for visualization purpose. b) Fixation precision defined as fixation span (Cherici et al., 2012) in each session. 4 example 2D distributions of eye position are shown. Distributions are normalized by their peak value for visualization purpose. Note binary logarithmic scale of y-axis.

3.3. Training on an orientation discrimination task

After training the head-free animal on the visual fixation task, we trained him to make a saccade to a target dot presented peripherally when the fixation dot was off (4 sessions). Thereafter we started to train him on an orientation discrimination task (16 sessions; Fig. 4a). 2 sessions were with 0.5 sec of pre-stimulus duration and 1.5 sec of stimulus presentation, and 14 sessions were 2 sec of stimulus presentation right after the fixation onset. In the both cases the total fixation duration per trial was 2 sec. The animal indicated his choice via a saccade to one of the two targets. The video-based eye-tracker successfully captured his choice saccades (examples from 4 sessions; Fig. 4b). We quantified the animals' psychometric performance as a psychometric threshold and found it on decrease over the course of training (Spearman's rank correlation: $r = -0.84$, $p < 10^{-4}$; Wilcoxson rank sum test: $p < 0.05$; Fig. 4c). This shows that we were indeed able to train the head-free animal on a task requiring precise measurements of eye position.

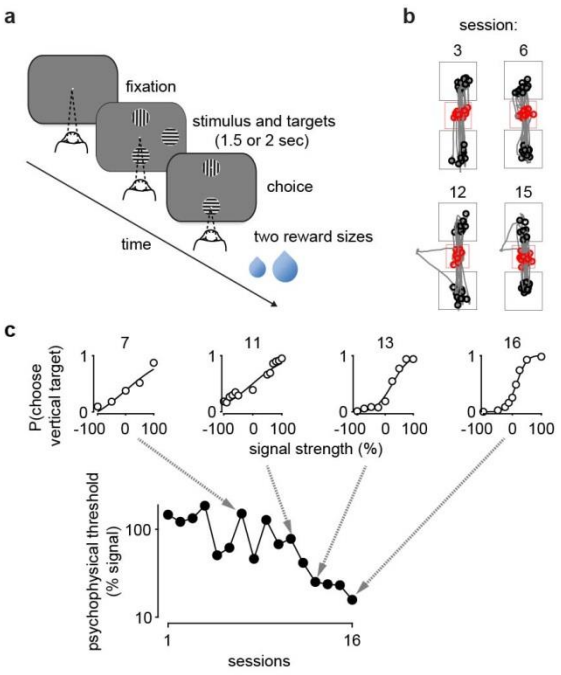

Fig. 4. The head-free animal's behaviors on an orientation discrimination task. a) Orientation discrimination task. The animal initiated a trial upon fixation. Visual stimulus and two targets were shown for 1.5 or 2 sec (2 and 14 sessions, respectively. 0.5 sec pre-stimulus duration was preceded when the stimulus duration was 1.5 sec). Once the fixation dot was off, the animal made a saccade to one of the targets. Available reward size was increased when the number of previous consecutive correct trials was > 2. Otherwise the available reward was reset to be an original value. b) Example saccades the animal made to indicate the choice from 4 sessions. Starting points of saccades are in red. End points are in black. Red and gray squares are fixation window and target window, respectively. c) Psychometric performance. Psychophysical thresholds decreased as a function of sessions, indicating improving psychophysical performance. Example psychometric functions were shown from 4 sessions.

We looked into the quality of the measured pupil size data with the head-free setup. Pupil size or diameter during fixation in isoluminant environment has been extensively used to infer subjects' arousal-linked internal state (Ebitz and Platt, 2015; Kawaguchi et al., 2018; Mitz et al., 2017; Rudebeck et al., 2014; Suzuki et al., 2016). To examine the quality of the pupil size data with the head-free setup, we sought to find widely-known modulation in pupil size by available reward size (Baruni et al., 2015; Varazzani et al., 2015). In the orientation discrimination task

trial-by-trial available reward size was determined based on the animal's previous consecutive correct trials and hence predictable. We computed pupil response from the average pupil size time-course in the 0% signal trials (Fig. 5a) separately for trials with small and large available reward size. Along with the previous studies, we found that the head-free animal's pupil response was significantly larger in large available reward trials than small available reward trials (n = 16 sessions, $p < 0.01$; Wilcoxon signed rank test; Fig. 5b). Our results suggest that pupillary research with macaques can be performed with the head-free setup.

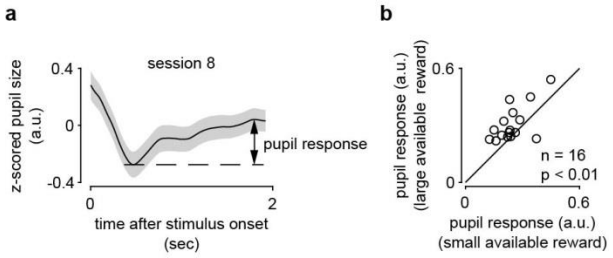

Fig. 5. Pupil size. a) Pupil response. Pupil response was defined as the difference between the minimum value during the initial sharp constriction and the maximum value during the dilation towards the stimulus offset in the average time-course of pupil size, shown for example session 8. b) Modulation in pupil response by available reward size. Pupil response in large available reward trials was larger than that in small available reward trials (n = 16 sessions, $p < 0.01$; Wilcoxon sign rank test).

Another important index of eye data during fixation is microsaccade. Microsaccade has been shown to be linked with sensory, motor, and cognitive processes (Chen et al., 2013, 2015; Hafed et al., 2011, 2013; Herrington et al., 2009; Lowet et al., 2018; Mcfarland et al., 2016). Therefore, accurate detection of microsaccade is desired for such a research. To see whether we could detect reasonable microsaccades of the head-free animal during fixation, we used a recently developed algorithm using a convolutional neural network (U'n'Eye; Bellet et al., 2018) with pretained weights based on multiple datasets. We found that the deep neural network successfully detected microsaccades (eye traces from two example trials in Fig. 6a). The rate of detected microsaccade was plausible, and its variance across sessions was small (1.14 ± 0.20 s^{-1}; mean ± SD). Finally we examined the "main sequence": a linear relationship between peak

velocity and amplitude in microsaccades (Zuber & Stark, 1965). We confirmed a positive correlation between amplitude and peak velocity in detected microsaccades (Pearson correlation: $r = 0.56$, $p < 10^{-9}$, $n = 44{,}124$ microsaccades from 16 sessions; Fig. 6b). Therefore, microsaccade can be reasonably detected in the head-free setup.

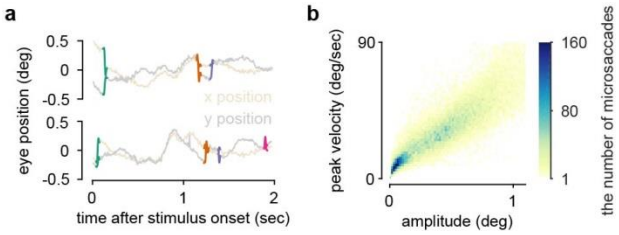

Fig. 6. Detected microsaccade by a convolutional neural network (Bellet et al., 2018). a) Detected microsaccades in eye traces from two example trials. b) Main sequence analysis. Among detected 44,124 microsaccades from 16 sessions movement amplitude and peak velocity were positively correlated (Pearson correlation: $r = 0.56$, $p < 10^{-9}$).

In conclusion, our results suggest that with this head-free setup, macaques can be trained on tasks requiring precise measurements of eye position.

4. Discussion

The head-free setup described here is, to our best knowledge, the simplest non-invasive approach to train macaque monkeys without head-fixation. Since sedation is not required during building the setup, it can be built independently in a workshop without the presence of monkeys. Potentially a single setup can be shared by different animals. In addition, it can be easily connected to a standard primate chair using bar-clamp holders (Fig. 1c). The cup-like structure of the setup allowed a monkey to move its head freely but reinforced its head to return to a stable position whenever the animal was seeking reward, which reduced variability in head-movements during tasks. We tested this head-free setup with a male rhesus monkey who was without a head-post and naïve to any behavioral trainings except for being seated in a standard primate chair. Presumably since animals could engage in a task voluntarily, the animal adapted

himself quickly to the setup (4 habituation sessions). The animal reached 2 sec of fixation per trail within 6 sessions (Fig. 2b), which was substantially earlier than two other in-house animals with head-posts (13 and 28 sessions each). We were able to use the fixation window smaller than 1.7^{o} x 1.7^{o} after session 8 (Fig. 2c) because the quality of visual fixation improved over the course of training (Fig. 3). After training on the fixation task, we were able to train the animal on an orientation discrimination task in which the animal indicated his choice via saccade (Fig. 4). We observed well-known properties of pupil size (Fig. 5) and microsaccade (Fig. 6). These results demonstrated that the head-free setup can be used to train animals with precise measurements of eye position.

We review the head-free setup against the eight criteria of non-invasive head-immobilization systems (Slater et al., 2016).

1) Customisable: the head-free setup can be individually customized for each animal simply by changing the diameter of the cup. The use of the same setup for different animals is potentially possible.

2) Access: the setup ensures access for visual stimulus presentation as well as the reward delivery. Auditory stimulation should be also possible given that animal's ears are not covered.

3) Minimising pressure points: after training we typically noticed marks on the animal's face along with the edge of the cup, which were caused by pressure of the animal's poking into the cup. The pressure can be reduced by increasing the distance in the reward tube inside the cup such that the animal can reach the reward drop without poking too strongly.

4) Comparisons to implanted head posts: the animal reached 2 sec of fixation per trail within 6 sessions (Fig. 2b), which was substantially earlier than other two in-house animals with head-posts (13 and 28 sessions, respectively). The quality of visual fixation of the head-free animal (median fixation precision = 0.33 deg^2; Fig. 3) was comparable to that of the same animal with head-fixation via the head-post in later sessions (median fixation precision = 0.28 deg^2). Therefore, we were able to train the head-free animal on a discrimination task requiring saccade (Fig. 4) and observed well-known properties of pupil size (Fig. 5) and microsaccade (Fig. 6) found in head-fixed animals in the previous studies.

5) Minimise distress: the head-free setup allowed the animal to engage on the task voluntary, and whenever the animal wanted to abort trials, he moved his head around or tried to move the cup with his month. Such behaviors were typically observed towards the end of the session.

6) Adaptable: the head-free setup can be easily mounted on a standard primate chair and therefore can be adapted by different labs. Since the setup allows animals to move heads freely, it is not suitable for neural recordings and imaging techniques. For those purposes other non-invasive approaches may be considered (neural recordings; Amemori et al., 2015; Drucker et al., 2015, transcranial magnetic stimulation; Drucker et al., 2015; electroencephalogram; Itoh et al., 2015, positron emission topography; Howell et al., 2001, magnetic resonance imaging; Srihasam et al., 2010; Hadj-Bouziane et al., 2014; Slater et al., 2016).

7) Voluntary engagement: the head-free setup allows totally voluntary engagement; an animal can move its head freely and poke inside the cup only when it was seeking reward.

8) Animal size: the head-free monkey in this study was 12 kg and relatively large as a macaque monkey. Since the setup does not cover animals' face or head like masks or helmets used in previous studies (Drucker et al., 2015; Machado & Nelson, 2011; Fairhall et al., 2006; Slater et al., 2016), the setup is presumably more invariant to animals' size. Animals with substantially heavier or lighter weight can be adapted to the setup by changing the size of the cup.

Although the head-free setup may not be versatile enough to be used in tandem with neural recordings or imaging techniques, it allows researchers to train animals with precise measurements of eye position before the head-post surgery. For some studies concerning eye data but without neural recordings or imaging techniques, it may be possible to finish data collection with this setup and without the head-post surgery. We believe that the head-free setup has a potential to accelerate research requiring extensive animal training on tasks requiring precise measurements of eye position.

5. Conclusions

We developed a head-free setup, which allowed researchers to train a macaque monkey with measurements of eye position without head-fixation. This setup can be built independently in a workshop without the presence of monkeys and easily integrated to a standard primate chair. We were able to train a monkey without a head-post on a visual fixation task and discrimination

task with this setup. The animal showed behaviors and eye data comparable to head-fixed animals. Therefore, the head-free setup has a potential to accelerate research requiring extensive animal training on tasks with precise measurements of eye position by allowing training to start before the head-post surgery.

Author contributions

H.N designed the head-free setup. K.K, L.S, P.P, and S.C performed data collection. K.K analyzed data. K.K and H.N wrote the paper.

Acknowledgements

This work was supported by a Starting Independent Researcher grant to H.N. from the European Research Council (NEUROOPTOGEN), by funds from the Deutsche Forschungsgemeinschaft awarded to the Centre for Integrative Neuroscience (DFG EXC 307). We are grateful to the animal care staff for all their husbandry expertise and Klaus Vollmer at the workshop in the UKT (Universitätsklinikum Tübingen) for building the head-free setup.

Reference

Adams, D. L., Economides, J. R., Jocson, C. M., & Horton, J. C. (2007). A biocompatible titanium headpost for stabilizing behaving monkeys. *Journal of neurophysiology*, *98*(2), 993-1001.

Amemori, S., Amemori, K. I., Cantor, M. L., & Graybiel, A. M. (2015). A non-invasive head-holding device for chronic neural recordings in awake behaving monkeys. *Journal of neuroscience methods*, *240*, 154-160.

Bellet, M. E., Bellet, J., Nienborg, H., Hafed, Z. M., & Berens, P. (2018). Human-level saccade detection performance using deep neural networks. *Journal of neurophysiology*.

Baruni, J. K., Lau, B., & Salzman, C. D. (2015). Reward expectation differentially modulates attentional behavior and activity in visual area V4. *Nature neuroscience*, *18*(11), 1656.

Betelak, K. F., Margiotti, E. A., Wohlford, M. E., & Suzuki, D. A. (2001). The use of titanium implants and prosthodontic techniques in the preparation of non-human primates for long-term neuronal recording studies. *Journal of neuroscience methods*, *112*(1), 9-20.

588 Brainard, D. H., & Vision, S. (1997). The psychophysics toolbox. *Spatial vision*, *10*, 433-436.
589 Cherici, C., Kuang, X., Poletti, M., & Rucci, M. (2012). Precision of sustained fixation in trained
590 and untrained observers. *Journal of Vision*, *12*(6), 31-31.

591 Choe, K. W., Blake, R., & Lee, S. H. (2016). Pupil size dynamics during fixation impact the
592 accuracy and precision of video-based gaze estimation. *Vision research*, *118*, 48-59.

593 Chen, C. Y., & Hafed, Z. M. (2013). Postmicrosaccadic enhancement of slow eye movements.
594 *Journal of Neuroscience*, *33*(12), 5375-5386.

595 Chen, C. Y., Ignashchenkova, A., Thier, P., & Hafed, Z. M. (2015). Neuronal response gain
596 enhancement prior to microsaccades. *Current Biology*, *25*(16), 2065-2074.

597 Drucker, C. B., Carlson, M. L., Toda, K., DeWind, N. K., & Platt, M. L. (2015). Non-invasive
598 primate head restraint using thermoplastic masks. *Journal of neuroscience methods*, *253*, 90-
599 100.

600 Ebitz, R. B., & Platt, M. L. (2015). Neuronal activity in primate dorsal anterior cingulate cortex
601 signals task conflict and predicts adjustments in pupil-linked arousal. *Neuron*, *85*(3), 628-640.

602 Engbert, R., & Kliegl, R. (2003). Microsaccades uncover the orientation of covert attention.
603 *Vision research*, *43*(9), 1035-1045.

604 Engbert, R., & Mergenthaler, K. (2006). Microsaccades are triggered by low retinal image slip.
605 *Proceedings of the National Academy of Sciences*, *103*(18), 7192-7197.

606 Fairhall, S. J., Dickson, C. A., Scott, L., & Pearce, P. C. (2006). A non - invasive method for
607 studying an index of pupil diameter and visual performance in the rhesus monkey. *Journal of*
608 *medical primatology*, *35*(2), 67-77.

609 Hadj-Bouziane, F., Monfardini, E., Guedj, C., Gardechaux, G., Hynaux, C., Farnè, A., & Meunier,
610 M. (2014). The helmet head restraint system: A viable solution for resting state fMRI in awake
611 monkeys. *NeuroImage*, *86*, 536-543.

612 Howell, L. L., Hoffman, J. M., Votaw, J. R., Landrum, A. M., & Jordan, J. F. (2001). An
613 apparatus and behavioral training protocol to conduct positron emission tomography (PET)
614 neuroimaging in conscious rhesus monkeys. *Journal of neuroscience methods*, *106*(2), 161-169.

615 Hafed, Z. M., Lovejoy, L. P., & Krauzlis, R. J. (2011). Modulation of microsaccades in monkey
616 during a covert visual attention task. *Journal of Neuroscience*, *31*(43), 15219-15230.

617 Hafed, Z. M., & Ignashchenkova, A. (2013). On the dissociation between microsaccade rate and
618 direction after peripheral cues: microsaccadic inhibition revisited. *Journal of Neuroscience*,
619 *33*(41), 16220-16235.

620 Herrington, T. M., Masse, N. Y., Hachmeh, K. J., Smith, J. E., Assad, J. A., & Cook, E. P. (2009).
621 The effect of microsaccades on the correlation between neural activity and behavior in middle

temporal, ventral intraparietal, and lateral intraparietal areas. *Journal of Neuroscience*, *29*(18), 5793-5805.

Itoh, K., Nejime, M., Konoike, N., Nakada, T., & Nakamura, K. (2015). Noninvasive scalp recording of cortical auditory evoked potentials in the alert macaque monkey. *Hearing research*, *327*, 117-125.

Kleiner, M., Brainard, D. H., & Pelli, D. G. (2007). What is new in Psychophysics Toolbox. *Perception*, *36*.

Lowet, E., Gomes, B., Srinivasan, K., Zhou, H., Schafer, R. J., & Desimone, R. (2018). Enhanced Neural Processing by Covert Attention only during Microsaccades Directed toward the Attended Stimulus. *Neuron*.

McFarland, J. M., Cumming, B. G., & Butts, D. A. (2016). Variability and correlations in primary visual cortical neurons driven by fixational eye movements. *Journal of Neuroscience*, *36*(23), 6225-6241.

Machado, C. J., & Nelson, E. E. (2011). Eye - tracking with nonhuman primates is now more accessible than ever before. *American journal of primatology*, *73*(6), 562-569.

Mitz, A. R., Chacko, R. V., Putnam, P. T., Rudebeck, P. H., & Murray, E. A. (2017). Using pupil size and heart rate to infer affective states during behavioral neurophysiology and neuropsychology experiments. *Journal of neuroscience methods*, *279*, 1-12.

Mountcastle, V. B., Lynch, J. C., Georgopoulos, A., Sakata, H., & Acuna, C. (1975). Posterior parietal association cortex of the monkey: command functions for operations within extrapersonal space. *Journal of neurophysiology*, *38*(4), 871-908.

Pelli, D. G. (1997). The VideoToolbox software for visual psychophysics: Transforming numbers into movies. *Spatial vision*, *10*(4), 437-442.

Rudebeck, P. H., Putnam, P. T., Daniels, T. E., Yang, T., Mitz, A. R., Rhodes, S. E., & Murray, E. A. (2014). A role for primate subgenual cingulate cortex in sustaining autonomic arousal. *Proceedings of the National Academy of Sciences*, *111*(14), 5391-5396.

Russell, W. M. S., Burch, R. L., & Hume, C. W. (1959). *The principles of humane experimental technique* (Vol. 238). London: Methuen.

Seillier, L., Lorenz, C., Kawaguchi, K., Ott, T., Nieder, A., Pourriahi, P., & Nienborg, H. (2017). Serotonin decreases the gain of visual responses in awake macaque V1. *Journal of Neuroscience*, 1339-17.

Slater, H., Milne, A. E., Wilson, B., Muers, R. S., Balezeau, F., Hunter, D., ... & Petkov, C. I. (2016). Individually customisable non-invasive head immobilisation system for non-human primates with an option for voluntary engagement. *Journal of neuroscience methods*, *269*, 46-60.

Srihasam, K., Sullivan, K., Savage, T., & Livingstone, M. S. (2010). Noninvasive functional MRI in alert monkeys. *Neuroimage*, *51*(1), 267-273.

Suzuki, T. W., Kunimatsu, J., & Tanaka, M. (2016). Correlation between pupil size and subjective passage of time in non-human primates. *Journal of neuroscience*, *36*(44), 11331-11337.

Urai, A. E., Braun, A., & Donner, T. H. (2017). Pupil-linked arousal is driven by decision uncertainty and alters serial choice bias. *Nature communications*, *8*, 14637.

Varazzani, C., San-Galli, A., Gilardeau, S., & Bouret, S. (2015). Noradrenaline and dopamine neurons in the reward/effort trade-off: a direct electrophysiological comparison in behaving monkeys. *Journal of Neuroscience*, *35*(20), 7866-7877.

Zuber, B. L., Stark, L., & Cook, G. (1965). Microsaccades and the velocity-amplitude relationship for saccadic eye movements. *Science*, *150*(3702), 1459-1460.

Systems/Circuits

Differentiating between Models of Perceptual Decision Making Using Pupil Size Inferred Confidence

Katsuhisa Kawaguchi,[1,2] Stephane Clery,[2] Paria Pourriahi,[2] Lenka Seillier,[2] Ralf M. Haefner,[3] and Hendrikje Nienborg[2]

[1]Graduate School of Neural and Behavioural Sciences, International Max Planck Research School, 72074 Tuebingen, Germany, [2]University of Tuebingen, Werner Reichardt Centre for Integrative Neuroscience, 72076 Tuebingen, Germany, and [3]Brain & Cognitive Sciences, University of Rochester, Rochester, New York 14627

During perceptual decisions, subjects often rely more strongly on early, rather than late, sensory evidence, even in tasks when both are equally informative about the correct decision. This early psychophysical weighting has been explained by an integration-to-bound decision process, in which the stimulus is ignored after the accumulated evidence reaches a certain bound, or confidence level. Here, we derive predictions about how the average temporal weighting of the evidence depends on a subject's decision confidence in this model. To test these predictions empirically, we devised a method to infer decision confidence from pupil size in 2 male monkeys performing a disparity discrimination task. Our animals' data confirmed the integration-to-bound predictions, with different internal decision bounds and different levels of correlation between pupil size and decision confidence accounting for differences between animals. However, the data were less compatible with two alternative accounts for early psychophysical weighting: attractor dynamics either within the decision area or due to feedback to sensory areas, or a feedforward account due to neuronal response adaptation. This approach also opens the door to using confidence more broadly when studying the neural basis of decision making.

Key words: **confidence; integration-to-bound; macaque; perceptual decision making; psychophysical reverse correlation; pupillometry**

Significance Statement

An animal's ability to adjust decisions based on its level of confidence, sometimes referred to as "metacognition," has generated substantial interest in neuroscience. Here, we show how measurements of pupil diameter in macaques can be used to infer their confidence. This technique opens the door to more neurophysiological studies of confidence because it eliminates the need for training on behavioral paradigms to evaluate confidence. We then use this technique to test predictions from competing explanations of why subjects in perceptual decision making often rely more strongly on early evidence: the way in which the strength of this effect should depend on a subject's decision confidence. We find that a bounded decision formation process best explains our empirical data.

Introduction

During perceptual discrimination tasks, subjects often rely more strongly on early, rather than late, sensory evidence, even when both are equally informative about the correct decision (e.g., Kiani et al., 2008; Neri and Levi, 2008; Nienborg and Cumming, 2009; Yates et al., 2017). But some studies in rodents and humans reported uniform weighting of the stimulus throughout the trial (Brunton et al., 2013; Raposo et al., 2014; Drugowitsch et al., 2016). From the perspective of maximizing the sensory information and hence performance, such early weighting is nonoptimal. Understanding this behavior may shed light on how the activity, or the read-out of sensory neurons limits our perceptual abilities, a major goal of contemporary neuroscience (e.g., Pitkow et al., 2015; Cumming and Nienborg, 2016; Clery et al., 2017). The classical explanation for such early psychophysical weighting is that it reflects an integration-to-bound decision process in which sensory evidence is ignored once an internal decision bound is reached (Kiani et al., 2008). For simple perceptual discrimination tasks, decision confidence can be defined statistically (Hangya et

Received March 20, 2018; revised June 22, 2018; accepted July 30, 2018.

Author contributions: R.M.H. and H.N. designed research; K.K. performed research; S.C., P.P., and L.S. contributed unpublished reagents/analytic tools; K.K. and H.N. analyzed data; K.K., R.M.H., and H.N. wrote the paper.

This work was supported by an European Research Council Starting Independent Researcher Grant (NEUROOPTOGEN) to H.N., by a grant from the Deutsche Forschungsgemeinschaft (within the CRC 1233 Robust Vision, University of Tuebingen) to H.N., funds of the Deutsche Forschungsgemeinschaft to the Centre for Integrative Neuroscience (Grant EXC 307), and by an NEI grant EY028811 to R.M.H.

The authors declare no competing financial interests.

Correspondence should be addressed to Dr. Hendrikje Nienborg, University of Tuebingen, Werner Reichardt Centre for Integrative Neuroscience, 72076 Tuebingen, Germany. E-mail: hnienb@gmail.com.

DOI:10.1523/JNEUROSCI.0735-18.2018

 0270-6474/18/388874-15$15.00/0

al., 2016), and hence also measured for such a model. Here, we derived new predictions of this model for how the temporal weighting of sensory evidence should vary as a function of decision confidence on individual trials. These revealed characteristic differences in the temporal weighting for high- and low-confidence trials, depending on the decision bound. We then sought to test these predictions in macaques performing a fixed duration visual discrimination task while also estimating the animal's subjective decision confidence.

Measuring decision confidence psychophysically is relatively difficult, particularly in animals, and increases the complexity of a task (e.g., for post-decision wagering) (Kiani and Shadlen, 2009; Komura et al., 2013), hence requiring additional training. To avoid these difficulties, we devised a metric based on the monkeys' pupil size. Combining this metric for decision confidence with psychophysical reverse correlation (Neri et al., 1999; Nienborg and Cumming, 2007, 2009) allowed us to quantify the animals' psychophysical weighting strategy for different levels of inferred decision confidence, and test our model predictions. The animals showed clear early psychophysical weighting on average. But separating this analysis by inferred decision confidence revealed that early psychophysical weighting was largely restricted to high-confidence trials. Indeed, on low inferred confidence trials, the animals weighted the stimulus relatively uniformly or even slightly more toward the end of the trial. Such behavior matched the predictions of the integration-to-bound model. Furthermore, the differences between both animals could be accounted for by the model by differences in its only two free parameters: internal decision bound as well as the level of uncertainty in our inference of decision confidence.

The animals' behavior was not as well explained by two alternative accounts of early psychophysical weighting. The first alternative account are models in which the decision stage provides self-reinforcing feedback to the sensory neurons (Wimmer et al., 2015), as suggested for example, for probabilistic inference (Haefner et al., 2016) or by attractor dynamics within the decision making area (Wang, 2002; Wong et al., 2007). The second, recent alternative proposal is that the early weighting simply reflects the feedforward effect of the dynamics (gain control or adaptation) of the activity of the sensory neurons (Yates et al., 2017). Although each of these alternatives predicts the early weighting, we were unable to fully capture the animals' data with the temporal weighting predictions of these models when separating trials by decision confidence.

Together, our data suggest that the animals rely on a bounded decision formation process. In this model, evidence at the end of the trial is only ignored once a certain level of decision confidence is reached, thereby reducing the impact on performance. Moreover, this combination of techniques provides a novel tool for a more fine-grained dissection of an animal's psychophysical behavior.

Materials and Methods

Animal preparation and surgery. All experimental protocols were approved by the local authorities (Regierungspräsidium Tübingen). Two adult male rhesus monkeys (Macaca mulatta), Animal A (7 kg; 11 years old) and Animal B (8 kg; 11 years old), housed in pairs, participated in the experiments. The animals were surgically implanted with a titanium headpost under general anesthesia using aseptic techniques as described previously (Seillier et al., 2017).

Visual discrimination task. The animals were trained to perform a two choice disparity discrimination task (see Fig. 2*a*). The animals initiated trials with the visual fixation on a small white fixation spot (size: 0.08°–0.12°) located on the center of the screen. After the animals maintained fixation for 500 ms, a visual stimulus was presented (median eccentricity for Animal A: 5.3°; range 3.0°-9.0°, median eccentricity for Animal B: 3.0°, range 2.3°–5.0°) for 1500 ms. After that two choice targets, each consisting of a symbol representing either a near or a far choice and whose positions were randomized between trials, appeared above and below the fixation spot. Once the fixation spot disappeared, the animals were allowed to make a choice via saccade to one of these targets. The animals received a liquid reward for correct choices. Randomizing target positions allowed us to disentangle saccade direction and choice.

Visual stimuli. Visual stimuli (luminance linearized) were back-projected on a screen using a DLP LED Propixx projector (ViewPixx; run at 100 Hz 1920 × 1080 pixel resolution, 30 cd/m^2 mean luminance) and an active circular polarizer (Depth Q; 200 Hz) for Animal B (viewing distance 97.5 cm), or two projection design projectors (F21 DLP; 60 Hz 1920 × 1080 pixel resolution, 225 cd/m^2 mean luminance, and a viewing distance of 149 cm) and passive linear polarizing filters for Animal A. The animals viewed the screen through passive circular (Animal A) or linear (Animal B), respectively, polarizing filter. Stimuli were generated with custom written software using MATLAB (The MathWorks) and the psychophysics toolbox (Brainard, 1997; Pelli, 1997; Kleiner et al., 2007).

The stimuli were circular dynamic random dot stereograms, which consisted of equal numbers of white and black dots, similar to those previously used (Nienborg and Cumming, 2009). Each random dot stereogram had a disparity-varying circular center (3° diameter) surrounded by an annulus (1° wide) shown at 0° disparity. On each video-frame, all center dots had the same disparity whose value was changed randomly on each video-frame according to the probability mass distribution set for the stimulus. For the 0% signal stimulus, the disparity was drawn from a uniform distribution (typically 11 values in 0.05° increments from −0.25° to 0.25°). The monkeys were rewarded randomly on half of the trials on 0% signal trials. These 0% signal trials were randomly interleaved with near disparity or far disparity signal trials. For each session, one near and one far disparity value was used to introduce disparity signal by increasing the probability of this disparity on each video-frame during the stimulus presentation on this trial. The range of signal strengths was adjusted between sessions to manipulate task difficulty and encourage performance at psychophysical threshold. Typical added signal values were 3%, 6%, 12%, 25%, and 50%.

The choice target symbols were random dot stereograms very similar to 100% signal stimuli, except that their diameter was smaller (2.2°).

To allow for constant mean luminance across the screen, equal numbers of black and white dots were used for the stimulus and the target symbols. Because we used a white fixation dot, systematic differences in fixation precision could, in principle, influence our findings. If this were the case, a black fixation marker should give the opposite results. We therefore also conducted control experiments using a black fixation marker, which yielded very similar results, indicating that systematic differences in fixation precision are insufficient to explain our findings.

Reward size. To discourage the animals from guessing, the available reward size was increased based on their task performance. After 3 consecutive trials with correct choices, the available reward size was doubled compared with the original reward size. After 4 consecutive trials with correct choices, the available reward size was again doubled (quadruple compared with the original size) and remained at this size until the next error. After every error trial, the available reward size was reset to the original. For the analyses in Figure 5, "large available reward" trials refer to both intermediate and large available reward trials collapsed.

Pupil data acquisition and analysis. During the experiments, the animals' eye positions and pupil size were measured at 500 Hz using an infrared video-based eye tracker (Eyelink 1000, SR Research), digitized and stored for the subsequent offline analysis. The eye tracker was mounted in a fixed position on the primate chair to minimize variability in pupil size measurements between sessions. Our pupil analysis focused on the period of animals' fixation in which the gaze angles were constant. The background of the display was at mid-gray levels throughout, resulting in considerable illumination of the darkened experimental booths. To nonetheless exclude the possibility that our results were substantially affected by the dark adaptation of the pupils after the animals entered the

experimental booths, we performed control analyses for which we excluded the initial 20 min of each experimental session, to allow for dark adaptation of the pupil (Hansen and Fulton, 1986), with very similar results (data not shown).

Only successfully completed trials (correct and error trials) were included for the analysis. During preprocessing, we first downsampled the pupil size data such that the sampling rate matched the refresh rates of our screens (60 Hz for Animal A, 100 Hz for Animal B), effectively low-pass filtering the data. We next high-pass filtered the data by subtracting on each trial the mean pupil size of the preceding 10 and following 10 trials (excluding the value of the current trial). This analysis removed linear trends on the pupil size within a session and was omitted for the analysis of pupil size changes throughout a session (see Fig. 3*a*). This analysis yielded qualitatively similar results to bandpass filtering (e.g., de Gee et al., 2014; Urai et al., 2017) the pupil size data. Finally, pupil size measurements were *z*-scored using the mean and SD during the stimulus presentation period across all trials.

When comparing pupil size across conditions, we aimed to minimize any mean difference of pupil size between conditions at stimulus onset. To do so, we computed a baseline pupil size, which was defined as the average pupil size in the epoch 200 ms before stimulus onset, and iteratively excluded trials in which the baseline value deviated most from the condition with the higher number of trials until the absolute mean difference of the *z* score of the baseline pupil size was ≤0.05. This procedure successfully made the baseline pupil size statistically indistinguishable across conditions with a small loss of trials in each session (for details, see Inclusion criteria).

Psychometric threshold. The animals' choice-behaviors were summarized as a psychometric function by plotting the percentage of "far" choices as a function of the signed disparity signals and then fitted with a cumulative Gaussian function using maximum likelihood estimation (see Fig. 2*b*). The SD of the cumulative Gaussian fit was defined as the psychophysical threshold and corresponds to the 84% correct level. The mean of the cumulative Gaussian quantified the subject's bias.

Psychophysical kernel. Psychophysical kernels were computed to quantify how the animals used the stimulus for their choices (Nienborg and Cumming, 2009, 2007). Only 0% signal trials were used for this analysis. First, the stimulus was converted into an $n \times m$ matrix (n, number of discrete disparity values used for the stimulus; m, number of trials) that contained the number of video-frames on which each disparity was presented per trial. Next, the trials were divided into "far" choice and "near" choice trials. The time-averaged psychophysical kernel was then computed as the difference between the mean matrix for "near" choice trials and that for "far" choice trials. We also computed a time-resolved psychophysical kernel as the psychophysical kernels for four nonoverlapping consecutive time bins (each of 375 ms duration) during the stimulus presentation period. Kernels were averaged across sessions, weighted by the number of trials in that session. The amplitude of the psychophysical kernels (PKAs) over time was calculated as the inner product between the time-averaged psychophysical kernel and the psychophysical kernel for each time bin. Kernel amplitudes separated by inferred decision confidence were then normalized by the maximum of the psychophysical kernel averaged across both conditions such that the relative differences between conditions remained. The SE of the amplitude was calculated by bootstrapping (1000 repeats). We also verified that our results were qualitatively similar when psychophysical kernels were computed using logistic regression (compare Yates et al., 2017).

Operationalizing decision confidence. When viewed from a statistical perspective, decision confidence can be linked to several behavioral metrics, such as accuracy, discriminability, and choices on error or correct trials (Hangya et al., 2016) (see Fig. 5*b*). Here, we simulated an observer's decision variables on each trial analogously to Urai et al. (2017). The decision variable (d) was drawn from a normal distribution whose mean depended on the signed signal strength (with negative and positive signal reflecting near and far stimuli, respectively) and the SD on the observer's internal noise (22.8% signal, the median of the animals' psychophysical thresholds). The sign of the d determined the choice on each trial. Assuming a category boundary $c = 0$ (no bias), trial-by-trial confidence (the distance between the decision variable and the category boundary) was transformed into an average across trials percent correct (Lak et al., 2014) as follows:

$$\text{confidence} = \frac{1}{n}\sum_{i=1}^{n} f(|d_i - c|)$$

where f is the cumulative density function of the normal distribution as follows:

$$\mathrm{f(x)} = \frac{1}{2}\left[1 + \mathrm{erf}\left(\frac{x}{\sigma\sqrt{2}}\right)\right] \times 100\%$$

To simulate the relationship between accuracy and confidence, we generated the d for 10^8 trials, binned these based on the level of confidence (20 bins), and computed the accuracy for each bin. To examine the relationship between confidence and psychophysical performance, we performed a median split of the trials based on confidence and measured the psychometric function for high- and low-confidence trials. Finally, we calculated the mean confidence as a function of signal strength separately for correct and error trials.

Perceptual decision models. To compare the animals' psychophysical kernels to different decision strategies, we simulated different perceptual decision models and calculated psychophysical kernels for the model data. For all simulations, only 0% signal trials were used, and the model "decision confidence" was defined as |decision variable| at the end of each trial, unless stated otherwise. PKAs were then computed separately for high- and low-confidence trials, after a median split based on this metric for decision confidence. To account for the imperfect relationship between pupil size and decision confidence, we allowed for noise ("confidence noise," Gaussian additive noise $\sim N(0, \sigma^2)$, where σ was scaled by the SD of the noise-free distribution of the confidence values) when assigning trials into the high- or low-confidence groups and fitting the model PKAs separated by confidence to the animals' data (compare results in Fig. 7). For this fitting procedure, we minimized the mean squared error using MATLAB fminsearchbnd. To compare the model performance, we used the Akaike Information Criterion (AIC) and normalized mean squared error (where the difference between model prediction and data point is divided by the SE of the respective data point).

Integration-to-bound model. In this model, the decision variable (d) is computed as the integrated time-varying difference of the population response of two pools of sensory neurons. For the disparity discrimination task, these would consist of one pool preferring near disparities, the other preferring far disparities. We computed the time-varying population response as the dot product between the time-varying stimulus (analogous to that used in the experiments) and an idealized version of the animals' time-averaged psychophysical kernel. On each trial, once the decision variable reached a decision bound (at decision time, t) (Mazurek et al., 2003; Kiani et al., 2008), the decision variable was fixed at that value (absorbing bound) until the end of the trial. The choice of the model was based on sign (d) at the end of the trial. We used two approaches to derive decision confidence for this model. First, it was defined as $|d|$ at the end of the trial. This approach ignores the decision time. This model had one free parameter (the height of the decision bound), which we varied to best account for the time courses of the PKAs for low- and high-confidence trials. In this model, all trials in which the decision bound was reached are assigned the same confidence. Second, we also generated predictions for the proposal that subjective confidence is higher for those trials in which the bound is reached earlier (Kiani and Shadlen, 2009; Kiani et al., 2014). Because our analysis only relied on the rank order of the trials based on confidence, our results are independent of how exactly this time is converted into confidence.

Neural sampling-based probabilistic inference model. We used the model by Haefner et al. (2016), implemented for an orientation discrimination task. In this model, the decision is based on a belief over the correct decision (posterior probability over the correct decision), which is updated throughout each trial. The decision confidence was computed as |posterior probability −0.5|, which effectively reflects the distance of the posterior to the category boundary. To approximate the time course of the PKA for high- and low-confidence trials, we varied the strength of

the feedback in the model, the contrast of the orientation-selective component of the stimulus and the trial duration. The parameters used to generate the sampling model predictions were the same as in the original paper ($\kappa = 2$, $\lambda = 3$, $\delta = 0.08$, $n_s = 20$; stimulus contrast on each individual frame = 10) (Haefner et al., 2016) and only differed in the number of sensory neurons ($n_x = 256$, $n_g = 64$) to reduce computation time. The decreasing PKA in this model is the result of a feedback loop between the decision making area and the sensory representation.

Evidence accumulation toy-model (idealized attractor model). To be able to systematically explore the predictions of attractor-based models for confidence-specific PKAs, we devised two simple abstract models. In the first, the decision variable d_t at time t is defined as follows:

$$d_t = d_{t-1}(1 + \alpha) + \mu_t$$

where μ_t is the sensory evidence at time t, and α is an acceleration parameter of the accumulation process (compare Brunton et al., 2013). For $\alpha = 0$, the model performs perfect integration. For $\alpha < 0$, it is a leaky integrator; and for $\alpha > 0$, the model implements a confirmation bias or attractor. In the second model, a variant of the previous one, the acceleration parameter α depends on a sigmoidal function of d such that instead:

$$d_t = d_{t-1} + \alpha \tanh(d_{t-1}) + \mu_t$$

For $\alpha > 0$, the behavior of the d_t can then be described by an attractor with a double-well energy landscape in which the minimum of each well corresponds to the choice attractors (compare Wimmer et al., 2015), a behavior also observed for the sampling model by Haefner et al. (2016).

Early sensory weighting model after Yates et al. (2017). We simulated psychophysical model decisions based on sensory responses of a linear-nonlinear model. The linear stage consisted of two temporal filters (k, one for contrast, one for disparity) as follows:

$$k(t) = e^{-t/\tau}(1 - e^{-t/\tau}) + at + b,$$

$$\text{where } 0 < t < t_{max}, \text{ a} \geq 0, \text{ b} \leq 0, \tau > 0.$$

The time-varying disparity stimulus and the stimulus contrast were each convolved with the temporal filter, and their sum ($x(t)$) was exponentiated to generate spike rates as follows:

$$\lambda(t) = e^{x(t)}$$

The model parameters a, b, t_{max}, τ as well as the relative weights of the disparity and contrast kernels were chosen such that the dynamics of the output of the linear-nonlinear model approximately matched that of the average peristimulus time histogram neurons in area MT (Yates et al., 2017, their Fig. 3*b*). Starting from these initial values we then varied these model parameters to explore a range of adaptation levels as shown in Fig. 8). To simulate the decision process, we used two of these MT responses but with opposite tuning, and computed the decision variable ($d(t)$) as the integral of the difference of these time-varying MT responses. The decision on each trial was based on sign ($d(t)$) at the end of the trial, and decision confidence defined as $|d|$ at the end of the trial.

We further explored an extension of this model to additionally account for the temporal autocorrelation of the spiking response, also after Yates et al. (2017). This variant was identical to the first, except that (1) we generated spikes based on the spike rates using a Poisson process; and (2) we included a spike history term such that:

$$\lambda(t) = e^{(x(t) + h * r(t-1))}$$

where h ("history filter," as in Yates et al., 2017, their Supplementary Math Note Fig. 1*c*) is the postspike weight that integrates the neuron's own spiking history ($r(t-1)$). This extension yielded similar results to the version without spike history (data not shown).

Inclusion criteria. Data from a total of 436 sessions (300 and 136 sessions from Animal A and B, respectively) were included. Trials with fixation errors were excluded, thereby reducing the number of included trials from 874,641 to 590,050 successfully completed trials (Animal A: 409,597 trials; Animal B: 180,453 trials). Additionally, to ensure that the differences in pupil size modulation across conditions were not simply a consequence of systematic differences in the baseline pupil size across conditions, we equalized baseline pupil size between conditions by iteratively removing trials until the mean difference of the z-scored baseline pupil size values between conditions was ≤0.05. This baseline equalization was done separately for the following conditions. (1) To explore the effect of signal strength (see Fig. 3*c*), signal trials were divided into easy (≥50% signal) and hard (>0% and <10% signal) trials, and the baseline equalized between these conditions, thereby removing 2457 trials from Animal A and 409 trials from Animal B. (2) To compute PKAs (see Figs. 2*c*, 7), and to explore the effect of available reward size on pupil size modulation (see Fig. 3*b*), only no-signal (0% signal) trials were used. To avoid that our metric used to infer decision confidence (mean pupil size during the last 250 ms before stimulus) and the pupil size modulation for available reward size merely reflected differences in baseline pupil size across conditions, we first separated trials into two groups: small and large (including both intermediate and large) available reward trials. Within each reward-size group, we divided trials according to our pupil size metric (median split) into two subgroups and equalized baseline across these subgroups. In a second step, we equalized baseline across the two reward-size groups. This two step procedure removed 7237 trials from Animal A and 2478 trials from Animal B. Additionally, we only included sessions in which the trials per session remaining after baseline correction exceeded 600, and in which each experimental condition had at least 10 trials. For each session, three psychometric functions were computed (one using all the completed trials, one each including only trials for which the available reward size was large or small, respectively). We fitted cumulative Gaussians to each of these psychometric functions, and only sessions for which each of these fits explained >90% of the variance were included. This selection resulted in 213 sessions from Animal A (312,998 trials) and 84 sessions from Animal B (122,897 trials) that were included for analysis. For our analyses based on inferred decision confidence (see Figs. 5, 7), we only used the last 40 sessions for Animal B after sufficient learning (compare Fig. 4). In control analyses, we verified that all our results were similar when instead no inclusion criteria were applied and all 590,050 successfully completed trials used.

Data and code availability. The code to reproduce the figures is available online at https://github.com/NienborgLab/Kawaguchi_et_al_2018, and the data at https://figshare.com/articles/Kawaguchi_et_al_2018/7076621.

Experimental design and statistical analyses. Two macaque monkeys (both male) were used in this study, reflecting the typical sample size of psychophysical or electrophysiological studies involving macaque monkeys. The statistical analyses for the results are presented in Figures 3–7.

Results

Integration-to-bound models predict characteristic differences in temporal sensory weighting when separating trials by decision confidence

Subjects during psychophysical discrimination tasks often give more weight to the early than late part of the stimulus presentation, even in tasks when both are equally informative about the correct answer (Kiani et al., 2008; Nienborg and Cumming, 2009; Yates et al., 2017). We refer to this behavior as early psychophysical weighting, and the standard computational account is that it reflects an integration-to-bound decision process (Kiani et al., 2008). In brief, this explanation suggests that subjects accumulate sensory evidence only up to a predefined bound, not only in reaction time tasks but also in tasks when the stimulus duration is fixed by the experimenter, and when a complete accumulation of evidence over the course of the entire trial would be optimal. As a result, sensory evidence is ignored after the internal bound is reached on a given trial and, together with a variable time at which this bound is reached, on average across trials, early evidence is weighted more strongly than evidence presented late in a

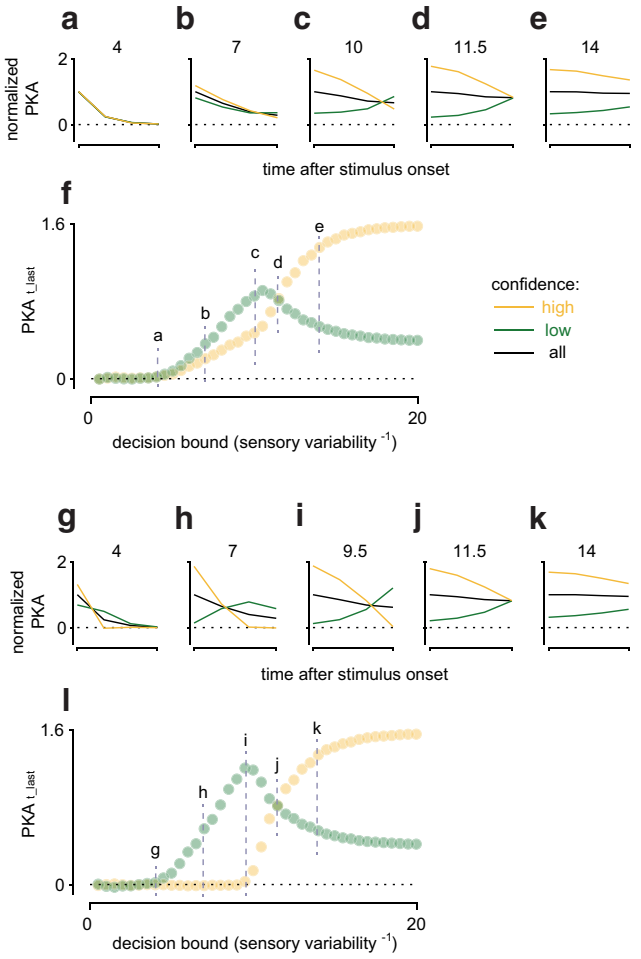

Figure 1. Integration-to-bound models predict characteristic differences in temporal sensory weighting for high- and low-confidence trials. ***a–e***, The PKA is plotted over time for integration-to-bound models with different decision bounds. PKAs for low confidence, high confidence, and averaged across all trials are shown in green, yellow, and black, respectively, and normalized by the peak of the average psychophysical kernel. For intermediate levels of the decision bound, the PKAs cross such that the PKA for low-confidence trials exceeds that for high-confidence trials at the end of the stimulus presentation. The value of the decision bound is marked in each panel. ***f***, PKA_{t_last} is plotted for high (yellow) and low (green) confidence trials. The difference, ΔPKA_{t_last}, depends characteristically on the level of the decision bound in the model and the stimulus strength. The decision bound is normalized by the SD of the sensory variability. The relationship between ΔPKA_{t_last} and the value of the decision bound therefore holds generally across tasks with different stimulus variability. ***g–l***, Same as ***a–f***, but for an integration-to-bound model in which decision confidence is based on both decision time and evidence. Because our analysis only relied on the rank order of the decision confidence, the results are independent of the relative weight of these influences on decision confidence.

trial. If this explanation for the observed early weighting is correct, then across trials in which the decision variable never reaches the bound, all evidence would be weighted equally, regardless of when it was presented during the trial.

Interestingly, for simple perceptual discrimination tasks, decision confidence can be defined statistically (Hangya et al., 2016) and directly linked to the decision variable. In an integration-to-bound model, it simply reflects the distance of the decision variable to the category boundary. Here, we exploited this link and systematically explored how the temporal weighting of the sensory stimulus should depend on decision confidence according to the integration-to-bound model. To do so, we categorized trials into high- or low-confidence trials (median split) and measured the temporal weighting of the sensory evidence as the PKA over time (see Materials and Methods) for each category. We compared these for high-confidence trials, low-confidence trials, and across all trials while systematically varying the decision bound of the model (Fig. 1). As expected, we found that the average PKA decreases more steeply if the decision bound is lower (Fig. 1*a–e*, black lines), indicating that the decision bound was reached earlier on average, and therefore the sensory evidence ignored from an earlier point in the trial. It is also intuitive that the PKA was typically larger for high- compared with low-confidence trials, reflecting the stronger sensory evidence, and hence confidence, on those trials. If the decision bound is low, the decision bound is reached on a large proportion of trials, and the assigned decision confidence identical. These trials are therefore randomly assigned to the high- and low-confidence category, resulting in the similarity of the PKAs (Fig. 1*a*). However, an interesting, nontrivial characteristic emerges for intermediate values of the decision bound (Fig. 1*b*,*c*). Relatively strong evidence early during the trial led to high-confidence and early reaching of the decision boundary, resulting in the pronounced decrease of the PKA for high-confidence trials. But for low-confidence trials, the PKA not only showed no decrease but an increase over time (Fig. 1*b–d*). As a result, the PKAs for high- and low-confidence trials crossed and the PKA for low-confidence trials exceeded that for high-confidence trials at the end of the stimulus presentation. Over a range of values of the decision bound, the difference between the PKA for high- and low-confidence trials was therefore negative (Fig. 1*f*). This characteristic behavior was even more pronounced when we defined decision confidence not only based on evidence but also decision time, as previously suggested (Kiani and Shadlen, 2009; Kiani et al., 2014) (compare Fig. 1*g–l*). A two race extension of the bounded integration model as used in van den Berg et al. (2016) produced similar results. Because our analysis depended only on the rank order of the decision confidence,

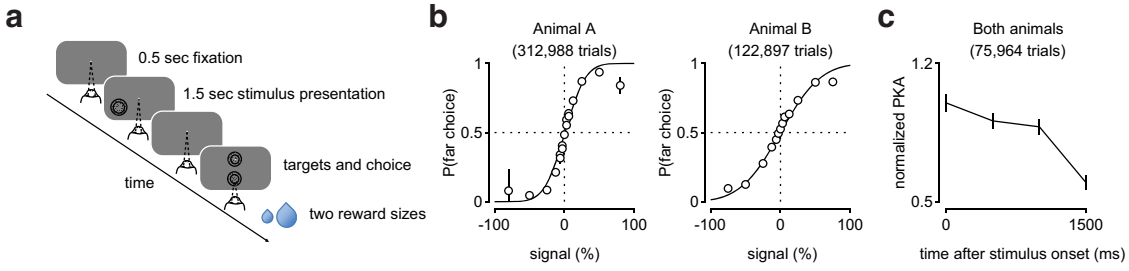

Figure 2. Task and early psychophysical weighting behavior. ***a***, Two choice disparity discrimination task. After the animals maintained fixation for 0.5 s, the stimulus was shown for 1.5 s. The animals had to decide whether the stimulus was "far" or "near" by making a saccade to one of two targets after the stimulus offset and received a liquid reward for correct choices. ***b***, Average psychophysical performance of Animal A (left) and Animal B (right) across all sessions, each fitted with a cumulative Gaussian function. The average psychophysical thresholds are 23% signal and 45% signal for Animal A and Animal B, respectively. ***c***, The time course of the PKA (normalized) shows that the animals weight the stimulus more strongly early during the trial. Data were obtained from 0% signal trials and collapsed across animals (A: 55,570 trials in 213 sessions; B: 20,394 trials in 84 sessions). Error bars indicate SEM derived by resampling.

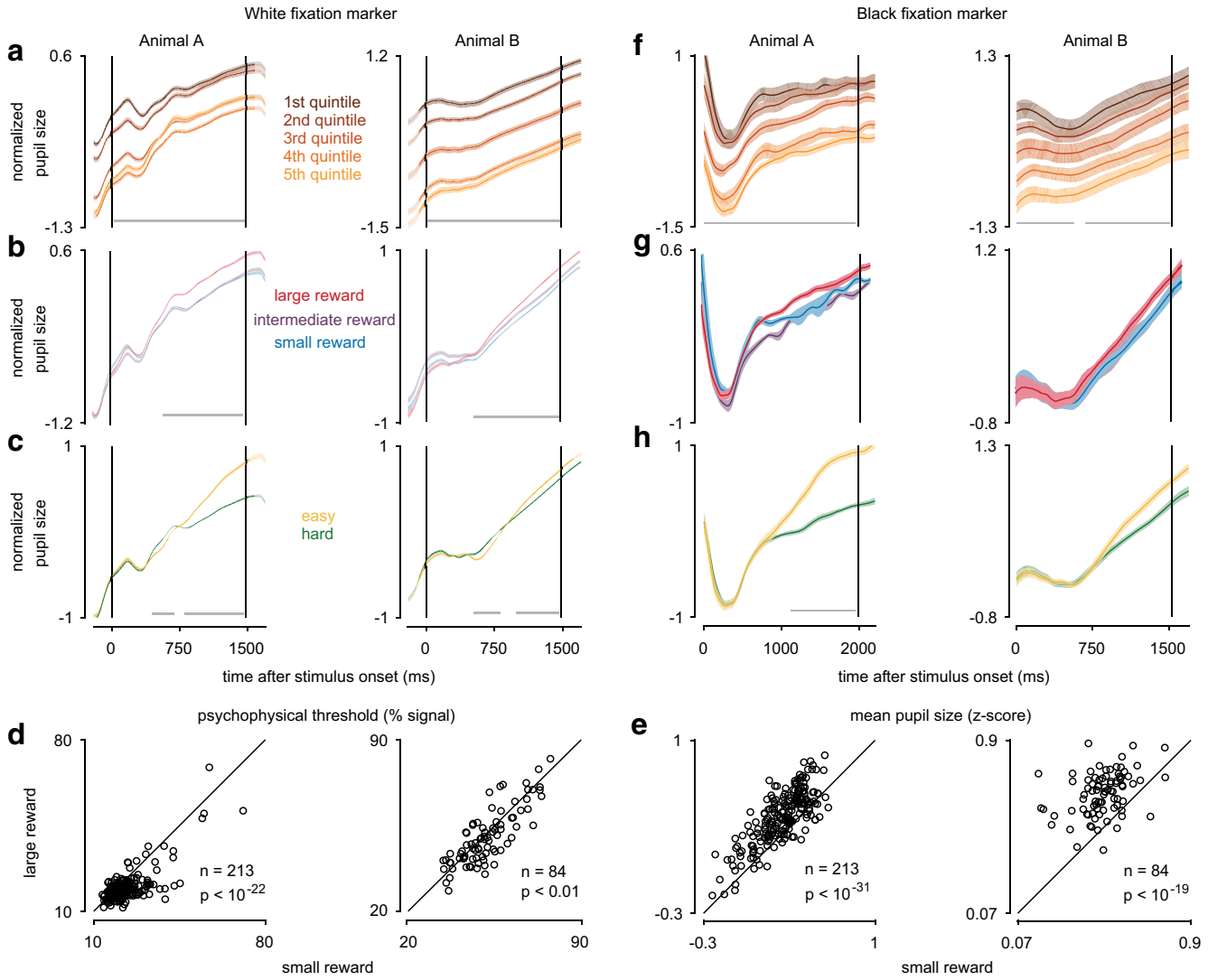

Figure 3. Pupil size modulation with task covariates is consistent with pupil-linked arousal. ***a–c***, Average *z* scores (across conditions) ± SEM of pupil size aligned on stimulus onset are shown for Monkey A (left) and Monkey B (right). Horizontal lines at the bottom of each panel indicate epochs of significant ($p < 0.05$, Bonferroni-corrected, 450 pupil size samples) pupil size modulation (by ANOVA in ***a***, two sample *t* tests in ***b***, ***c***). ***a***, Mean pupil size for five equally sized bins throughout each experimental session. Only small available reward 0% signal trials are used. Pupil size decreases throughout the session as expected for decreasing motivation (Monkey A: 6987 trials from 213 sessions; Monkey B: 2571 trials from 84 sessions). ***b***, Average time courses of pupil size on 0% signal trials that followed a correct trial for large (red), intermediate (purple), and small (blue) available reward trials (Monkey A: 18,700 small available reward trials, 5468 intermediate available reward trials, and 13,035 large available reward trials from 213 sessions; Monkey B: 6897 small available reward trials, 2011 intermediate available reward trials, and 4843 large available reward trials from 84 sessions). ***c***, Average time courses of pupil size on hard (<10%, excluding 0% signal, green) and easy (≥50% signal, yellow) trials. Only trials with small available reward that followed a correct trial were used (Monkey A: 39,390 hard trials and 8651 easy trials from 213 sessions; Monkey B: 10,813 hard trials and 14,020 easy trials from 84 sessions). ***d***, Psychophysical thresholds on large available reward trials were significantly smaller than in small available reward trials (Monkey A: $n = 213, p < 10^{-22}$; Monkey B: $n = 84, p < 0.01$). ***e***, Average pupil size during the 250 ms before the stimulus offset was significantly larger compared with small available reward trials (Monkey A: $n = 213, p < 10^{-31}$; Monkey B: $n = 84, p < 10^{-19}$, all paired *t* tests). ***f–h***, Control sessions for which a black fixation marker was used were included when the number of trials exceeded 600 and the number of trials in each condition per session was at least 10 (9 and 12 sessions, for Animal A and Animal B, respectively). ***f–h***, Colors same as in ***a–c***. ***f***, Monkey A: 139 trials in each time bin from 9 sessions; Monkey B: 221 trials in each time bin from 12 sessions. ***g***, Monkey A: 411 small available reward trials, 102 intermediate available reward trials, and 403 large available reward trials from 9 sessions; Monkey B: 558 small available reward trials, 198 intermediate available reward trials, and 407 large available reward trials from 12 sessions. The pupil size averaged over 250 ms before stimulus offset of the stimulus presentation tended to be larger compared with small available reward trials ($p = 0.12$ for Animal A, $p < 0.01$ for Animal B, paired *t* tests). ***h***, Monkey A: 775 hard trials and 465 easy trials from 9 sessions; Monkey B: 1347 hard trials and 1169 easy trials from 12 sessions. Similar to our results for white fixation markers, the pupil size averaged over the last 250 ms before stimulus offset on easy trials (yellow) significantly exceeded that for hard trials ($p < 10^{-4}$ for Animal A and Animal B, respectively). Data are mean ± SEM.

these results hold generally, regardless of the relative weighting of time and evidence for decision confidence (see Materials and Methods). After sorting zero-signal trials by decision variable, the PKA cannot easily be interpreted as a weight on the stimulus. For instance, the temporal weights on any one trial are always a non-zero constant starting at the beginning of the trial, and zero after some point. As a result, the averaged weights across all trials must be decreasing. The fact that the PKA may be increasing is the result of sorting the trials by confidence which separates the stimulus distributions between the high-and the low-signal trials. Equally, the more pronounced early difference in PKAs for low-decision bounds (compare Fig. 1*a* with Fig. 1*g*) reflects the fact that, when decision confidence is based on both time and evidence, trials with stronger early sensory evidence, and hence early decision times, are assigned to the high-confidence category. Nonetheless, these simulations reveal characteristic predictions

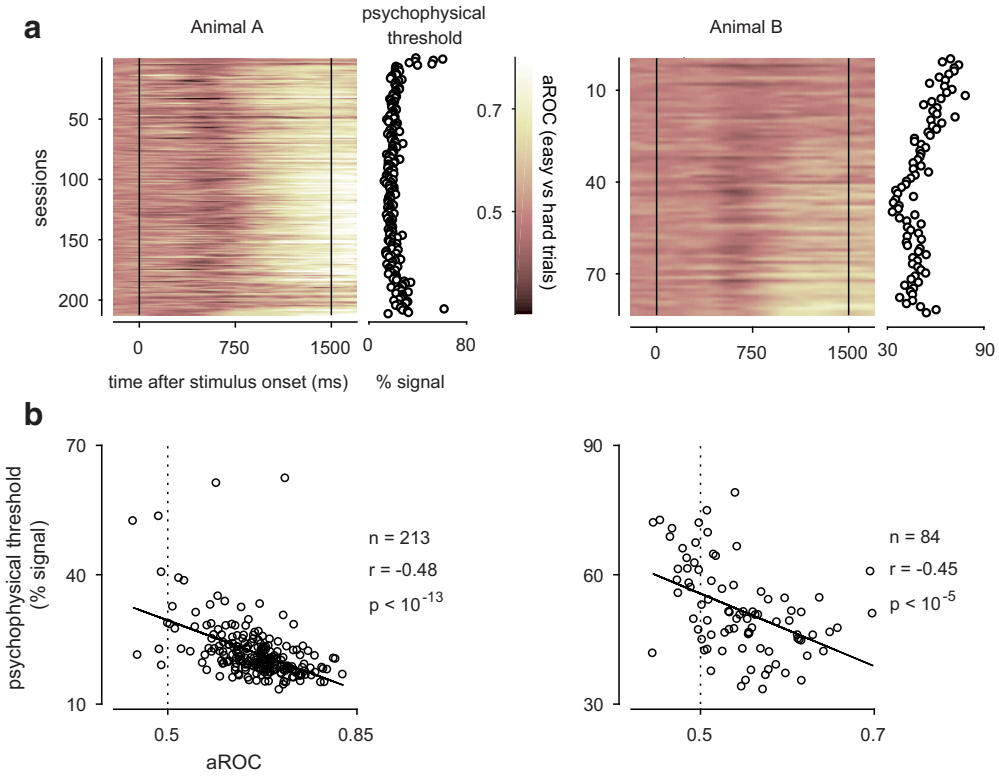

Figure 4. The signature of decision confidence requires good task performance. ***a***, Discriminability between hard (<10%, excluding the 0% signal) and easy (≥50% signal) trials, quantified as aROC for each session (ordinate; 213 sessions from Animal A, 84 sessions from Animal B), plotted as a function of time (abscissa) in the trial after stimulus onset. The systematically larger pupil size for easy trials (bright colors) late in the trial emerges only after extensive training, particularly in Monkey B. ***b***, The average aROC during the 250 ms before the stimulus offset is significantly correlated with the psychophysical threshold (A: $n = 213, r = -0.48, p < 10^{-13}$, B: $n = 84, r = -0.45, p < 10^{-5}$; Pearson's correlation coefficient).

about how a particular statistic (the psychophysical kernel as measured by taking the difference between the choice-triggered averages) should vary as a function of confidence for a bounded decision formation process. We therefore next aimed to test these predictions in monkeys performing a visual discrimination task for which early psychophysical weighting was previously reported (Nienborg and Cumming, 2009).

The animals exhibit early psychophysical weighting behavior in this task

Two macaque monkeys performed a coarse disparity discrimination task (Fig. 2*a*), similar to that described previously (Nienborg and Cumming, 2009). The animals initiated each trial by fixating on a small fixation marker; and after a delay of 500 ms, a dynamic random dot stimulus was presented for a fixed duration of 1500 ms. The stimulus was a circular random dot pattern defining a central disk and a surrounding annulus. The animals' task was to determine whether the disparity-varying center was either protruding ("near") or receding ("far") relative to the surrounding annulus. Following the stimulus presentations, two choice targets appeared above and below the fixation point: one symbolizing a "near" choice, the other a "far" choice. Importantly, the positions of the choice targets were randomized between trials such that the animals' choices were independent of their saccade direction. While the animals performed this task, we measured their eye positions and pupil size.

Our animals performed the task well (Fig. 2*b*). Similar to previous findings (e.g., Kiani et al., 2008; Nienborg and Cumming, 2009; Yates et al., 2017), the animals relied more strongly on the stimulus early than late during the stimulus presentation. We quantified this as a decrease in the PKA (see Materials and Methods) throughout the stimulus presentation (Fig. 2*c*). To test the model predictions separated by decision confidence in the animals' data, we therefore sought to devise an approach to infer the animals' decision confidence from pupil size measurements in this task.

Pupil size is systematically associated with experimental covariates, consistent with pupil-linked changes in arousal

Pupil size has been linked to a subject's arousal in both humans (Bradley et al., 2008) and monkeys (Rudebeck et al., 2014; Ebitz and Platt, 2015; Suzuki et al., 2016; Mitz et al., 2017). Our animals performed a substantial number of trials in each session (mean; Animal A: 828; Animal B: 1067). We therefore wondered whether a signature of their decreasing motivation with increased satiation during the behavioral session could be found in the animals' pupil sizes. To this end, we split the trials of each session into five equally sized bins (quintiles) and computed the average pupil size aligned on stimulus onset (Fig. 3*a*). For these averages, only 0% signal trials on which the available reward size was small (see Materials and Methods) were used. Moreover, to allow for the detection of slow trends throughout the session, the pupil size data were not high-pass filtered for this analysis. We found that, in both animals, pupil size systematically decreased throughout the session, as expected for a decrease in arousal with decreased motivation or task engagement with progressive satiation.

We next explored the effect of varying the available reward size in a predictable way (see Materials and Methods). Consistent with previous results (Cicmil et al., 2015), the animals' psychophysical performance on large available reward trials exceeded

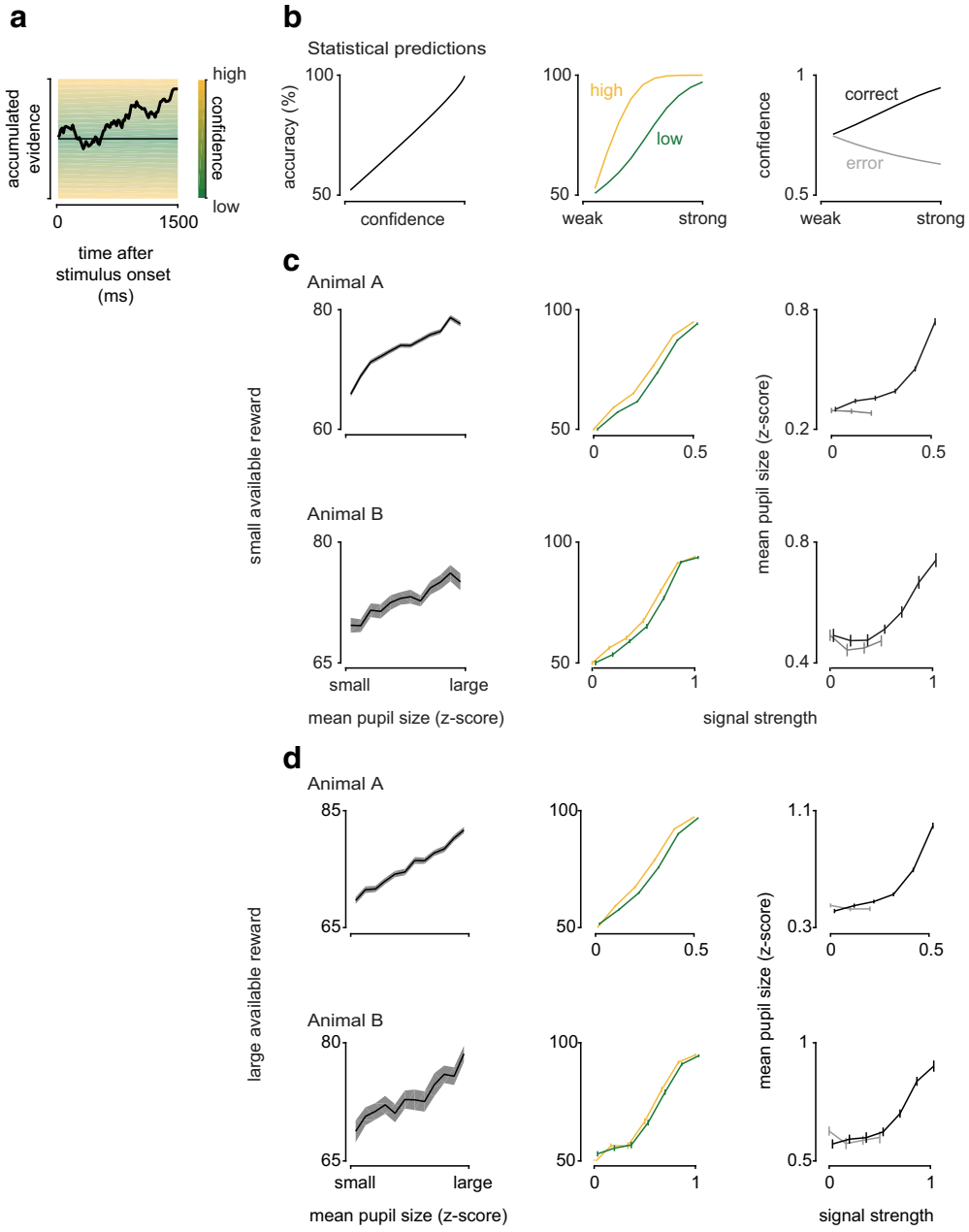

Figure 5. Pupil size shows signatures of decision confidence. ***a***, Schematic of a drift-diffusion model in which the decision confidence depends on the distance of the decision variable to the category boundary. ***b***, Signatures of statistical decision confidence. Left, Statistical decision confidence predicts accuracy. Middle, For high decision confidence, statistical decision confidence predicts steeper psychometric functions than for low decision confidence. Right, Decision confidence is predicted to increase with signal strength in correct trials and decrease with signal strength in error trials. ***c***, ***d***, Metric based on pupil size (mean pupil size during the 250 ms before stimulus offset for small (**c**) or large (**d**) available reward trials) shows characteristics of decision confidence. Left column, Mean pupil size increases monotonically with accuracy. Middle column, The monkeys' psychometric functions separated by mean pupil size are slightly steeper for large compared with small mean pupil size, as predicted for decision confidence. Right column, Mean pupil size increases for correct and slightly decreases on error trials (Monkey A), and for low signal strengths in Monkey B. Data points are slightly offset for better visualization. For Animal A, all 213 sessions were included. For Animal B, analyses are restricted to the last 40 sessions with good performance (compare Fig. 4). Data are mean ± SEM.

that on small available reward trials (Fig. 3*d*). When averaging the time course of the pupil size for 0% signal trials separated by available reward size, we found that pupil size for large available reward trials increased progressively compared with that on small available reward trials (Fig. 3*b*). The animals were rewarded after correct choices following the stimulus presentation. The time course of this pupil size modulation with available reward size is therefore consistent with modulation related to the animals' expectation of the reward toward the end of the trial. Indeed, the difference in mean pupil with available reward size over the last 250 ms of the stimulus presentation was highly statistically reliable (Fig. 3*e*), similar to previous findings (Baruni et al., 2015).

Previous studies that revealed arousal linked pupil size modulation typically used long intertrial intervals (ITIs) lasting several seconds (Rudebeck et al., 2014; Ebitz and Platt, 2015; Suzuki et al., 2016; Mitz et al., 2017), which were deemed necessary to stabilize pupil size before stimulus or trial onset. Conversely, our task allowed for short ITIs (Animal A: 65–4772 ms, median: 136 ms; Animal B: 115–3933, median: 146 ms) to yield a large number of trials per session. Nonetheless, the above analyses revealed

robust signatures of pupil size modulation with experimental manipulations of arousal also for this task.

Given the relatively short ITIs and the sluggishness of the pupil response, we performed a number of control analyses to verify that these results did not merely reflect effects from the preceding trials. First, we equalized the baseline pupil size before stimulus onset across conditions (see Materials and Methods). Second, we explored the effect of the preceding saccade direction, ITI, and the mean pupil size during the last 250 ms of the stimulus presentation on the preceding trial. While there was no systematic effect difference in pupil size as a function of the saccade direction on the preceding trial ($p = 0.75$ and $p = 0.92$ for Monkey A and Monkey B, respectively), there was a systematic correlation between ITI and mean pupil size in 1 animal ($p = 0.50$ and $p = 0.002$, for Monkey A and Monkey B, respectively), and between the mean pupil size on the preceding and current trial in both animals ($p < 10^{-6}$ and $p < 10^{-7}$, for Monkey A and Monkey B, respectively; for the distribution of Spearman's correlation coefficients across sessions). We therefore performed additional analyses to verify that the effects of available reward size and task difficulty were found, even when ITI or mean pupil size on the preceding trial was matched. To this end, we divided trials into five groups of similar average ITI or mean pupil size on the preceding trial each and repeated the analysis (Fig. 3*b*,*c*) for each of these quintiles and found that the main characteristics in pupil size modulation were robust.

Previous work in humans found that pupil size increased with task difficulty, which is thought to reflect changes in arousal related to "cognitive load" or "mental effort" (Hess and Polt, 1964; Kahneman and Beatty, 1966; Alnæs et al., 2014). To explore whether such a signature was evident for our task, we divided our data into easy (≥50% signal) and hard trials (<10% signal, excluding 0% signal trials) (Fig. 3*c*). To remove effects of available reward size, this analysis was restricted to small available reward trials. Consistent with the expected modulation for cognitive load, pupil size in hard trials weakly exceeded that for easy trials in the initial period of the stimulus presentation (before ~750 ms after stimulus onset). However, the more pronounced modulation with task difficulty occurred in the opposite direction toward the end of the trial.

Remarkably, plotting this modulation across training sessions revealed that this late modulation only emerged once the animals knew the task well (Fig. 4*a*) and was correlated with task performance (Fig. 4*b*). This late modulation appears to reflect the animals' expectation to receive a reward based on their knowledge of the probability of being correct given the stimulus difficulty. It might thus be interpretable as a modulation based on the animal's confidence to make the correct decision. We will show next that this modulation indeed exhibits established key signatures (Hangya et al., 2016; Urai et al., 2017) of decision confidence, supporting this interpretation.

Pupil size in this task can be used to infer the animal's decision confidence

For a two-alternative sensory discrimination task analogous to the one used here, decision confidence is monotonically related to the distance to a category boundary (Kepecs et al., 2008; Hangya et al., 2016), that is, the integrated sensory evidence, as schematically shown in Figure 5*a*. From a statistical perspective, decision confidence in such discrimination tasks should be systematically associated with evidence discriminability, accuracy, and choice outcome (model predictions in Fig. 5*b*). Empirically, we found that mean pupil size during the 250 ms before stimulus

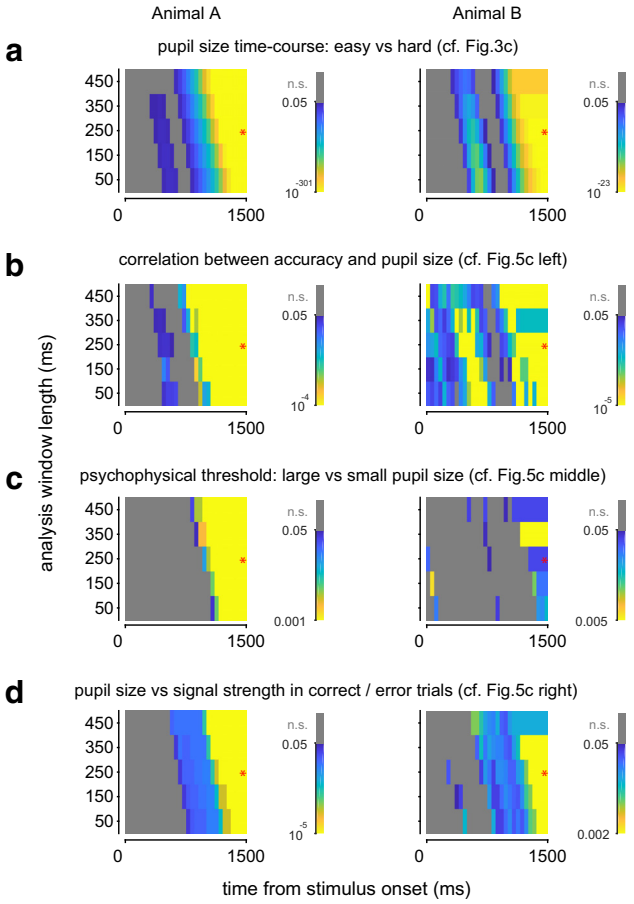

Figure 6. Time window for signature of decision confidence in pupil size within the trial. ***a–d***, *p* values for different analyses are shown for different times within the trial (*x*-axis) and lengths of the analysis window (*y*-axis) over which pupil size was averaged. Data for Animals A and B are shown in the left and right columns, respectively. Red star indicates the time window used for the analyses in this study. ***a***, Bonferroni-corrected *p* values for comparison between pupil size in easy versus hard trials, as in Figure 3*c*. ***b***, *p* values for the Spearman's correlation between accuracy and mean pupil size within each window, as in Fig. 5*c* (left column). ***c***, *p* values derived by resampling for comparing psychometric thresholds for low- versus high-inferred confidence trials, as in Fig. 5*c* (middle column). ***d***, *p* values for the Spearman's correlation between mean pupil size in the respective window and the predicted confidence, as in Fig. 5*c* (right column).

offset showed the three characteristics of statistical decision confidence keeping reward size constant (Fig. 5*c*): we restricted these analyses to small available reward trials to eliminate the effect of available reward size. The findings were qualitatively the same when only analyzing large available reward trials (Fig. 5*d*). First, in both animals, pupil size was correlated with performance accuracy (Fig. 5*c*,*d*, left column; $p < 10^{-4}$ and $p < 0.01$ for Animal A and B, respectively, Spearman's rank correlation). Second, when separating trials based on pupil size (median split), the animals showed better discrimination performance for trials on which pupil size was larger, as expected for improved evidence discrimination with higher decision confidence (Hangya et al., 2016) (Fig. 5*c*,*d*, middle column; $p < 10^{-3}$ and $p = 0.014$ for Animal A and B, respectively, by resampling). Third, as predicted, when separating correct and error trials, decision confidence increased on correct and decreased on error trials (Fig. 5*c*,*d*, right column; $p < 10^{-5}$ and $p < 0.01$ for Animal A and $p < 0.001$ and $p < 0.05$ for Animal B in Fig. 5*c* and Fig. 5*d*, respectively; Spearman's rank correlation with the model predictions in Fig. 5*b*). Interestingly, we also observe a slight increase in pupil

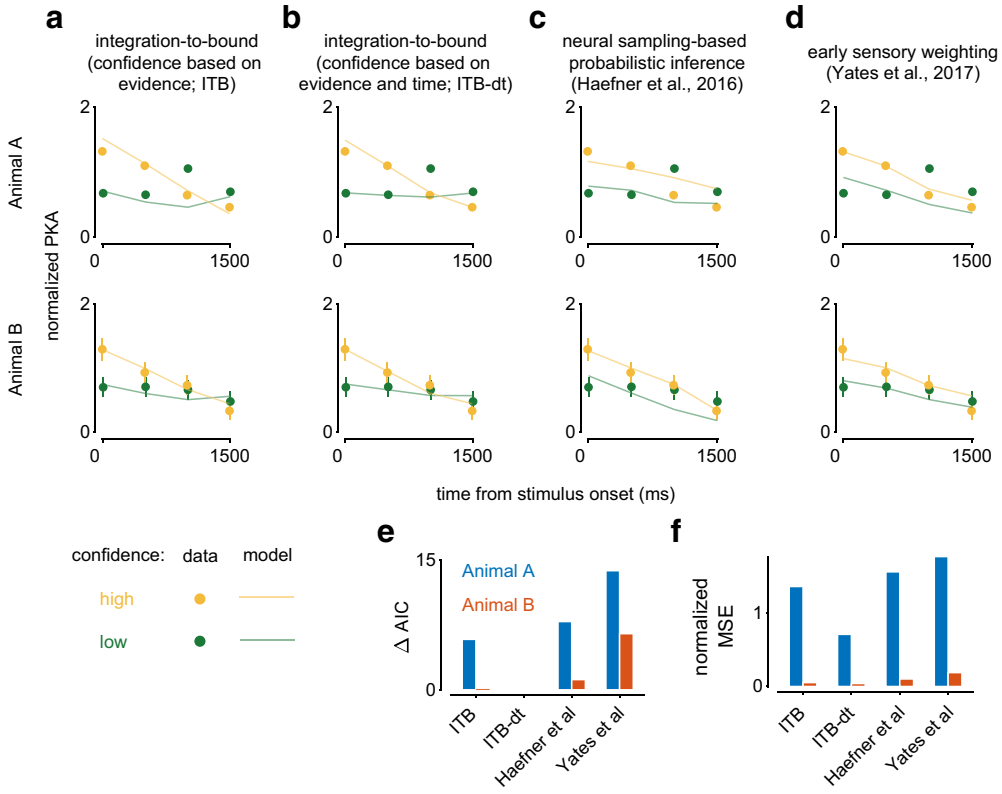

Figure 7. The animals' psychophysical weighting on low- and high-confidence trials is compared with model predictions. ***a–d***, Circles represent PKAs for high (yellow) and low (green) inferred confidence trials (median split) for Animal A (top row) and Animal B (bottom row), plotted as a function of time (A: 213 sessions; B: 40 sessions). To avoid confounding the pupil size modulation for available reward size with that for inferred decision confidence, the median split based on pupil size to assign trials to the high- or low-confidence bin was performed separately for small and large available reward trials. Error bars indicate SEM derived by resampling. ***a***, The integration-to-bound model in which trials were separated based on decision confidence defined as |decision variable| (ITB) provides a reasonably good fit to the animals' data, including the characteristic higher PKA for lower confidence trials in the last time bin, resulting in a crossover of PKAs. ***b***, The integration-to-bound model with decision confidence depended on both |decision variable| and the model's decision time on each trial yields improved fits, in particular for Animal A for which the crossover of PKA was more pronounced. Both the neural sampling-based probabilistic inference model for which decision confidence is defined by the Bayesian posterior probability (***c***) and the early sensory weighting model after Yates et al. (2017) based on a linear-nonlinear model reflecting the response dynamics (gain control) of sensory neurons (***d***) are unable to capture the crossover in PKA separated by confidence late in the trial resulting in worse fits. Model performance is compared using ΔAIC, the difference in AIC compared with the best performing model (ITB-dt) (***e***), and the normalized mean squared error (***f***).

size with signal strength for higher signal strengths in Animal B. Such a pattern is expected if decision confidence is informed not only by the strength of the sensory evidence, as described above, but also by decision time as observed in human observers (Kiani et al., 2014; see also Adler and Ma, 2017) for how increasing confidence ratings may actually be compatible with Bayesian confidence. Indeed, fits of the model by Kiani et al. (2014) correlated well with the data ($p < 10^{-4}$ and $p < 0.01$ for Animal A, and $p < 10^{-6}$ and $p < 0.01$ for Animal B in Fig. 5*c* and Fig. 5*d*, respectively; Spearman's rank correlation).

To explore when within the trial pupil size could be used to infer decision confidence, we systematically repeated the statistical analyses in Figures 3*c* and 5 when varying the time within the trial and the duration over which pupil size was averaged (Fig. 6). The results show that pupil size toward the end of the trial over a range of analysis windows could be used to infer decision confidence.

Because we used a white fixation marker, our results with pupil size measurements might in principle have been affected by the animals' fixation precision. To control for this potential confound, we therefore performed a number of control sessions in which, instead of a white fixation dot, we used a black fixation marker. If our results were mostly driven by differences in luminance resulting from differences in fixation precision across conditions, the modulation with our experimental covariates should reverse. However, our results were robust when, instead of a white fixation marker, we used a black fixation marker (Fig. 3*f–h*). Together, these analyses support our conclusion that mean pupil size at the end of the stimulus presentation can be used to infer the animals' decision confidence.

The animals' data separated by inferred decision confidence support the predictions of the integration-to-bound model

Having established the relationship between pupil size and decision confidence in our task, we now use it to test the confidence-related predictions of the integration-to-bound model using our data. To do so, we computed the animals' psychophysical kernels separately after categorizing high- or low-inferred decision confidence trials (median split based on the pupil size metric). For inferred high-confidence trials, we observed a decrease in PKA for both monkeys (Fig. 7*a–d*). In contrast, for inferred low-confidence trials, the PKA either stayed relatively constant throughout the trial (Monkey B, Fig. 7*a–d*, bottom row), or first increased and then decreased (Monkey A, Fig. 7*a–d*, top row). Furthermore, the PKA at the end of low-confidence trials was approximately equal (Monkey B) or higher (Monkey A) than the PKA for high-confidence trials. We then fit the two variants of the integration-to-bound model (compare Fig. 1) while allowing for

noise in our assignment of trials as high versus low confidence (to account for the imperfect relationship between pupil size and decision confidence) before computing the models' PKAs for high- and low-confidence trials (Fig. 7*a*,*b*). Importantly, the data for both monkeys best agree with the predictions of an integration-to-bound model when subjective confidence is based on both evidence and time (Kiani et al., 2014) (Fig. 7*b*,*e*,*f*) with the difference between the 2 animals explainable by slightly differing internal integration bounds (compare Fig. 1*i* and Fig. 1*j*), as well as different levels of noise to infer decision confidence (Table 1). Interestingly, the noise to infer decision confidence is lower for Animal A, which is plausible given this animal's more extensive learning of the task (compare Fig. 4).

We next wondered whether the data were also explainable by two alternative accounts of the early psychophysical weighting: (1) models with attractor dynamics resulting from recurrent feedback; or (2) a purely feedforward account that includes adaptation.

To test the first alternative account, we implemented a model (Haefner et al., 2016) in which the decrease of the PKA results from self-reinforcing feedback from decision neurons to sensory neurons. Because of its recurrent connectivity, this model exhibits attractor dynamics, in which early evidence is effectively weighted more strongly than evidence presented late in the trial. Other recurrent models of perceptual decision making, whether across cortical hierarchies (Wimmer et al., 2015), or proposing attractor dynamics within the decision area itself (Wang, 2002; Wong et al., 2007), share this attractor behavior. In these models, the behavior of the decision variable after stimulus onset can be described by a double-well energy landscape, where the minimum of each well corresponds to a choice attractor (compare Wimmer et al., 2015, their Fig. 2*d*, inset). As a result, the effect of early evidence on the decision variable will be amplified by the subsequent pull exerted by whatever attractor toward which the early evidence had pushed the decision variable. While this behavior resembles that of the integration-to-bound model, it differs in its predictions when separating trials according to confidence (Fig. 7*c*). Analogous to our fits of the integration-to-bound models, we included a noise parameter to allow for an imperfect assignment of trials to the high- or low-confidence group when fitting this model to the monkeys' data. These fits were worse than those for the integration-to-bound models (Fig. 7*c*,*e*,*f*). Specifically, we were unable to identify model parameters for which the kernel amplitude in low-confidence trials exceeded that for high-confidence trials at the end of the stimulus presentation (Fig. 8*a*). To convince ourselves that an attractor dynamic by itself is indeed unable to account for our data, we confirmed this finding for two idealized attractor models in which attractor strength and hence slope of the PKA were determined by a single parameter (similar to the integration-to-bound model; Fig. 8*b*,*c*). As for the neural sampling-based probabilistic inference model, varying this parameter did not yield kernels for which the kernel amplitude in low-confidence trials exceeded that for high-confidence trials at the end of the stimulus presentation. Indeed, in the absence of confidence noise, the only way to achieve a similar late-trial PKA for high and low confidence was to strengthen the attractor dynamics in one of the models to a degree that made the late-trial PKA close to zero, in contradiction to the data (Fig. 8*c*).

Finally, we tested the behavior of two versions of an early sensory weighting model after Yates et al. (2017, their Figs. 4*a*, 6*a*), in which the decrease in PKA results from adaptation of the sensory responses in a purely feedforward way. The model generates choices based on the integrated inputs of stimulus-selective sensory neurons, whose response decreases over the time of the stimulus presentation. Such decrease in response amplitude after response onset is typically observed for sensory neurons and may reflect a gain control mechanism or stimulus-dependent adaptation. As expected, we found a decreasing PKA across all trials. But like for the attractor-based models investigated above, and unlike for our data, the amplitude of the high-confidence PKA was consistently larger than

Table 1. Model parameters used in each figure[a]

Parameter	Value
Integration-to-bound model (Figs. 1, 9)	Range (0, 20)
Decision bound	
Integration-to-bound model (Fig. 7*a*,*b*)	
Decision bound	8.24 (Fig. 7*a*, Animal A)
	8.67 (Fig. 7*a*, Animal B)
	8.77 (Fig. 7*b*, Animal A)
	8.67 (Fig. 7*b*, Animal B)
Confidence noise (σ)	0.02 (Fig. 7*a*, Animal A)
	1.49 (Fig. 7*a*, Animal B)
	1.36 (Fig. 7*b*, Animal A)
	2.08 (Fig. 7*b*, Animal B)
Neural sampling-based probabilistic inference model (Fig. 7*c*)	
Trial duration	15 (Fig. 7*c*, Animal A) (a.u.)
	25 (Fig. 7*c*, Animal B) (a.u.)
Confidence noise (σ)	2.53 (Fig. 7*c*, Animal A)
	2.41 (Fig. 7*c*, Animal B)
Neural sampling-based probabilistic inference model (Fig. 7*c*, 8*a*)	
κ	2
λ	3
δ	0.08
n_x	256
n_g	64
n_s	20
Stimulus contrast	10
Evidence-accumulation toy model (Fig. 8*b*,*c*)	
α	Range (0.04, 0.4) (Fig. 8*b*)
	Range (0.01, 0.1) (Fig. 8*c*)
Trial duration	Range (20, 1000) (a.u.)
Early sensory weighting model (Fig. 7*d*)	
t_{max}	411 ms (Fig. 7*d*, Animal A)
	415 ms (Fig. 7*d*, Animal B)
τ	26.7 ms (Fig. 7*d*, Animal A)
	28.9 ms (Fig. 7*d*, Animal B)
a	0.493 (Fig. 7*d*, Animal A; for stimulus kernel)
	0.584 (Fig. 7*d*, Animal B; for stimulus kernel)
	0 (for contrast kernel)
b	−0.0135 (Fig. 7*d*, Animal A)
	−0.0160 (Fig. 7*d*, Animal B)
Weight of contrast kernel relative to stimulus kernel	1.08 (Fig. 7*d*, Animal A)
	0.78 (Fig. 7*d*, Animal B)
Confidence noise (σ)	2.77 (Fig. 7*d*, Animal A)
	2.98 (Fig. 7*d*, Animal B)
Early sensory weighting model (Fig. 8*d*)	
t_{max}	Range (100, 500) (ms)
τ	Range (10, 100) (ms)
a	Range (0, 1.37) (for stimulus kernel), 0 (for contrast kernel)
b	Range (−0.0375, 0)
Weight of contrast kernel relative to stimulus kernel	Range (0, 3)

[a]For parameter description, see Materials and Methods., a.u., Arbitrary units.

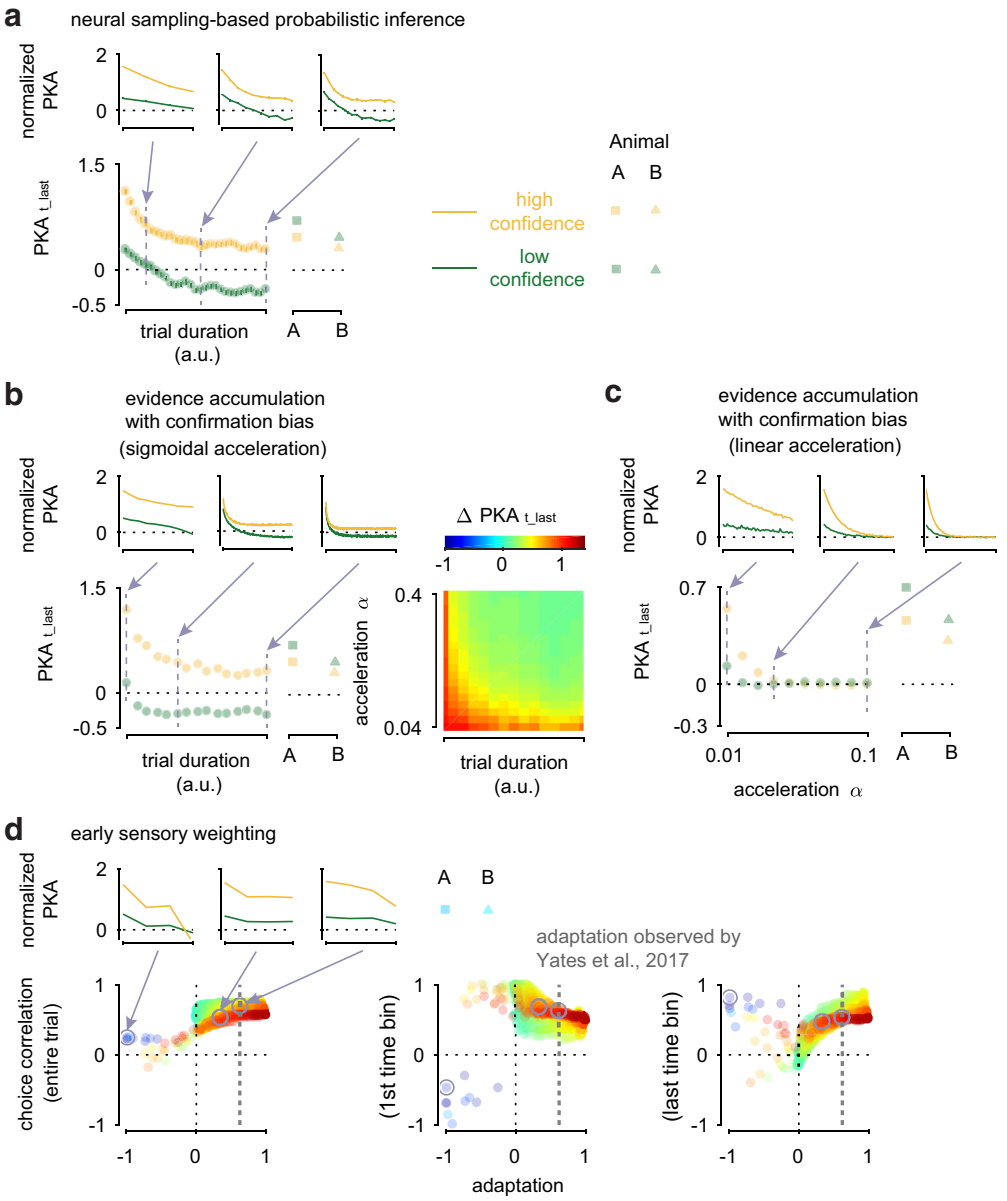

Figure 8. Exploring the parameter space of the models. Quantifying the PKA in the last time bin (PKA_{t_last}) for high- and low-confidence trials. Insets, PKAs separated by confidence (colors as in Figs. 1, 7) predicted by each model. Values for Animal A and B are included for comparison. ***a***, Exploring parameters of the neural sampling-based probabilistic inference model (Haefner et al., 2016). Model parameters were chosen such that the average PKA decreased. We then explored PKA_{t_last} when systematically increasing the trial duration. While systematically decreasing with trial duration, for high-confidence trials, $PKA_{t\_last,high\_confidence} > PKA_{t\_last,low\_confidence}$ across all parameters. ***b***, Simplified model of evidence accumulation with confirmation bias (sigmoidal acceleration; see Materials and Methods), mimicking the behavior of ***a*** or of a choice attractor (Wimmer et al., 2015) and a bimodal distribution of the decision variable late in the trial (double-well energy landscape). Similar to ***a***, $PKA_{t\_last,high\_confidence} > PKA_{t\_last,low\_confidence}$. Moreover, ΔPKA_{t_last} decreases with trial duration and with increasing the confirmation bias (parametrized by acceleration parameter α) but consistently remains positive, contrasting with the monkeys' data. ***c***, Simplified model of evidence accumulation with confirmation bias (linear acceleration; see Materials and Methods) but a consistently unimodal distribution of the decision variable, in contrast to Wimmer et al. (2015) and Wong et al. (2007). When increasing α PKA_{t_last} approaches 0 for both high- and low-confidence trials, in contradiction with the animals' data. ***d***, Exploring parameters of the early sensory weighting model after Yates et al. (2017). We systematically changed the relative weights and the width of the stimulus and contrast kernel (parameters a, b, t_{max}, τ), thereby varying the degree and time course of the adaptation. The level of adaptation was evaluated in response to the preferred stimulus and quantified as the response at the end of the stimulus presentation relative to the peak response. Negative values for adaptation correspond to adaptation below baseline. Vertical dashed line indicates the degree of adaptation observed by Yates et al. (2017) for MT neurons. Only simulations for which a decrease in the overall kernel amplitude over time is observed, and for which the PKA in high-confidence trials exceeds that for low-confidence trials in the first time bin were included. We plot ΔPKA_{t_last} (color code as defined in ***b***, right) as a function of the degree of adaptation (abscissa) and the neuron's correlation with the choice of the model (choice correlation, quantified as defined by Pitkow et al., 2015). Choice correlation was evaluated for the entire trial (left) and the first (middle) and last (right) time bin. We found that $\Delta PKA_{t\_last} < 0$ (blue data points) only for sensory responses that were otherwise inconsistent with empirical data (i.e., suppression of the sensory response below baseline or negative correlation with choice early during the trial; compare middle panel).

the low-confidence PKA (Fig. 7*d*). As for the previous model fits, we additionally included a noise parameter to allow for an imperfect assignment of trials into the high- and low-confidence groups. This pattern remained unchanged over a wide range of model parameters that yielded plausible sensory responses (compare Fig. 8*d*).

Together, these results indicate that, while each of these models could account for early psychophysical weighting, a decision

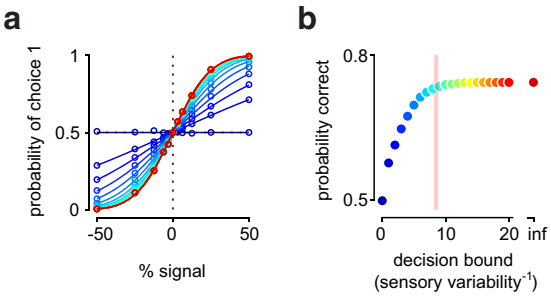

Figure 9. Exploring the cost of the decision bound on performance. ***a***, Model psychophysical performance is shown for integration-to-bound models with different decision bounds (color coded as depicted in ***b***). ***b***, Plotting the model performance across all trials as a function of the decision bound. Because correct answers are assigned arbitrarily on 0% signal trials, the maximal performance is <100% correct. Vertical bar represents the range of values of the decision bound for model fits to the animals' data in Fig. 7*a*, *b*. It shows that their decision bound is close to where performance asymptotes, and supports the view that the cost of the decision bound on performance is small.

bound was necessary to account for the monkeys' behavioral differences with inferred decision confidence.

Given the importance of a decision bound to account for the data, we explored the cost of a decision bound on performance in our task (Fig. 9). The psychophysical performance is shown for models with different decision bounds and best in the absence of a decision bound, as expected (Fig. 9*a*, red curve). The cost on performance (percent correct) resulting from the decision bound is depicted in Figure 9*b*. The vertical red bar marks the range of the animals' decision bounds obtained from the model fitting (compare Fig. 7*a*,*b*). The performance for this value has reached asymptotic values (exceeding 95% maximal performance), suggesting that the cost on performance for the animals is small (see Discussion).

Discussion

The frequently observed (Kiani et al., 2008; Neri and Levi, 2008; Nienborg and Cumming, 2009; Yates et al., 2017) early weighting of sensory evidence in perceptual decision making tasks has classically been explained to reflect an integration-to-bound decision process (Mazurek et al., 2003; Kiani et al., 2008). Here, we first derived decision confidence-specific predictions for this account. Second, to test these predictions, we devised a metric based on pupil size that allowed us to estimate 2 macaques' subjective decision confidence on individual trials without the use of a wagering paradigm. Finally, we compared our confidence-specific data with two alternative accounts of early weighting (attractor dynamics and response adaptation) and found that neither of those models could explain our data. This combined approach provided new insights into the animals' decision formation process. It revealed that the frequently observed (Kiani et al., 2008; Neri and Levi, 2008; Nienborg and Cumming, 2009; Yates et al., 2017) early weighting of the sensory evidence was largely restricted to high-confidence trials, approximately consistent with findings in humans (Zylberberg et al., 2012), and that the shape of the PKA confirmed our predictions based on the integration-to-bound model. Indeed, the match between data and model was best when we incorporated a recent proposal about how subjective confidence was not just based on the strength of the presented evidence, but also integration time (Kiani et al., 2014). Moreover, our data could not be fully explained by other computational accounts for early psychophysical weighting, such as sensory adaptation (Yates et al., 2017) or models of perceptual decision making with recurrent processing (Wong et al., 2007; Wimmer et al., 2015; Haefner et al., 2016). We note that our findings do not preclude the contribution of these alternative models. However, our results highlight that none of these accounts is sufficient to explain the data by itself and that a decision rule that implements an early stopping of the evidence integration process appears necessary.

Our analysis of pupil size showed that, even without the stabilizing effect of long ITIs, pupil size was reliably correlated with experimental covariates and could be used to infer the animal's decision confidence. The correlation of pupil size with decision confidence is similar to that in a recent psychophysical study in humans (Krishnamurthy et al., 2017) that queried decision confidence directly. As we did here, this study found a positive correlation between subjects' pupil size before they made their judgment and their reported decision confidence. Previous work inferring an animal's decision confidence typically relied on behavioral measurements, such as postdecision wagering (Kiani and Shadlen, 2009; Komura et al., 2013) and the time an animal is willing to wait for a reward (Lak et al., 2014), which increases the complexity of the behavioral paradigm and hence the required training of the animals. To our knowledge, the present study is the first to relate pupil size measurements in animals to decision confidence. Such a pupil size-based metric opens up studies of decision making in animals to include decision confidence without increasing the complexity of the behavioral paradigm.

In our task, the animals were rewarded on each trial directly after making their choice. Consistent with modulation of pupil-linked arousal due to reward expectation (Baruni et al., 2015; Varazzani et al., 2015), pupil size was progressively larger toward the end of the trial when the (known) available reward was large compared with when it was small (compare Fig. 3*b*). Such reward-based interpretation of the pupil size modulation associated with decision confidence may explain our findings here and those of Krishnamurthy et al. (2017), which contrasts with studies associating increases in pupil size with uncertainty (e.g., Satterthwaite et al., 2007; Nassar et al., 2012; Lempert et al., 2015; de Berker et al., 2016; Urai et al., 2017). Specifically, a recent study (Urai et al., 2017) observed the opposite relationship between inferred decision confidence and pupil size, measured after the subject's perceptual report: larger pupil size after the subject's report, and before receiving feedback, was associated with higher decision uncertainty. Access to information (e.g., whether or not a choice is correct) can be rewarding by itself (Behrens et al., 2007; Bromberg-Martin and Hikosaka, 2009). It may therefore be that, in Urai et al. (2017), the reward was such access to information (i.e., the feedback on each trial). When the confidence about the correct choice is low, the information is more valuable, hence resulting in the observed negative correlation with pupil size. Alternatively, this discrepancy may also reflect methodological differences, such as the time interval used for the analysis (before or after the choice was made) (but see also Lempert et al., 2015). More generally, these findings underscore the importance to consider a subject's motivational context when interpreting pupil size modulation.

Moreover, pupil size modulation by cognitive factors has been linked to a number of neural circuits mirroring the complexity of the signal. These include the locus coeruleus noradrenergic system (Aston-Jones and Cohen, 2005; Joshi et al., 2016), a brain-wide neuromodulatory system involved in arousal, the inferior and superior colliculi, which mediate a subject's orienting response to salient stimuli (Wang et al., 2012; Wang and Munoz, 2015), but the dopaminergic system has also been implicated

(Lak et al., 2017; Colizoli et al., 2018), and there is evidence for an association with cholinergic modulation (Polack et al., 2013; Reimer et al., 2016), which is also linked to attention.

The emergence of a reliable signature of decision confidence required that the animals performed the task well (compare Fig. 4). We propose two possible, not mutually exclusive, accounts for this. First, in line with the notion that the observed pupil size modulation linked to decision confidence is driven in part by reward expectation, it may reflect the animal's improved knowledge of the timing of the task and hence the anticipation of the reward. Second, it may reflect the fact that to engage the pupil-linked arousal circuitry a certain threshold of decision confidence needs to be exceeded. Such an interpretation would mean that, once the signature of decision confidence emerges, a higher level of decision confidence is reached at least on some trials.

Our animals' psychophysical behavior separated by inferred decision confidence was well described by a bounded accumulation decision process. These results imply that in a subset of trials sensory evidence was ignored after a certain level of decision confidence had been gained. We find that, in our task, across all difficulty levels, the loss in performance is small for the bounds required to explain our data (Fig. 9). Because the overall loss will differ between different experiments, it might explain some of the differences seen in the temporal profile of PKAs across studies (e.g., Kiani et al., 2008; Neri and Levi, 2008; Nienborg and Cumming, 2009; Wyart et al., 2012; Brunton et al., 2013; Drugowitsch et al., 2016; Yates et al., 2017).

References

Adler WT, Ma WJ (2017) Limitations of proposed signatures of Bayesian confidence. bioRxiv. Advance online publication. Retrieved from Nov. 13, 2017. doi:10.1101/218222.

Alnæs D, Sneve MH, Espeseth T, Endestad T, van de Pavert SH, Laeng B (2014) Pupil size signals mental effort deployed during multiple object tracking and predicts brain activity in the dorsal attention network and the locus coeruleus. J Vis 14:1. CrossRef Medline

Aston-Jones G, Cohen JD (2005) Adaptive gain and the role of the locus coeruleus-norepinephrine system in optimal performance. J Comp Neurol 493:99–110. CrossRef Medline

Baruni JK, Lau B, Salzman CD (2015) Reward expectation differentially modulates attentional behavior and activity in visual area V4. Nat Neurosci 18:1656–1663. CrossRef Medline

Behrens TE, Woolrich MW, Walton ME, Rushworth MF (2007) Learning the value of information in an uncertain world. Nat Neurosci 10:1214–1221. CrossRef Medline

Bradley MM, Miccoli L, Escrig MA, Lang PJ (2008) The pupil as a measure of emotional arousal and autonomic activation. Psychophysiology 45:602–607. CrossRef Medline

Brainard DH (1997) The psychophysics toolbox. Spat Vis 10:433–436. CrossRef Medline

Bromberg-Martin ES, Hikosaka O (2009) Midbrain dopamine neurons signal preference for advance information about upcoming rewards. Neuron 63:119–126. CrossRef Medline

Brunton BW, Botvinick MM, Brody CD (2013) Rats and humans can optimally accumulate evidence for decision making. Science 340:95–98. CrossRef Medline

Cicmil N, Cumming BG, Parker AJ, Krug K (2015) Reward modulates the effect of visual cortical microstimulation on perceptual decisions. Elife 4:e07832. CrossRef Medline

Clery S, Cumming BG, Nienborg H (2017) Decision related activity in macaque V2 for fine disparity discrimination is not compatible with optimal linear read-out. J Neurosci 37:715–725. CrossRef Medline

Colizoli O, de Gee JW, Urai A, Donner TH (2018) Task-evoked pupil responses reflect internal belief states. bioRxiv. Advance online publiaction. Retrieved from March 3, 2018. https://doi.org/10.1101/275776.

Cumming BG, Nienborg H (2016) Feedforward and feedback sources of choice probability in neural population responses. Curr Opin Neurobiol 37:126–132. CrossRef Medline

de Berker AO, Rutledge RB, Mathys C, Marshall L, Cross GF, Dolan RJ, Bestmann S (2016) Computations of uncertainty mediate acute stress responses in humans. Nat Commun 7:10996. CrossRef Medline

de Gee JW, Knapen T, Donner TH (2014) Decision related pupil dilation reflects upcoming choice and individual bias. Proc Natl Acad Sci U S A 111:E618–E625. CrossRef Medline

Drugowitsch J, Wyart V, Devauchelle AD, Koechlin E (2016) Computational precision of mental inference as critical source of human choice suboptimality. Neuron 92:1398–1411. CrossRef Medline

Ebitz RB, Platt ML (2015) Neuronal activity in primate dorsal anterior cingulate cortex signals task conflict and predicts adjustments in pupil-linked arousal. Neuron 85:628–640. CrossRef Medline

Haefner RM, Berkes P, Fiser J (2016) Perceptual decision making as probabilistic inference by neural sampling. Neuron 90:649–660. CrossRef Medline

Hangya B, Sanders JI, Kepecs A (2016) A mathematical framework for statistical decision confidence. Neural Comput 28:1840–1858. CrossRef Medline

Hansen RM, Fulton AB (1986) Pupillary changes during dark adaptation in human infants. Invest Ophthalmol Vis Sci 27:1726–1729. Medline

Hess EH, Polt JM (1964) Pupil size in relation to mental activity during simple problem-solving. Science 143:1190–1192. CrossRef Medline

Joshi S, Li Y, Kalwani RM, Gold JI (2016) Relationships between pupil diameter and neuronal activity in the locus coeruleus, colliculi, and cingulate cortex. Neuron 89:221–234. CrossRef Medline

Kahneman D, Beatty J (1966) Pupil diameter and load on memory. Science 154:1583–1585. CrossRef Medline

Kepecs A, Uchida N, Zariwala HA, Mainen ZF (2008) Neural correlates, computation and behavioural impact of decision confidence. Nature 455:227–231. CrossRef Medline

Kiani R, Shadlen MN (2009) Representation of confidence associated with a decision by neurons in the parietal cortex. Science 324:759–764. CrossRef Medline

Kiani R, Hanks TD, Shadlen MN (2008) Bounded integration in parietal cortex underlies decisions even when viewing duration is dictated by the environment. J Neurosci 28:3017–3029. CrossRef Medline

Kiani R, Corthell L, Shadlen MN (2014) Choice certainty is informed by both evidence and decision time. Neuron 84:1329–1342. CrossRef Medline

Kleiner M, Brainard DH, Pelli DG, Ingling A, Murray R, & Broussard C. (2007) What's new in Psychtoolbox-3? Perception 36:1–16.

Komura Y, Nikkuni A, Hirashima N, Uetake T, Miyamoto A (2013) Responses of pulvinar neurons reflect a subject's confidence in visual categorization. Nat Neurosci 16:749–755. CrossRef Medline

Krishnamurthy K, Nassar MR, Sarode S, Gold JI (2017) Arousal-related adjustments of perceptual biases optimize perception in dynamic environments. Nat Hum Behav 1:0107. CrossRef Medline

Lak A, Costa GM, Romberg E, Koulakov AA, Mainen ZF, Kepecs A (2014) Orbitofrontal cortex is required for optimal waiting based on decision confidence. Neuron 84:190–201. CrossRef Medline

Lak A, Nomoto K, Keramati M, Sakagami M, Kepecs A (2017) Midbrain dopamine neurons signal belief in choice accuracy during a perceptual decision. Curr Biol 27:821–832. CrossRef Medline

Lempert KM, Chen YL, Fleming SM (2015) Relating pupil dilation and metacognitive confidence during auditory decision making. PLoS One 10:e0126588. CrossRef Medline

Mazurek ME, Roitman JD, Ditterich J, Shadlen MN (2003) A role for neural integrators in perceptual decision making. Cereb Cortex 13:1257–1269. CrossRef Medline

Mitz AR, Chacko RV, Putnam PT, Rudebeck PH, Murray EA (2017) Using pupil size and heart rate to infer affective states during behavioral neurophysiology and neuropsychology experiments. J Neurosci Methods 279:1–12. CrossRef Medline

Nassar MR, Rumsey KM, Wilson RC, Parikh K, Heasly B, Gold JI (2012) Rational regulation of learning dynamics by pupil-linked arousal systems. Nat Neurosci 15:1040–1046. CrossRef Medline

Neri P, Levi D (2008) Temporal dynamics of directional selectivity in human vision. J Vis 8:22 1–11. CrossRef Medline

Neri P, Parker AJ, Blakemore C (1999) Probing the human stereoscopic system with reverse correlation. Nature 401:695–698. CrossRef Medline

Nienborg H, Cumming BG (2007) Psychophysically measured task strategy

for disparity discrimination is reflected in V2 neurons. Nat Neurosci 10: 1608–1614. CrossRef Medline

Nienborg H, Cumming BG (2009) Decision related activity in sensory neurons reflects more than a neuron's causal effect. Nature 459:89–92. CrossRef Medline

Pelli DG (1997) The VideoToolbox software for visual psychophysics: transforming numbers into movies. Spat Vis 10:437–442. CrossRef Medline

Pitkow X, Liu S, Angelaki DE, DeAngelis GC, Pouget A (2015) How can single sensory neurons predict behavior? Neuron 87:411–423. CrossRef Medline

Polack PO, Friedman J, Golshani P (2013) Cellular mechanisms of brain state-dependent gain modulation in visual cortex. Nat Neurosci 16:1331–1339. CrossRef Medline

Raposo D, Kaufman MT, Churchland AK (2014) A category-free neural population supports evolving demands during decision making. Nat Neurosci 17:1784–1792. CrossRef Medline

Reimer J, McGinley MJ, Liu Y, Rodenkirch C, Wang Q, McCormick DA, Tolias AS (2016) Pupil fluctuations track rapid changes in adrenergic and cholinergic activity in cortex. Nat Commun 7:13289. CrossRef Medline

Rudebeck PH, Putnam PT, Daniels TE, Yang T, Mitz AR, Rhodes SE, Murray EA (2014) A role for primate subgenual cingulate cortex in sustaining autonomic arousal. Proc Natl Acad Sci U S A 111:5391–5396. CrossRef Medline

Satterthwaite TD, Green L, Myerson J, Parker J, Ramaratnam M, Buckner RL (2007) Dissociable but inter-related systems of cognitive control and reward during decision making: evidence from pupillometry and event-related fMRI. Neuroimage 37:1017–1031. CrossRef Medline

Seillier L, Lorenz C, Kawaguchi K, Ott T, Nieder A, Pourriahi P, Nienborg H (2017) Serotonin decreases the gain of visual responses in awake macaque V1. J Neurosci 37:11390–11405. CrossRef Medline

Suzuki TW, Kunimatsu J, Tanaka M (2016) Correlation between pupil size and subjective passage of time in non-Human primates. J Neurosci 36: 11331–11337. CrossRef Medline

Urai AE, Braun A, Donner TH (2017) Pupil-linked arousal is driven by decision uncertainty and alters serial choice bias. Nat Commun 8:14637. CrossRef Medline

van den Berg R, Anandalingam K, Zylberberg A, Kiani R, Shadlen MN, Wolpert DM (2016) A common mechanism underlies changes of mind about decisions and confidence. Elife 5:e12192. CrossRef Medline

Varazzani C, San-Galli A, Gilardeau S, Bouret S (2015) Noradrenaline and dopamine neurons in the reward/effort trade-off: a direct electrophysiological comparison in behaving monkeys. J Neurosci 35:7866–7877. CrossRef Medline

Wang CA, Munoz DP (2015) A circuit for pupil orienting responses: implications for cognitive modulation of pupil size. Curr Opin Neurobiol 33: 134–140. CrossRef Medline

Wang CA, Boehnke SE, White BJ, Munoz DP (2012) Microstimulation of the monkey superior colliculus induces pupil dilation without evoking saccades. J Neurosci 32:3629–3636. CrossRef Medline

Wang XJ (2002) Probabilistic decision making by slow reverberation in cortical circuits. Neuron 36:955–968. CrossRef Medline

Wimmer K, Compte A, Roxin A, Peixoto D, Renart A, de la Rocha J (2015) Sensory integration dynamics in a hierarchical network explains choice probabilities in cortical area MT. Nat Commun 6:6177. CrossRef Medline

Wong KF, Huk AC, Shadlen MN, Wang XJ (2007) Neural circuit dynamics underlying accumulation of time-varying evidence during perceptual decision making. Front Comput Neurosci 1:6. CrossRef Medline

Wyart V, de Gardelle V, Scholl J, Summerfield C (2012) Rhythmic fluctuations in evidence accumulation during decision making in the human brain. Neuron 76:847–858. CrossRef Medline

Yates JL, Park IM, Katz LN, Pillow JW, Huk AC (2017) Functional dissection of signal and noise in MT and LIP during decision making. Nat Neurosci 20:1285–1292. CrossRef Medline

Zylberberg A, Barttfeld P, Sigman M (2012) The construction of confidence in a perceptual decision. Front Integr Neurosci 6:79. CrossRef Medline

Systems/Circuits

Serotonin Decreases the Gain of Visual Responses in Awake Macaque V1

Lenka Seillier,[1]* Corinna Lorenz,[1]* Katsuhisa Kawaguchi,[1] Torben Ott,[2] Andreas Nieder,[1,2] Paria Pourriahi,[1] and Hendrikje Nienborg[1]

[1]Werner Reichardt Centre for Integrative Neuroscience and [2]Department of Animal Physiology, Institute of Neurobiology, University of Tübingen, 72076 Tübingen, Germany

Serotonin, an important neuromodulator in the brain, is implicated in affective and cognitive functions. However, its role even for basic cortical processes is controversial. For example, in the mammalian primary visual cortex (V1), heterogenous serotonergic modulation has been observed in anesthetized animals. Here, we combined extracellular single-unit recordings with iontophoresis in awake animals. We examined the role of serotonin on well-defined tuning properties (orientation, spatial frequency, contrast, and size) in V1 of two male macaque monkeys. We find that in the awake macaque the modulatory effect of serotonin is surprisingly uniform: it causes a mainly multiplicative decrease of the visual responses and a slight increase in the stimulus-selective response latency. Moreover, serotonin neither systematically changes the selectivity or variability of the response, nor the interneuronal correlation unexplained by the stimulus ("noise-correlation"). The modulation by serotonin has qualitative similarities with that for a decrease in stimulus contrast, but differs quantitatively from decreasing contrast. It can be captured by a simple additive change to a threshold-linear spiking nonlinearity. Together, our results show that serotonin is well suited to control the response gain of neurons in V1 depending on the animal's behavioral or motivational context, complementing other known state-dependent gain-control mechanisms.

Key words: **awake macaque; extracellular recordings; gain modulation; iontophoresis; serotonin; striate cortex**

Significance Statement

Serotonin is an important neuromodulator in the brain and a major target for drugs used to treat psychiatric disorders. Nonetheless, surprisingly little is known about how it shapes information processing in sensory areas. Here we examined the serotonergic modulation of visual processing in the primary visual cortex of awake behaving macaque monkeys. We found that serotonin mainly decreased the gain of the visual responses, without systematically changing their selectivity, variability, or covariability. This identifies a simple computational function of serotonin for state-dependent sensory processing, depending on the animal's affective or motivational state.

Introduction

Perceptually guided behavior depends on context. Such context includes an animal's prior experience or knowledge of the environment and task, and its behavioral and motivational state (Harris and Thiele, 2011). The context dependence of perceptually driven behavior relies, in part, on the context-dependent neuromodulation of sensory processing (Hurley et al., 2004; Harris and Thiele, 2011). One mode of such neuromodulation involves subcortical nuclei that have widespread projections throughout the brain (Jacobs and Azmitia, 1992). These are ideally suited to modulate processing in extended networks according to changing behavioral–motivational conditions (Dayan, 2012).

One important neuromodulatory system is the serotonin system. Serotonin [5-hydroxytryptamine (5-HT)] in the brain has been implicated in a variety of affective, cognitive, and sensorimotor functions, but identifying an account of its computational role even for the intensely studied links to reward signaling has proved challenging (Ranade et al., 2014; Dayan and Huys, 2015). Similarly, the reported effects of serotonin on sensory processing have been heterogeneous (Waterhouse et al., 1990; Hurley et al., 2004; Petzold et al., 2009; Watakabe et al., 2009; Lottem et al.,

Received May 16, 2017; revised Sept. 9, 2017; accepted Sept. 12, 2017.

Author contributions: L.S. and H.N. designed research; L.S., K.K., P.P., and H.N. performed research; T.O. and A.N. contributed unpublished reagents/analytic tools; C.L., K.K., and H.N. analyzed data; L.S., C.L., and H.N. wrote the paper.

This work was supported by a Starting Independent Researcher grant to H.N. from the European Research Council (NEUROOPTOGEN), by funds from the Deutsche Forschungsgemeinschaft awarded to the Centre for Integrative Neuroscience (DFG EXC 307), and by a postdoctoral fellowship to L.S. from the Alexander von Humboldt Foundation.

*L.S. and C.L. contributed equally to this work.

Correspondence should be addressed to Hendrikje Nienborg at the above address. E-mail: hendrikje.nienborg@cin.uni-tuebingen.de.

DOI:10.1523/JNEUROSCI.1339-17.2017

2016) and a simple computational account remains elusive. For example, in the primary visual cortex (V1) of anesthetized animals' bidirectional modulation of the responses (Watakabe et al., 2009) and variable effects on receptive field properties have been observed (Waterhouse et al., 1990; Hurley et al., 2004; Bachatene et al., 2013). However, despite this multitude of effects on sensory processing, the serotonergic effects on perceptually driven behavior have been surprisingly uniform and consistent with a decreased perceptual response (Davis et al., 1980; Dugué et al., 2014). Potential reasons for these apparent differences are that cortical neuronal modulation in some studies was examined using receptor-selective rather than the endogenous ligand (Watakabe et al., 2009), and these studies were all performed using anesthetized animals. Under anesthesia, substantial fluctuations in brain state that affect responses in the primary sensory cortex have been observed (Ecker et al., 2014). Moreover, anesthesia, such as isofluorane, can directly influence the activity of serotonergic neurons (Johansen et al., 2015). It may therefore be that in awake animals, where the serotonergic system may be in a more controlled state, a less diverse modulation would be seen.

We therefore set out to characterize the modulatory effect of serotonin on sensory processing in the awake animal. To this end, we focused on the macaque V1. The macaque V1 receives extensive projections from the dorsal and medial raphe nuclei, the major source of serotonin in the brain. Serotonergic input projections are most pronounced in the input layers of V1 (de Lima et al., 1988). This pattern is approximately mirrored by the laminar profile of the expression of serotonin receptors in V1 (Watakabe et al., 2009). From a functional perspective, such a bias toward the input layers would be expected, for example, for a mechanism involved in adjusting the gain of the sensory input, as previously suggested (Hurley et al., 2004; Disney et al., 2007). Here, we leveraged the extensive knowledge of the spatiotemporal tuning properties in V1 to quantify the serotonergic modulation on visual processing in awake monkeys along several stimulus dimensions.

Serotonergic neurons are thought to convey a variety of signals on different time scales, as found, for example, for their phasic versus tonic response components (Ranade and Mainen, 2009; Cohen et al., 2015; Fonseca et al., 2015; Hayashi et al., 2015; Correia et al., 2017), versus long-term (days) effects of phasic activation (Correia et al., 2017). In this study we focused on time scales that are consistent with the tonic component of the response by iontophoretically applying serotonin in the minute range time scale.

We find that across the population of neurons in V1 and across different stimulus dimensions, the serotonergic modulation is surprisingly simple: serotonin predominantly decreases the gain of the visual responses, with little change to the tuning properties. A simple additive change to a threshold-linear spiking nonlinearity can account for the observed modulation. Gain modulation is an important computation to change response levels without affecting tuning (Atallah et al., 2012). It has been implicated in the modulation by cognitive states, such as attention (McAdams and Maunsell, 1999), and is subject to cholinergic modulation at the cortical input (Disney et al., 2007). Our results show that serotonin is well suited to control the response gain of neurons in V1, potentially complementing these known gain control mechanisms.

Materials and Methods

Animals. Two adult male rhesus monkeys (*Macaca mulatta*; M, 8 kg, 11 years old; K, 12 kg, 7 years old; housed in pairs) participated in the experiments. Using aseptic techniques, the monkeys were implanted with a titanium head-post and titanium chambers over the operculum of V1 under general anesthesia. All experimental procedures followed guidelines for animal experimentation and were approved by the local authorities, the Regierungspräsidium Tübingen, Germany.

Electrophysiological recordings and iontophoresis. We recorded extracellular single-unit activity in V1 while the animals performed a 2 s fixation task (fixation within 0.75° of a small 0.1° fixation dot on the center of the screen) for fluid rewards while we presented stimuli in the receptive field of the recorded unit. The positions of both eyes were recorded at 500 Hz using an infrared optical recording system (Eyelink 1000, SR Research). Experimental control and stimulus presentation was done using custom-written software in Matlab modified after Eastman and Huk (2012) using the psychophysics toolbox (Brainard, 1997; Pelli, 1997; Kleiner et al., 2007).

Recordings and iontophoresis were done using custom-made tungsten-in-glass electrodes flanked by two pipettes as described previously (Thiele et al., 2006; Jacob et al., 2013). This electrode pipette was mounted inside a guide tube and inserted transdurally without a dura-piercing guide tube using a custom-made electric microdrive. Iontophoretic application was controlled by an MVCS iontophoresis system (NPI Electronic). Neuronal signals were amplified, digitized, and filtered (250 Hz to 5 kHz) with the Ripple Grapevine System (Ripple). Spike sorting was performed offline using the Plexon Offline Sorter. Spike clusters were computed based on a variety of features, including principal components, energy, peak, trough, and spike amplitude. Single-unit clusters were identified using the features that provided the best separation. Spike isolation was quantified by computing the isolation distance and L ratio (Schmitzer-Torbert et al., 2005). For 763 of 780 (98%) included experimental blocks, the isolation distance was >20 and the L ratio <0.1. For the remaining 17 (2%) experimental blocks that did not meet these criteria, unit isolation was verified by visual inspection. One barrel of the electrode pipette was filled with serotonin hydrochloride (Sigma-Aldrich; 10 mM in double-distilled water; pH 3.5–3.8), the other with pH-matched saline (NaCl; 0.9%). The electrodes typically had impedances between 0.3 and 1.6 MΩ (measured at 1 kHz) and tip sizes of 10–15 μm. The ejection current ranged between 2 and 50 nA (median, 10 nA) for serotonin and between 5 and 20 nA (median, 11 nA) for saline. To better quantify effects on the neuronal tuning properties, we aimed for relatively small modulatory effects. The values of the ejection currents used were therefore toward the lower end of the range of values previously used in the macaque cortex (Williams et al., 2002). In a subset of experiments, we used different ejection currents across blocks to examine the dose dependence of the effect (Fig. 1*B*). We typically used ejection currents less than or equal to the value for which the serotonergic modulation seemed to asymptote (Fig. 1*B*), which we observed at values between 20 and 30 nA, and this limited range of currents may have contributed to the homogeneity of our results. The retention current was −8 nA to prevent leakage from the drug barrels during the control conditions. The pipette resistance ranged from 10 to 150 MΩ, as was used previously (Ott et al., 2014). To minimize long-term effects of serotonin (Maya Vetencourt et al., 2008; Correia et al., 2017), we avoided recording from nearby locations in V1 in consecutive recording sessions.

For each unit we initially quantified the center of the receptive field from receptive-field profiles along a horizontal and vertical axis as described previously (Nienborg et al., 2004) by presenting an elongated rectangular grating (height, 3–5°; width, 0.2°) at different horizontal or vertical positions across the receptive field and its immediate surroundings. Subsequent stimuli were centered on the receptive field at a median eccentricity of 3.6° (range, 1.6 to 6.4°). We initially measured neuronal tuning curves without applying serotonin or saline to establish the baseline using the retention current. We then started to apply serotonin or saline using the ejection current in blocks and then remeasured a tuning curve during the application (note that our analyses of the time course of the response modulation across trials averaged over all experiments did not reveal a systematic difference between the baseline, saline control, and serotonin experiments, suggesting that the lead time of the serotonin application of several seconds was, on average, sufficient). Following the application of the drug, we remeasured the tuning in subsequent blocks using the retention current to obtain the recovery of the response if it was possible to maintain unit isolation. Thus, if it was possible to maintain unit

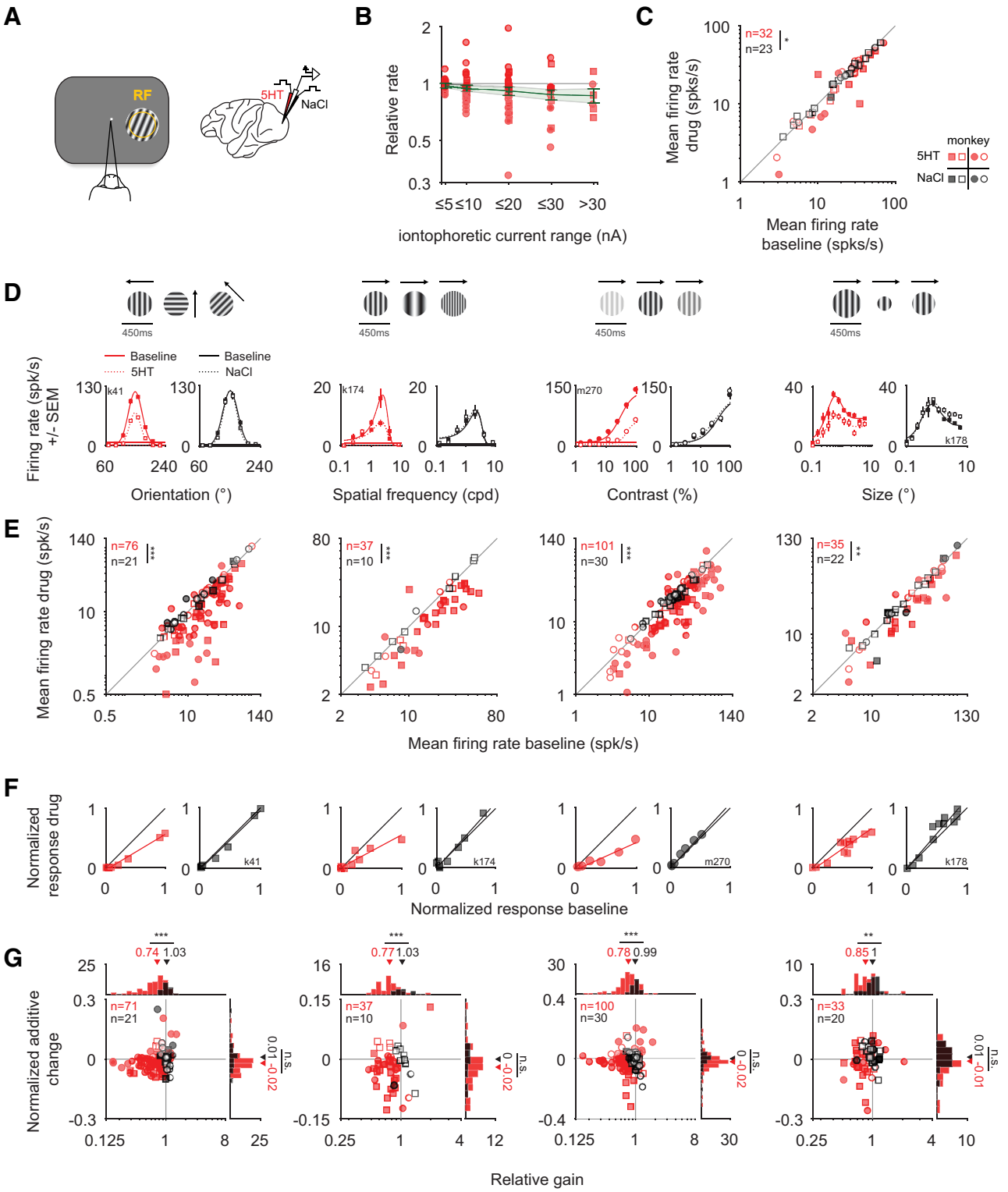

Figure 1. Iontophoretic application of serotonin leads mainly to a gain decrease. ***A***, Schematic of the experimental setup. While the monkey performed a fixation task, grating stimuli were presented in a neuron's receptive field (RF) during blockwise iontophoretic application of serotonin (5HT; red) or pH-matched saline (NaCl; black). ***B***, Dose dependence of the serotonergic modulation. The relative firing rate is plotted as a function of the applied iontophoretic current range of 90 serotonin blocks from $n = 36$ units. Each unit is shown only once per bin. The green line represents the geometric mean ± SEM. ***C***, Modulation for the subset of units for which the duration of unit isolation allowed for a full sequence of baseline, drug application, and recovery. Note that for four units for which tuning for >1 stimulus dimensions was tested, only the first comparison is included. The median of the average firing rate decreased from 27 to 24 spikes/s for serotonin but not for saline application [20 spikes/s for the baseline, 21spikes/s for saline application; $p = 0.03$, $n_{5\text{-HT}} = 32$, $n_{\text{NaCl}} = 23$; 11 of 32 (34%) of units were significantly suppressed, 2 of 32 (6%) were significantly enhanced for serotonin application; 1 of 23 (4%) was significantly enhanced and suppressed for saline application]. ***D–G***, Orientation, spatial frequency, contrast, and size were varied in blocks, and results are shown in the first, second, third, and last column, respectively. ***D***, Example tuning curves are shown for the baseline condition (red solid line, filled symbols) or the application of serotonin (dotted line, open symbols). Note the decrease in the response amplitude during the application of serotonin. No such change is observed during control experiments when saline is applied instead: the open and closed black symbols largely overlap. ***E***, The mean firing rate (average across the tuning curves as in ***D***, including the blank response) for the baseline condition is compared with that for application of serotonin (red) or saline (black). Note the systematic decrease of the response for serotonin but not for the application (*Figure legend continues.*)

isolation and keep the monkey working, each block of drug application was followed by ≥1 block of recovery before the next application of the drug. Full recovery was evaluated by observation during recording but verified statistically off-line: the responses to each stimulus parameter were *z*-scored to remove the stimulus-driven variability of the response, and the *z* scores for the baseline and recovery block were then required to be statistically indistinguishable ($p > 0.05$, Wilcoxon rank-sum test). The median time to achieve full recovery [possible for $n = 90$ serotonin experiments for which the inclusion criteria (see below) were met; this value includes multiple experiments per unit, e.g., for our dose–response measurements; Fig. 1*B*] after the serotonin application was 32 s (range, 15 to 1171 s). Note that these values reflect the upper bound of the times to full recovery since we occasionally inserted wait times of variable duration after the serotonin application experiment to ensure full recovery while keeping the animal motivated to perform additional trials afterward.

Stimuli. Visual stimuli were back-projected on a screen using DLP LED Propixx projector (1920 × 1080 pixels resolution; 30 cd/m^2 mean luminance; linearized gray values; run at 100 Hz/eye, combined with an active circular polarizer, DepthQ, run at 200 Hz) at a distance of 98 cm in front of the animals. The animals viewed the screen through passive circular polarizing filters monocularly or binocularly. Visual stimuli were generated in Matlab (Mathworks) using the Psychophysics toolbox (Brainard, 1997; Pelli, 1997; Kleiner et al., 2007).

Stimuli were circular drifting sinusoidal luminance gratings centered on and slightly exceeding a neuron's receptive field and presented for 450 ms (temporal frequency typically 7 Hz) binocularly or monocularly to the preferred eye. For each experimental block, either the direction (16 equally spaced values), the spatial frequency [eight logarithmically spaced values from 0.125 to 16 cycles per degree (cpd)], the contrast (typically seven logarithmically spaced values from 1.56 to 100%), or the size (typically 12 logarithmically spaced values from 0.3 to 8°) of the grating was pseudorandomly varied, randomly interleaved by blank stimuli, with all other parameters constant at approximately the preferred value for each unit. Within each experimental block each stimulus was typically presented 8–10 times.

For the subspace reverse correlation, we briefly flashed sinusoidal luminance gratings (flash duration typically 10 ms; 100% contrast; preferred spatial frequency; presented binocularly or monocularly to the preferred eye) that randomly varied in orientation (eight equally spaced values) and spatial phase (equally spaced values), randomly interleaved by blank stimuli (also 10 ms duration, presented with equal probability as each orientation).

Data analysis. All analyses were done in Matlab (Mathworks). For experiments using drifting gratings, we computed the mean firing rate during the 450 ms stimulus presentation. To obtain orientation tuning curves, we averaged the responses for directions 180° apart. Tuning curves were computed as the mean firing rate as a function of orientation, spatial frequency, contrast, and size, respectively, and fit with standard descriptive functions.

Orientation tuning curves were fit with Gaussian functions for which all parameters were constrained to values >0. To avoid an overestimation of the amplitude resulting from placing the preferred orientation between two sparsely measured values, we further restricted the amplitude to be smaller than twice the peak value of the tuning curve.

Spatial frequency tuning curves were also fit with Gaussian functions, either in linear or logarithmic units, whichever resulted in better fits.

Contrast tuning curves were fit with the Naka–Rushton function (Albrecht and Hamilton, 1982): $R(c) = R_{\max} c^n/(c_{50}^n + c^n) + R_{\text{offset}}$, where c is the stimulus contrast, c_{50} is the semisaturation contrast, and n is the exponent influencing the shape of the curve. All parameters were restricted to values >0, and additionally $R_{\max} + R_{\text{offset}}$ could not exceed the peak response of the tuning curve to ensure that fits reached saturation within the contrast range of 0 to 100%. For the model comparison in Figure 6, we first fit the Naka–Rushton function to the baseline condition. In a second step, to account for the serotonin-induced modulation of the response, we allowed one parameter of this fit to the baseline to change: $R_{\max}$ for the response-gain model, or c_{50} for the contrast-gain model (Williford and Maunsell, 2006).

Size tuning curves were fit with a ratio-of-Gaussians function (Cavanaugh et al., 2002). All parameters had to be positive, and the width of the center Gaussian had to be less than or equal to that of the surround Gaussian function. The preferred size was defined as the smallest size that evoked 98% of the maximal response based on the fitted data (Nienborg et al., 2013). The suppression index was computed as the difference between the neuron's maximum response and the response to the maximum size, divided by the maximum response. Goodness of fit was quantified as variance explained and all fits had to explain ≥70% of the variance.

For a subset of units we also measured temporal frequency tuning with stimulus presentations of 2 s each. We used these longer stimulus presentations to quantify the selectivity to spatial phase for each unit as the $f1/f0$ ratio (Skottun et al., 1991) measured at the preferred temporal frequency of that unit, where $f1$ corresponds to the amplitude of response modulation at the stimulus temporal frequency and $f0$ to the mean firing rate. For these analyses, eye movements within the fixation window were not factored out, which may have contributed to the modest phase selectivity across the population.

Orientation selectivity was quantified using the circular variance (Ringach et al., 2002). Direction selectivity was computed as a simple contrast metric $(r_\theta - r_{\theta-180})/(r_\theta + r_{\theta-180})$, where $r_{\theta \text{ and } \theta-180}$ correspond to the response at the neuron's preferred direction θ and that at 180° away from preferred, respectively.

Receptive field size was quantified as the mean of the equivalent widths (w; Bracewell, 1986) in both the vertical and horizontal directions: If A is the area under the horizontal or vertical receptive field profile, and h is the peak response of the receptive field profile, then $w = A/h$. The median equivalent width was 0.56° (range, 0.25 to 1.34°).

To evaluate significant response modulation during the serotonin or saline condition, we *z*-transformed the mean response for each stimulus condition and compared the *z* scores across all stimuli between the serotonin or saline condition and the baseline condition using Wilcoxon rank-sum test (two-sided, 5% significance threshold).

For the experiments with flashed gratings, we quantified the tuning curves using reverse correlation subspace analysis (Ringach et al., 1997). We smoothed the stimulus-triggered spike-density function (SDF) using a 4 ms boxcar. The SDFs were used to compute the mean number of spikes elicited by each frame to yield "orientation subspace maps," analogous to an approach described previously in the disparity domain (Nienborg and Cumming, 2009). SEs were estimated based on bootstrapping (1000 resamples). To estimate the dynamics of the orientation-selective component of the response, we first computed the SD across the SDFs for each orientation. Response latencies were defined as the first point in time after frame onset for which the SD exceeded the half-height between the baseline variability and peak deviation (Lee et al., 2007). The baseline variability was computed as the average of the first 20 ms after frame onset. For inclusion of latency estimates, the orientation-selective response component had to exceed four times the baseline variability. Additionally, latencies were restricted to 25–100 ms after frame onset. To

←

(*Figure legend continued.*) of saline. The size of the change in firing rate induced by serotonin or saline, respectively, differs statistically (for orientation: $p < 10^{-5}$; for spatial frequency: $p < 10^{-3}$; for contrast: $p < 10^{-3}$; for size: $p = 0.001$; all Wilcoxon ranked-sum tests). ***F***, To quantify the size of the additive and multiplicative component of the change in the response (normalized to the peak response in the baseline condition), we performed linear (type II) regression on the tuning curves [baseline condition plotted on the abscissa against application of serotonin (red) or saline (black) on the ordinate]. The slope reflects the multiplicative change (relative gain) and the intercept the additive change. ***G***, For each cell, we compared the relative gain and the normalized additive change (normalized by the peak response in the baseline condition). Note that for all stimulus dimensions, the relative gain after applying serotonin is significantly smaller than in the control condition (for orientation: $p < 10^{-5}$, $n = 71$ for serotonin; $n = 21$ for saline; for spatial frequency: $p < 10^{-3}$; $n = 37$ for serotonin; $n = 10$ for saline; for contrast: $p < 10^{-4}$; $n = 100$ for serotonin; $n = 30$ for saline; for size: $p = 0.003$; $n = 33$ for serotonin; $n = 20$ for saline; all Wilcoxon ranked-sum tests). Circles and squares correspond to data from monkey M and K, respectively. Filled symbols represent units with significant mean response modulation ($p < 0.05$, Wilcoxon ranked-sum test). *: <0.05; **: <0.005; ***: $<5*10^{-4}$

ensure that changes in latency could not be explained by differences in the response variability between conditions, we estimated the dependence of the latency estimate on baseline variability by randomly subsampling the data in the baseline condition and computing latency for the subsampled data. The change in latency was then predicted from the change in baseline variability using linear regression, and the actually measured latency was corrected by the predicted change (see Fig. 5*D*). For comparison, we also quantified response latency using maximum likelihood estimation to identify the critical change point of the dynamics of the response (Friedman and Priebe, 1998). This approach assumes one Poisson process for the baseline response and one for the stimulus-evoked component of the response, and we required significantly different Poisson processes for inclusion. This analysis yielded similar results.

Analysis of fixational eye movements. To examine potential effects on fixational eye movements, we explored the fixation precision as well as the amplitude and frequency of microsaccades. Microsaccades within the fixation window were identified as defined previously (Nienborg and Cumming, 2006, 2014; Clery et al., 2017). Fixation precision was defined by Cherici et al. (2012) as the area around the mean gaze position that encompassed the 75th percentile of the gaze positions.

Noise correlations. Stimulus-independent covariability ["noise correlations," (Cohen and Kohn, 2011)] was calculated between the single-unit activity and the simultaneously measured multiunit activity recorded from the same electrode. Note that since this approach overestimates the absolute value of noise correlation (Ecker et al., 2010), we only explored the changes in noise correlation with serotonin, not the absolute value. To reduce the effect of slow fluctuations on nonstationarities (Ecker et al., 2014; Goris et al., 2014; Rabinowitz et al., 2015) resulting from the onset of the serotonin application, we removed the initial 20 stimulus presentations of each experimental block for this analysis. Responses for each stimulus condition were first *z*-scored, and noise correlations computed as the Pearson correlation coefficient of the *z* scores for single-unit and multiunit activity across all trials. Noise correlations have typically been found to depend on the neuronal spike rate (Cohen and Kohn, 2011). We estimated this dependence in our dataset for the baseline condition by linear regression and corrected the noise correlation by that predicted from the change in firing rate.

Fano factor. For each stimulus condition, we computed the Fano factor as the ratio between the variance and the mean response for each stimulus for each experimental block, excluding the initial 20 stimulus presentations to reduce variability from potential nonstationarities due to onset of serotonin. The average of the Fano factors for each stimulus was then calculated as the Fano factor for that unit.

Membrane potential-based model. The responses of the membrane potential-based model were explored for the stimulus used for orientation subspace mapping described earlier. The membrane potential was orientation selective and the selectivity described by a Gaussian function [amplitude, 20 mV; similar to empirically observed values (Priebe and Ferster, 2008)]. The width of the Gaussian function describing the orientation selectivity of the membrane potential (SD ranged from 10 to 40°) was chosen such that the bandwidth of the orientation subspace maps was within the range of those of the neuronal data in the baseline condition. The time-varying stimulus (a sequence of oriented gratings each flashed for 10 ms) induced fluctuations in membrane potential $V_m(t)$ that were convolved by a temporal kernel that consisted of a Gaussian temporal filter (chosen to be within the range of the neuronal data: SD, 6 ms; mean, 57 ms after stimulus onset to account for the lag of the response). Spike rates [$k(t)$] were derived from the following threshold-linear function:

$$k(t) = \begin{cases} c \cdot (V_m(t) - V_{thresh}) & if\ V_m(t) > V_{thresh} \\ 0 & otherwise \end{cases}$$

where $V_m(t)$ denotes the membrane potential at time t, V_{thresh} is the spiking threshold, and c is a scalar value set to 15, approximating the value previously obtained for the cat striate cortex (Carandini, 2004). The spiking rate was converted to Poisson spike events, which were analyzed like the neuronal data.

The serotonergic modulation was imitated by a subtractive shift in the membrane potential (equivalent to changing V_{thresh}). We explored shifts over a range of 1 to 8 mV, similar to empirically observed changes in membrane potential in response to serotonin (Ko et al., 2016). We adjusted the number of stimulus repetitions to obtain a comparable level of baseline variability for the baseline and serotonin condition.

Inclusion criteria. For each unit, we required a minimum response to the neuron's preferred stimulus of 10 spikes/s, a minimum of four presentations per stimulus condition (except for the noise correlation and Fano factor analysis, where ≥8 presentations per stimulus condition were required), and that the neuron showed selectivity for the respective stimulus dimension (orientation, spatial frequency, contrast, size; evaluated by an ANOVA at a significance threshold of $p < 0.01$). To be included in the comparison of additive and multiplicative changes (Figs. 1, 2, 5), the type-II regression had to account for ≥70% of the variance.

Results

Two macaque monkeys performed a standard fixation task while we recorded the activity of single units in their V1 during block-wise iontophoretic application of serotonin (Fig. 1*A*). We examined the effect of serotonin on the visual responses to drifting gratings that varied systematically in orientation, spatial frequency, contrast, or size, and to briefly flashed gratings of varying orientation (see Materials and Methods). We recorded a total of 265 single units in macaque V1 (118 from monkey M, and 147 from monkey K). To be included for further analysis, we required a minimum response to the neuron's preferred stimulus of 10 spikes/s, ≥4 presentations per stimulus condition, and that the neuron showed selectivity for the respective stimulus dimension as evaluated by an ANOVA at a significance threshold of $p < 0.01$. These criteria were passed by 229 units (108 for monkey M; 121 for monkey K). Of these, 206 (100 for monkey M; 106 for monkey K) were recorded with serotonin application and 65 (39 for monkey M; 26 for monkey K) with pH-matched saline (NaCl) application as control experiments (thus, in a subset of 42 units, we were able to measure responses for both serotonin and saline application in consecutive blocks; moreover, whenever possible, experiments along several stimulus dimensions were done on the same unit in consecutive blocks).

Serotonin predominantly decreases the responses in V1 by multiplicative changes of the tuning curves

The most salient consequence of the serotonin application was a substantial decrease in the visual responses. This effect was evident for the tuning curves for orientation, spatial frequency, contrast, and size, respectively, in four example neurons (Fig. 1*D*, red symbols). We found that these response changes could not be explained by the iontophoretic current application: control experiments with pH-matched saline (NaCl) did not result in such modulation of the neuronal responses (Fig. 1*D*, black symbols). Indeed, across the population, the mean firing rate in response to gratings of different orientations decreased for the serotonin condition (the median decrease was from 18 to 10 spikes/s) but not for the saline application (median values, 14 and 15 spikes/s, respectively), and the changes differed significantly between conditions [Fig. 1*E*; $p < 10^{-5}$, $n_{\text{5-HT}} = 76$, $n_{\text{NaCl}} = 21$; monkey M: $p < 10^{-3}$, $n_{\text{5-HT}} = 45$, $n_{\text{NaCl}} = 11$; monkey K: $p < 10^{-3}$, $n_{\text{5-HT}} = 31$, $n_{\text{NaCl}} = 10$; significant modulation for serotonin: 51 of 76 units (67%) were suppressed; 4 of 76 units (5%) were enhanced; significant modulation for saline: 4 of 21 units (19%) were suppressed; 3 of 21 units (14%) were enhanced]. These results were similar for gratings of varying spatial frequency, contrast, and size (Fig. 1*E*). For spatial frequency, the median average firing rate for serotonin decreased from 15 to 12 spikes/s and remained constant at 11 spikes/s for saline application [$p < 10^{-3}$, $n_{\text{5-HT}} = 37$, $n_{\text{NaCl}} = 10$; monkey M: $p = 0.41$, $n_{\text{5-HT}} = 11$, $n_{\text{NaCl}} = 2$; monkey

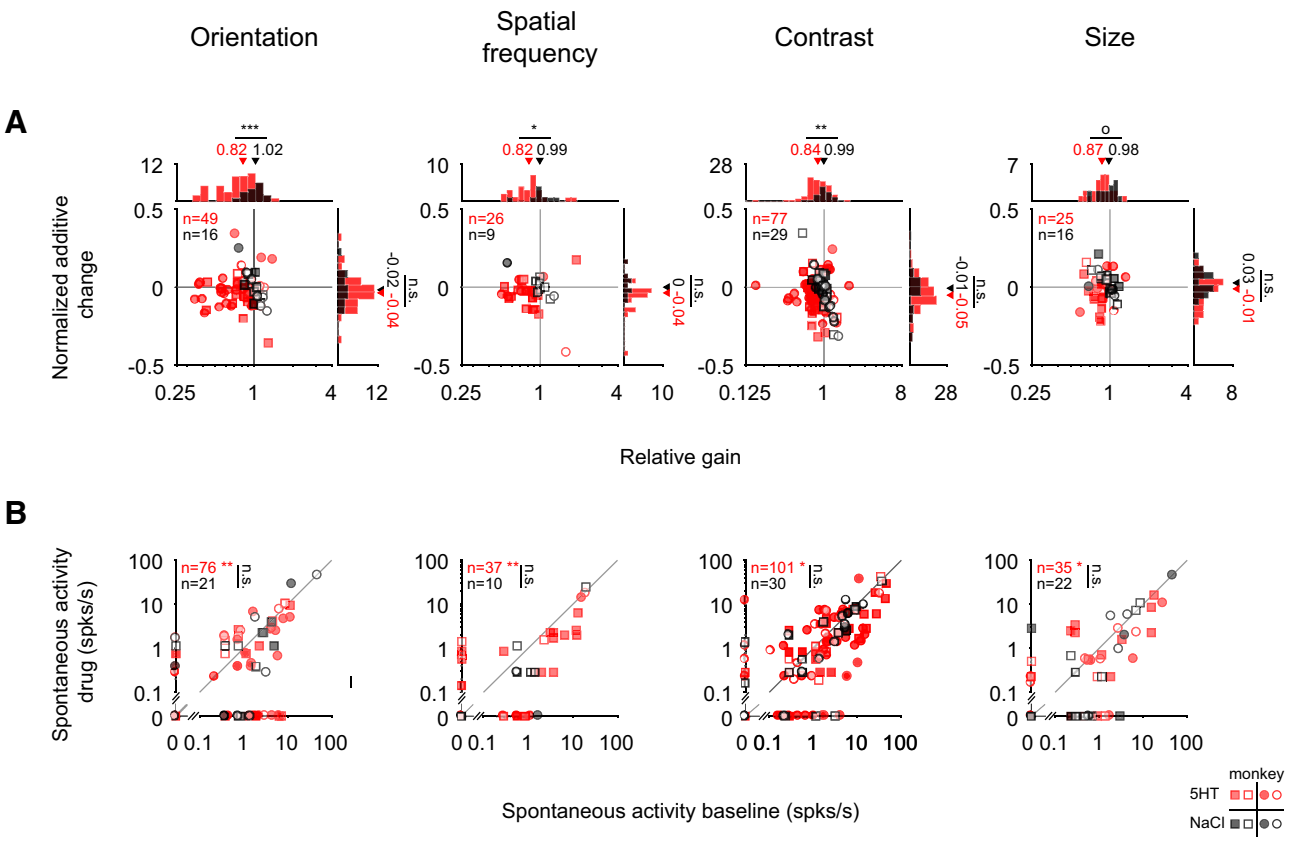

Figure 2. The gain decrease with serotonin does not merely reflect the iceberg effect. Symbols are the same as in Figure 1. Note that filled symbols reflect units with significant response modulation based on the full tuning curves as in Figure 1*E*. ***A***, Comparing the gain and additive changes to the tuning curves as in Figure 1*G* but after restricting the datapoints to those whose responses were >0 spikes/s to explore the serotonergic modulation independent of the iceberg effect. In this reduced dataset, we also observe a significant gain decrease (relative gain for orientation: 0.82 for serotonin and 1.02 for saline, $p < 10^{-3}$, $n_{5\text{-HT}} = 49$, $n_{\text{NaCl}} = 16$; for spatial frequency: 0.82 for serotonin and 0.99 for saline, $p = 0.016$, $n_{5\text{-HT}} = 26$, $n_{\text{NaCl}} = 9$; for contrast: 0.84 for serotonin, 0.99 for saline, $p = 0.003$, $n_{5\text{-HT}} = 77$, $n_{\text{NaCl}} = 29$; for size: 0.87 for serotonin, 0.98 for saline, $p = 0.075$, $n_{5\text{-HT}} = 25$, $n_{\text{NaCl}} = 16$). ***B***, The application of serotonin mainly resulted in a decrease of the blank response (blank interleaved in orientation ($p_{5\text{-HT}} = 0.005$, $n_{5\text{-HT}} = 76$; $p_{\text{NaCl}} = 0.35$, $n_{\text{NaCl}} = 21$), spatial frequency ($p_{5\text{-HT}} = 0.001$, $n_{5\text{-HT}} = 37$; $p_{\text{NaCl}} = 0.58$, $n_{\text{NaCl}} = 10$), contrast ($p_{5\text{-HT}} = 0.02$, $n_{5\text{-HT}} = 101$; $p_{\text{NaCl}} = 0.09$, $n_{\text{NaCl}} = 30$), or size ($p_{5\text{-HT}} = 0.03$, $n_{5\text{-HT}} = 35$, $p_{\text{NaCl}} = 0.50$, $p_{\text{NaCl}} = 22$) experiment (all Wilcoxon paired signed-rank tests).

K: $p = 0.001$, $n_{5\text{-HT}} = 26$, $n_{\text{NaCl}} = 8$; significant modulation for serotonin: 24 of 37 units (65%) were suppressed, 2 of 37 units (5%) were enhanced; significant modulation for saline: 1 of 10 units (10%) was suppressed]. For contrast tuning, the median firing rate decreased from 26 to 19 spikes/s for serotonin [the respective values for saline application were 23 and 22 spikes/s; $p < 10^{-3}$, $n_{5\text{-HT}} = 101$, $n_{\text{NaCl}} = 30$; monkey M: $p = 0.04$, $n_{5\text{-HT}} = 66$, $n_{\text{NaCl}} = 15$; monkey K: $p = 0.004$, $n_{5\text{-HT}} = 35$, $n_{\text{NaCl}} = 15$; significant modulation for serotonin: 58 of 101 units (57%) were suppressed, 8 of 101 (8%) units were enhanced; significant modulation for saline: 4 of 30 (13%) were suppressed]. Similarly, the mean firing rate decreased for the size tuning curves [29 to 25 spikes/s for serotonin; constant at 18 spikes/s for saline, $p = 0.001$, $n_{5\text{-HT}} = 35$, $n_{\text{NaCl}} = 22$; monkey M: $p = 0.65$, $n_{5\text{-HT}} = 14$, $n_{\text{NaCl}} = 6$; monkey K: $p < 10^{-4}$, $n_{5\text{-HT}} = 21$, $n_{\text{NaCl}} = 16$; all Wilcoxon rank-sum tests; significant modulation for serotonin: 19 of 35 (54%) were suppressed, 5 of 35 (14%) were enhanced; significant modulation for saline: 2 of 22 (9%) were suppressed, 5 of 22 (23%) were enhanced].

In a subset of experiments, unit isolation was maintained and the animal worked for sufficiently long for a full sequence of baseline, drug application, and recovery. The results for this subset of experiments are shown in Figure 1*C* (same format as Fig. 1*E*), also supporting the significant decrease in firing when serotonin was applied. The proportion of units for which full, statistically defined (see Materials and Methods), recovery was achieved was relatively small mainly because of sessions in which the monkeys were not motivated to continue to work or the unit isolation was lost. However, this relatively small proportion does not affect the interpretation of the main results of this paper, which relies on a comparison of the serotonergic modulation with that for pH-matched saline, and this comparison was robust when restricting the data to the subset of units with full recovery and saline control experiments (Fig. 1*C*). To additionally verify that a lack of recovery for some serotonin experiments did not impact the saline control experiments, we also performed two additional analyses. First, we compared the serotonergic modulation with that for saline for units for which only one substance (either serotonin or saline) per unit was applied. Second, we compared the serotonergic modulation for units with full recovery with the subset of the same dataset for which we also applied saline. For both analyses, we found a significant difference between the modulation for serotonin and that for saline (comparison across units: $p < 10^{-7}$, $n_{5\text{-HT}} = 53$, $n_{\text{NaCl}} = 23$ and comparison for units with full recovery: $p = 0.04$, $n_{5\text{-HT}} = 32$, $n_{\text{NaCl}} = 11$, respectively; note that for each unit only the first experiment per condition was included; Wilcoxon rank-sum tests). Moreover, our analysis of the responses to the interleaved blank stimuli revealed that the change in firing was not limited to the stimulus-driven response, but also observed in response to the blank stimuli (Fig. 2*B*).

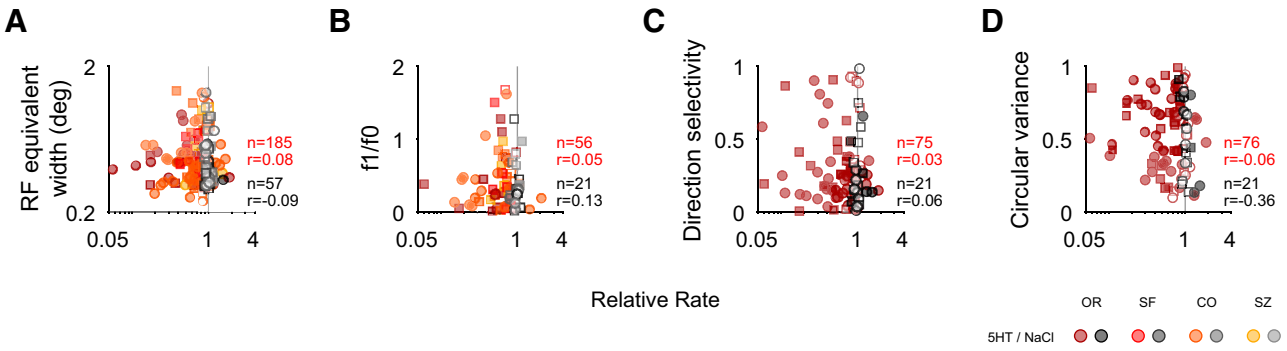

Figure 3. Probing the serotonergic modulation as a function of receptive field (RF) size and phase, direction, and orientation selectivity. ***A–D***, Symbols are the same as in Figure 1. Shading represents the type of experiment for which the modulation by drug application [serotonin (5HT) or saline (NaCl)] was quantified. The modulation was quantified as the relative rate based on the average firing rates across the tuning curve (compare Fig. 1*E*) for the drug condition (compare Fig. 1*E*, ordinate), divided by that for the baseline condition (compare Fig. 1*E*, abscissa). Neither RF size, quantified as equivalent width (***A***); phase selectivity, quantified as f1/f0 (***B***); direction selectivity (***C***); nor orientation selectivity, quantified as circular variance (***D***), were correlated with the modulation by serotonin or saline. Note that low values for circular variance reflect strong orientation selectivity (all Spearman's rank correlation).

For the example tuning curves (Fig. 1*D*) serotonin seems to primarily scale down the tuning curve, indicative of a gain decrease (multiplicative effect). We then quantified across the population whether the effect of serotonin was primarily additive or multiplicative. To do so, we compared the tuning curves with and without serotonin application, fit by type-II regression (Fig. 1*F*). The slope and intercept of the regression line reflect the multiplicative (relative gain) and additive change. When comparing these values for each unit across the population, we found that the changes in the tuning curve were primarily accounted for by a gain decrease for each type of tuning curve. For orientation tuning curves, the median gain decreased to 74% after serotonin application, in contrast to saline (median relative gain for saline: 103%; $p < 10^{-5}$, $n_{5\text{-HT}} = 71$, $n_{\text{NaCl}} = 21$; monkey M: $p < 0.01$, $n_{5\text{-HT}} = 43$, $n_{\text{NaCl}} = 11$; monkey K: $p < 10^{-4}$, $n_{5\text{-HT}} = 28$, $n_{\text{NaCl}} = 10$; Fig. 1*G*). Similarly, for spatial frequency, the gain reduced on average to 77% for serotonin (median relative gain for saline: 103%; $p < 10^{-3}$, $n_{5\text{-HT}} = 37$, $n_{\text{NaCl}} = 10$; monkey M: $p = 0.23$, $n_{5\text{-HT}} = 11$, $n_{\text{NaCl}} = 2$; monkey K: $p < 10^{-3}$, $n_{5\text{-HT}} = 26$, $n_{\text{NaCl}} = 8$). For contrast tuning, the gain decreased on average to 78% for serotonin (for saline the median relative gain was 99%; $p < 10^{-4}$, $n_{5\text{-HT}} = 100$, $n_{\text{NaCl}} = 30$; monkey M: $p < 0.01$, $n_{5\text{-HT}} = 66$, $n_{\text{NaCl}} = 15$; monkey K: $p < 10^{-4}$, $n_{5\text{-HT}} = 34$, $n_{\text{NaCl}} = 15$). As for the other stimulus dimensions, the median gain for size tuning was a decrease (to 85%) for serotonin while for saline the median relative gain was unchanged at 100% ($p = 0.003$, $n_{5\text{-HT}} = 33$, $n_{\text{NaCl}} = 20$; monkey M: $p = 0.78$, $n_{5\text{-HT}} = 13$, $n_{\text{NaCl}} = 5$; monkey K: $p < 10^{-3}$, $n_{5\text{-HT}} = 20$, $n_{\text{NaCl}} = 15$; all comparisons Wilcoxon rank-sum tests). The normalized additive suppressive effect differed significantly from 0 for the serotonin but not for the saline conditions for orientation, spatial frequency, and contrast (for orientation: −0.02 for serotonin, $p < 10^{-3}$, $n = 76$; 0.01 for saline, $p = 0.96$, $n = 21$; for spatial frequency: median normalized additive change for serotonin was −0.02, $p < 0.01$, $n = 37$; change for saline was 0.00, $p = 0.56$, $n = 10$; for contrast the median normalized additive change for serotonin was −0.02, $p < 10^{-3}$, $n = 100$ and 0.00 for saline, $p = 0.45$, $n = 30$; for size: the corresponding changes were −0.01 for serotonin, $p = 0.62$, $n = 33$, and 0.01 for saline, $p = 0.26$, $n = 20$; Wilcoxon signed-rank test) but given the variability in the control condition, the additive suppression for serotonin did not significantly exceed that for the control condition (for orientation: $p = 0.12$, $n_{5\text{-HT}} = 71$, $n_{\text{NaCl}} = 21$; for spatial frequency: $p = 0.29$, $n_{5\text{-HT}} = 37$, $n_{\text{NaCl}} = 10$; for contrast: $p = 0.21$, $n_{5\text{-HT}} = 100$, $n_{\text{NaCl}} = 30$; for size: $p = 0.20$, $n_{5\text{-HT}} = 33$, $n_{\text{NaCl}} = 20$; Wilcoxon rank-sum test). Moreover, the absence of an additive suppressive effect seemed to at least partially result from the "iceberg effect" (Carandini and Ferster, 2000): as a consequence of the spiking nonlinearity, spike rates are restricted to values >0 such that subtractive changes are limited by the minimum response of the tuning curve. In support of this, we found a significant correlation between the size of the normalized additive change and the minimum response of the tuning curve for the baseline condition ($r = -0.41$, $p < 10^{-8}$, $n_{5\text{-HT}} = 198$; Spearman's rank correlation; for this comparison we combined data for different stimulus dimensions but included only one data point per unit; data not shown). To verify that the observed gain decrease was not merely a consequence of the iceberg effect, we repeated the regression analysis after removing all data for which the responses were 0. In the subset of units for which the regression fits to the reduced dataset met the inclusion criteria (see Materials and Methods), we also found a significant gain decrease (Fig. 2*A*). Together, the additive and multiplicative changes provided an excellent fit to the data. Indeed, this simple linear model accounted for 90% of the variance (averaged across all regression fits for serotonin in Fig. 1*G*; note that the quality of the fits was similar for the saline controls: 92%). These results suggest that a simple linear transformation, predominantly multiplicative, can account for the serotonergic modulation of visual responses along several visual dimensions.

Given that serotonin receptors are differentially expressed across layers and on different cell types in the macaque V1 (Watakabe et al., 2009) the overall homogeneity of the effect is surprising. We therefore wondered whether the serotonergic modulation was systematically related to parameters that have been reported to vary to a certain degree with layer, such as receptive field size, orientation, direction, and spatial-phase selectivity (Ringach et al., 2002; Gur et al., 2005). To test this, we compared each of these parameters with the strength of serotonergic modulation (Fig. 3). Our analyses revealed no correlation of the serotonergic modulation with these parameters ($r = 0.08$, $p = 0.28$, $n = 185$ for equivalent width; $r = 0.05$, $p = 0.72$, $n = 56$ for *f*1/*f*0 ratio; $r = 0.03$, $p = 0.77$, $n = 75$ for direction tuning index; $r = -0.06$, $p = 0.62$, $n = 76$ for circular variance; Spearman's rank correlation with serotonergic modulation ratio for each). Moreover, we did not observe a systematic difference in the serotonergic modulation for narrow spiking compared with broad spiking (defined by a spike waveform width of <200 or ≥200 μs, respectively) units ($p = 0.49$; $n = 206$; Wilcoxon rank-sum test). Together,

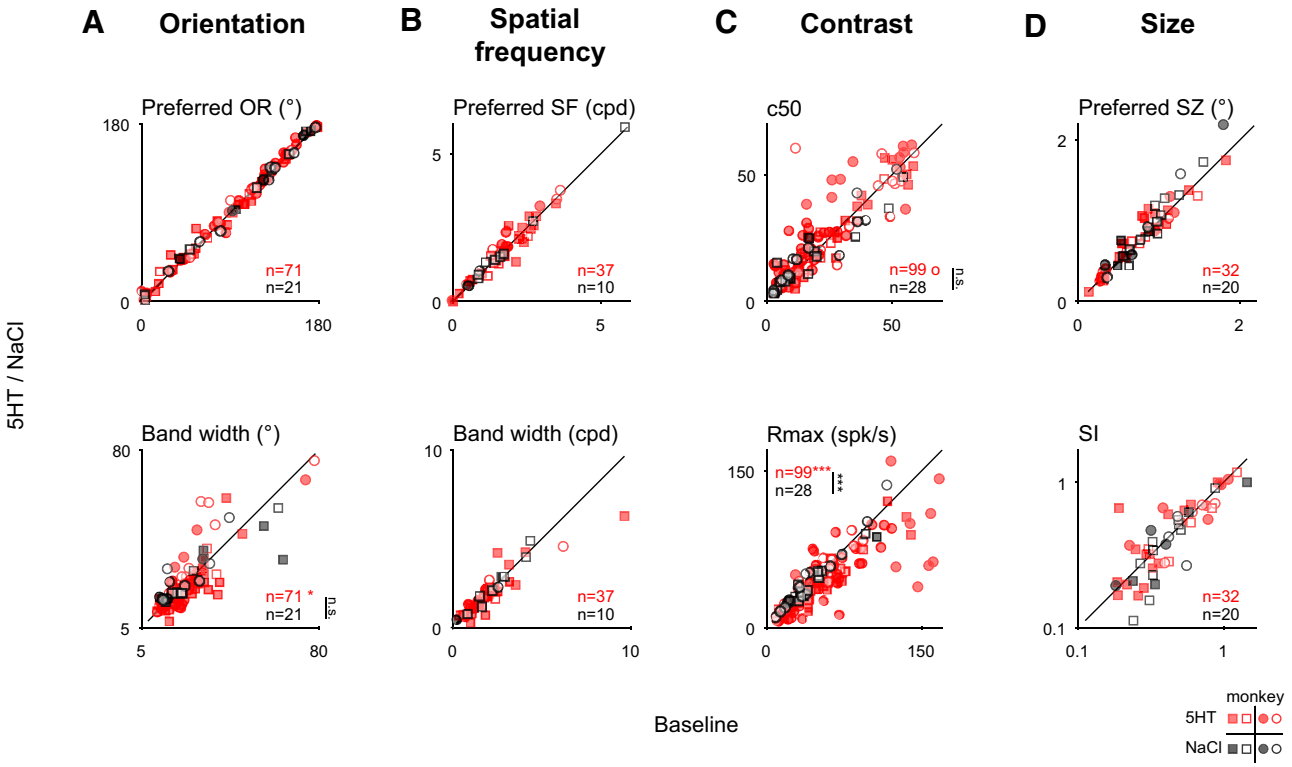

Figure 4. Serotonin does not systematically change the neuronal selectivity. Filled symbols reflect units with significant response modulation based on the full tuning curves as in Figure 1*E*. ***A–D***, The neuronal tuning curves for orientation (***A***), spatial frequency (***B***), contrast (***C***), and size (***D***) were fit with descriptive functions (see Materials and Methods) to quantify changes in selectivity. Symbols are the same as in Figure 1. ***A***, For orientation tuning, we compared the mean (preferred orientation, top) and the SD (orientation tuning width, bottom) of Gaussian fits. There was no significant change for either parameter that exceeded changes observed for saline (preferred orientation: $p = 0.29$, $n = 71$ for serotonin; $p = 0.66$, $n = 21$ for saline; bandwidth: $p = 0.05$, $n = 71$ for serotonin; $p = 0.93$, $n = 21$ for saline; $p = 0.24$ for the Wilcoxon ranked-sum test). ***B***, For the spatial frequency tuning curves, neither the mean (preferred spatial frequency, top) nor the SD (bandwidth, bottom) of the fitted Gaussians differed significantly (mean: $p = 0.50$, $n = 37$ for serotonin; $p = 0.92$, $n = 10$ for saline; SD: $p = 0.11$, $n = 37$ for serotonin; $p = 0.85$, $n = 10$ for saline). ***C***, For the contrast tuning, the contrast at half-maximum showed a nonsignificant trend toward higher values (top; C_{50}; $p = 0.06$, $n = 99$ for serotonin; $p = 1.0$, $n = 28$ for saline). The maximum response (R_{max}, bottom) decreased significantly for serotonin, as expected for a gain decrease. Indeed, the change in the maximum response differed significantly between the serotonin and the saline conditions ($p < 10^{-4}$, $n = 99$ for serotonin, $n = 28$ for saline; Wilcoxon ranked-sum test). ***D***, For size tuning, we found no significant difference in the preferred size (top; $p = 0.70$, $n = 32$ for serotonin; $p = 0.09$, $n = 20$ for saline) or surround index (bottom; $p = 0.54$, $n = 32$ for serotonin; $p = 0.30$, $n = 20$ for saline). All paired comparisons used the Wilcoxon paired signed-rank test.

these analyses suggest that the observed serotonergic modulation was not restricted to a particular cell type or layer.

Serotonin leaves visual tuning properties largely unchanged

We next wondered whether the serotonin application additionally resulted in a systematic modulation of the visual encoding properties along one of the visual stimulus dimensions we explored. To this end we fit descriptive functions (see Materials and Methods) to the tuning curves and examined the effect of serotonin parametrized by these fits. For orientation tuning, the serotonergic modulation changed neither the preferred orientation (Fig. 4*A*, top; $p = 0.29$, $n_{5\text{-HT}} = 71$; monkey M: $p = 0.34$, $n_{5\text{-HT}} = 41$; monkey K: $p = 0.63$, $n_{5\text{-HT}} = 30$) nor the orientation bandwidth (Fig. 4*A*, bottom; $p = 0.05$, $n_{5\text{-HT}} = 71$; monkey M: $p = 0.18$, $n_{5\text{-HT}} = 41$; monkey K: $p = 0.23$, $n_{5\text{-HT}} = 30$; Wilcoxon paired sign-rank tests; note that the slight decrease in bandwidth did not significantly differ from the saline condition, $p = 0.24$, $n_{\text{NaCl}} = 21$). Similarly, serotonin did not alter the preferred spatial frequency (Fig. 4*B*, top; $p = 0.50$, $n_{5\text{-HT}} = 37$; monkey M: $p = 0.32$, $n_{5\text{-HT}} = 11$; monkey K: $p = 0.12$, $n_{5\text{-HT}} = 26$) or spatial frequency bandwidth of the recorded neurons (Fig. 4*B*, bottom; $p = 0.11$, $n_{5\text{-HT}} = 37$; monkey M: $p = 0.97$, $n_{5\text{-HT}} = 11$; monkey K: $p = 0.11$, $n_{5\text{-HT}} = 26$; Wilcoxon paired sign-rank tests). However, the amplitude of the fits was significantly reduced for both orientation ($p < 10^{-4}$, $n_{5\text{-HT}} = 71$, $n_{\text{NaCl}} = 21$; monkey M: $p < 0.01$, $n_{5\text{-HT}} = 41$, $n_{\text{NaCl}} = 11$; monkey K: $p < 0.01$, $n_{5\text{-HT}} = 30$, $n_{\text{NaCl}} = 10$) and spatial frequency ($p < 0.01$, $n_{5\text{-HT}} = 37$, $n_{\text{NaCl}} = 10$; monkey M: $p = 0.41$, $n_{5\text{-HT}} = 11$, $n_{\text{NaCl}} = 2$; monkey K: $p < 0.01$, $n_{5\text{-HT}} = 26$, $n_{\text{NaCl}} = 8$; all Wilcoxon sign-rank tests), as expected given the observed reduction in gain. Also as expected from the reduction in gain, we observed a significant reduction in R_{max} for contrast tuning (Fig. 4*C*, bottom; $p < 10^{-4}$, $n_{5\text{-HT}} = 99$, $n_{\text{NaCl}} = 28$; monkey M: $p < 0.01$, $n_{5\text{-HT}} = 66$, $n_{\text{NaCl}} = 14$; monkey K: $p < 10^{-3}$, $n_{5\text{-HT}} = 33$, $n_{\text{NaCl}} = 14$; Wilcoxon sign-rank test). Conversely, the sensitivity for changes in contrast (i.e., the steepness of the tuning curve parametrized by the exponent n in the Naka–Rushton function; see Materials and Methods), did not change ($p = 0.15$, $n = 99$; monkey M: $p = 0.43$, $n = 66$; monkey K: $p = 0.19$, $n = 33$; Wilcoxon paired sign-rank test; data not shown). Interestingly, we also found that the contrast that yielded half the maximum response (c_{50}) was slightly increased. We note that this trend did not reach statistical significance in the population and was only significant in one of the animals ($p = 0.06$, $n_{5\text{-HT}} = 99$; monkey M: $p = 0.01$, $n_{5\text{-HT}} = 66$; monkey K: $p = 0.56$, $n_{5\text{-HT}} = 33$). Nonetheless, this trend raises the question whether serotonin engages a similar mechanism as contrast gain control, which we will address in more detail below.

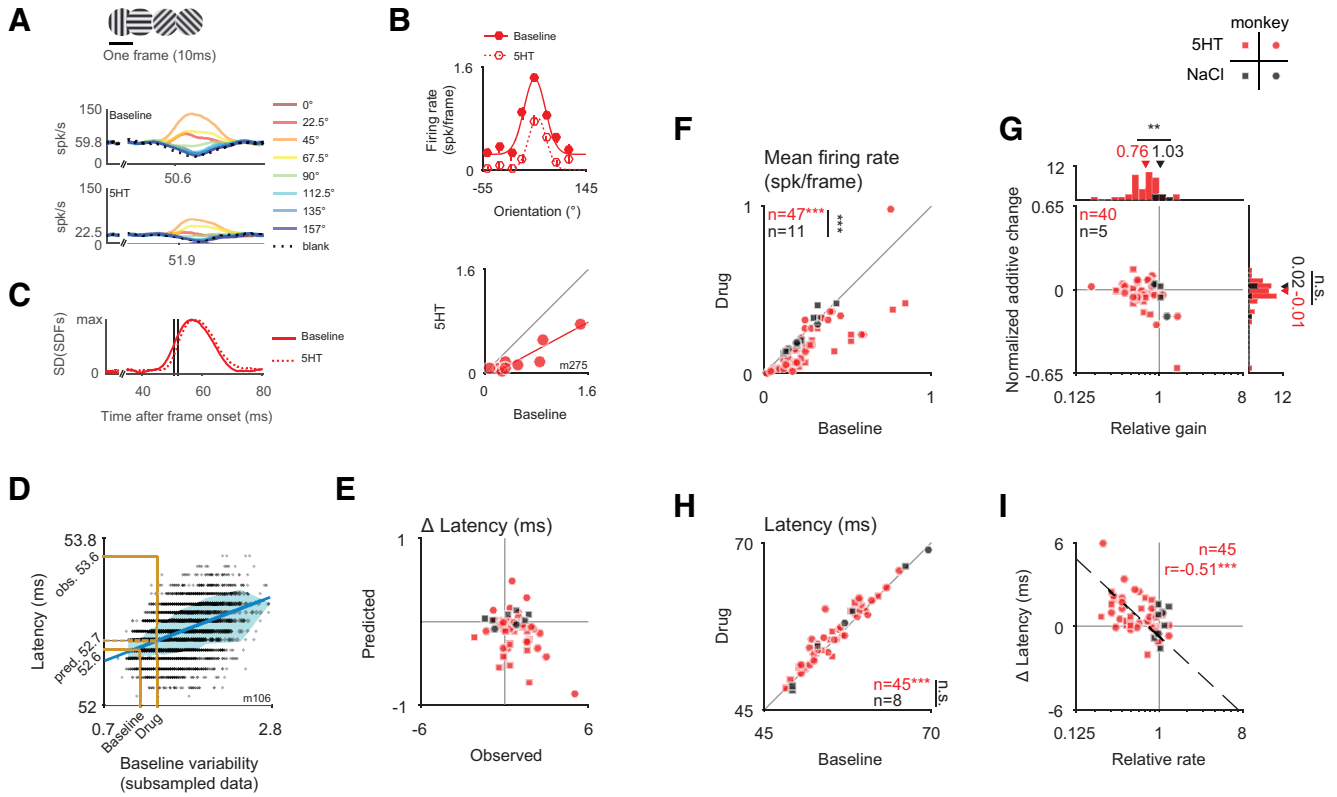

Figure 5. A slight modulation of the response dynamics by serotonin. Symbols are the same as in Figure 1. ***A***, SDFs separated by orientation for one example neuron without (top) and with (bottom) application of serotonin obtained for random sequences of briefly (10 ms) flashed gratings of different orientations. ***B***, The serotonergic application for this unit resulted in both a modest subtractive change and a divisive change of the tuning curve. ***C***, To quantify the dynamics of the response, we computed the SD across the SDFs for each orientation. These SDs are superimposed for the baseline (solid) and serotonin condition. Latency was defined as the time to the half-maximum response. Note the slight increase in latency for the serotonin condition. ***D***, In control analyses, we subsampled the data of the baseline condition to quantify changes in latency estimates due to changes in baseline variability. ***E***, The predicted changes in latency from changes in baseline variability cannot account for the observed latency changes. Note the different scales of abscissa and ordinate. ***F***, The mean firing rate for the orientation subspace stimulus decreases significantly with the application of serotonin (red, $p < 10^{-6}$, $n = 47$), but not for the saline (black, $p = 0.70$, $n = 11$). The change in mean firing with the iontophoretic application differs significantly between both conditions ($p < 10^{-4}$, $n = 47$ for serotonin, $n = 11$ for saline, Wilcoxon rank-sum test). ***G***, The gain of the tuning curves decreases substantially more for the serotonin than for the saline condition ($p = 0.006$, $n = 40$ for serotonin, $n = 5$ for saline) while the subtractive change does not differ across conditions ($p = 0.99$, both Wilcoxon rank-sum test). ***H***, The response latency increases slightly for serotonin ($p < 10^{-3}$, $n = 45$) but not for the saline condition ($p = 0.55$, $n = 8$). Note that due to the small sample for saline, this difference in modulation across conditions does not reach significance ($p = 0.38$). ***I***, The serotonin-induced changes in latency and mean firing rate are correlated ($r = -0.51$, $p < 10^{-3}$, $n = 45$, Spearman's rank correlation).

Finally, we examined whether serotonin had a systematic effect on receptive field size, as suggested by previous work in anesthetized rats (Waterhouse et al., 1990). To address this question, we first compared the stimulus size for which the visual response was maximal ("preferred size") with and without application of serotonin. In contrast to the previous suggestion, we found no systematic change in the preferred size of the neurons (Fig. 4*D*, top; $p = 0.70$, $n_{5\text{-HT}} = 32$; monkey M: $p = 0.41$, $n_{5\text{-HT}} = 12$; monkey K: $p = 0.30$, $n_{5\text{-HT}} = 20$; Wilcoxon paired sign-rank tests). To explore the effect of center surround interactions, we also examined the degree to which the visual responses to large stimuli decreased the visual stimuli compared with stimuli of a neuron's preferred size ("suppression index"). Similar to the results for preferred size, we found no significant effect of serotonin on the neurons' surround suppression quantified by the suppression index (Fig. 4*D*, bottom; $p = 0.54$, $n_{5\text{-HT}} = 32$; monkey M: $p = 0.38$, $n_{5\text{-HT}} = 12$; monkey K: $p = 0.74$, $n_{5\text{-HT}} = 20$; Wilcoxon paired signed-rank tests).

Together these analyses corroborate our finding that the observed serotonergic modulation is dominated by a multiplicative change and modest additive change of the visual responses. Beyond that, serotonin leaves the receptive field properties largely unchanged.

Serotonin weakly increases the latency of the orientation selective response

We next wondered whether serotonin influenced the dynamics of the visual response, since previous work reported serotonergic influences on the dynamics of subcortical auditory processing in bats (Hurley and Pollak, 2005). To address this question, we used orientation subspace reverse correlation (Ringach et al., 1997), an approach that allows for detailed quantification of the dynamics of the orientation-selective response. The stimulus consisted of a random sequence of gratings of the same spatial frequency but different spatial phases and orientations, updated every 10 ms (see Materials and Methods). Figure 5*A* shows the average SDFs for each orientation for one example neuron for the baseline (top) and serotonin (bottom) blocks. We extracted tuning curves ("orientation subspace maps") from these SDFs (Nienborg and Cumming, 2009; Fig. 5*B*) and quantified the changes in tuning as additive and multiplicative changes using type-II regression. Similar to the results for drifting gratings, we found a significant decrease in the mean response (Fig. 5*F*; $p < 10^{-4}$, $n_{5\text{-HT}} = 47$, $n_{\text{NaCl}} = 11$; monkey M: $p = 0.08$, $n_{5\text{-HT}} = 34$, $n_{\text{NaCl}} = 3$; monkey K: $p < 10^{-3}$, $n_{5\text{-HT}} = 13$, $n_{\text{NaCl}} = 8$) that was largely explained by multiplicative changes in the tuning curves (Fig. 5*G*; relative gain: $p = 0.007$, $n_{5\text{-HT}} = 40$, $n_{\text{NaCl}} = 5$; monkey M: $p = 0.06$, $n_{5\text{-HT}} = 31$,

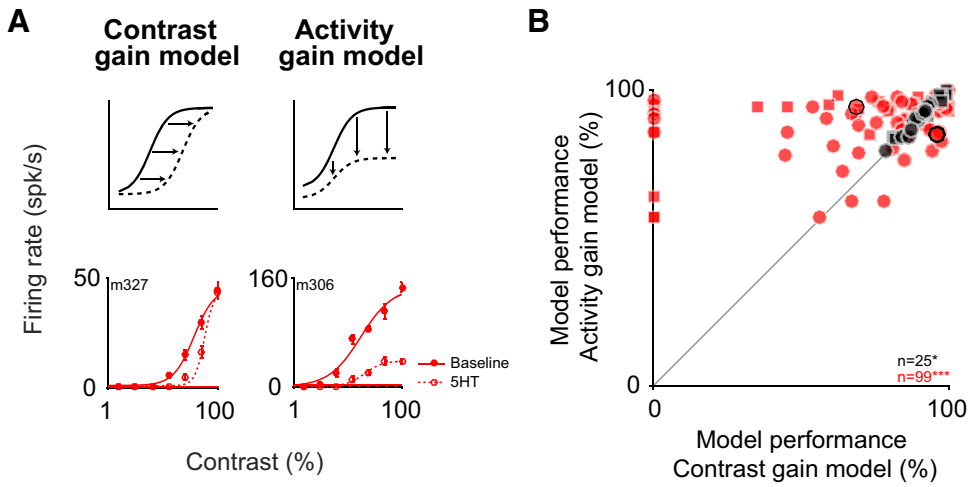

Figure 6. The serotonergic modulation cannot be accounted for by a contrast-gain model. ***A***, If the serotonergic modulation reflected a mechanism similar to contrast-gain control, the serotonergic modulation of the contrast tuning curve should result in a horizontal shift of the curve, without changing the response maximum (dashed line, top left), and an example neuron (bottom left) is compatible with such a change. Alternatively, under an activity-gain model (top right) serotonin application would result in a multiplicative downscaling of the tuning curve, as found for the example (bottom right). ***B***, Symbols are the same as in Figure 1. The activity-gain model in most cases explains a higher percentage of the variance than the contrast-gain model ($p < 10^{-6}$, $n = 99$; Wilcoxon paired test). The change in variance explained differs significantly ($p = 0.02$, $n = 99$ for serotonin, $n = 25$ for saline, Wilcoxon rank-sum test) between the serotonin (5HT; red) and the saline control condition (NaCl; black). Example units in ***A*** are marked by the black circles.

$n_{NaCl} = 3$; monkey K: $p = 0.15$, $n_{5\text{-HT}} = 9$, $n_{NaCl} = 2$; additive chane: $p = 0.99$, $n_{5\text{-HT}} = 40$, $n_{NaCl} = 5$; monkey M: $p = 0.86$, $n_{5\text{-HT}} = 31$, $n_{NaCl} = 3$; monkey K: $p = 0.44$, $n_{5\text{-HT}} = 9$, $n_{NaCl} = 2$). To explore the dynamics of the orientation-selective response, we computed the SD across the SDFs over time (Fig. 5*C*). For the example cell, we find that the response latency for the orientation-selective component of the response is slightly longer after serotonin application (Fig. 5*A*,*C*). Importantly, our control analysis (Fig. 5*D*,*E*; see Materials and Methods) reveals that this effect cannot be explained by the decreased signal-to-noise ratio owing to the reduced spike rate in the serotonin condition. Indeed, across the population, we observed a small but consistent and statistically significant increase in response latency (Fig. 5*H*; $p < 10^{-3}$, $n_{5\text{-HT}} = 45$; monkey M: $p < 0.01$, $n_{5\text{-HT}} = 33$; monkey K: $p = 0.02$, $n_{5\text{-HT}} = 12$), which was correlated with the size of the serotonergic modulation in firing rate (Fig. 5*I*; $r = -0.51$, $p < 10^{-3}$, $n_{5\text{-HT}} = 45$; monkey M: $r = -0.56$, $p < 10^{-3}$, $n_{5\text{-HT}} = 33$; monkey K: $r = -0.20$, $p = 0.54$, $n_{5\text{-HT}} = 12$).

The serotonin-induced changes differ quantitatively from contrast gain, but are accounted for by a simple membrane potential-based model

The main serotonin-dependent changes of the tuning curves (i.e., a largely divisive change in the response and a slight increase in the response latency) are reminiscent of the divisive reduction and phase delay when lowering contrast (Carandini et al., 1997), which are accounted for by a model using divisive normalization (Heeger, 1992; Carandini et al., 1997). We therefore wondered whether the serotonin-induced changes mimic a reduction in contrast, suggesting it may engage a mechanism similar to contrast normalization. To test this hypothesis, we therefore compared the performance of two descriptive models, a contrast-gain model and an activity-gain model (Fig. 6*A*). For the contrast-gain model, the modulation by serotonin would only mimic a change in contrast, resulting in a horizontal shift of the tuning curve (Fig. 6*A*, left). Conversely, for the activity-gain model, the modulation by serotonin would result in a downscaling of the entire tuning curve (Fig. 6*A*, right). While the contrast-gain model provided a better fit to the data for a small number of cells in support of the hypothesis that the modulation by serotonin engages a similar mechanism as contrast, the activity-gain model performed substantially better in most cases (Fig. 6*B*; $p < 10^{-6}$, $n_{5\text{-HT}} = 99$; monkey M: $p < 0.01$, $n_{5\text{-HT}} = 66$; monkey K: $p < 10^{-4}$, $n_{5\text{-HT}} = 33$; Wilcoxon paired signed-rank test). This indicates that modulation by serotonin relies on a mechanism that differs from contrast-gain control.

Finally we wondered whether a simple membrane potential-based model could account for the divisive change in the response and the slight increase in response latency. Specifically, we explored whether a linear change at the level of the membrane potential would suffice to account for the observed effects by serotonin (Fig. 7). This membrane potential-based model consisted of an orientation-selective response at the level of the membrane potential followed by a temporal low-pass filter to fit the orientation bandwidth and average latency of the neuronal response to the stimulus used for orientation subspace reverse correlation (see Materials and Methods; Fig. 7*A*). The time-varying response of the membrane potential was then passed through a threshold-linear spiking nonlinearity. To account for the effect of serotonin, a subtractive shift was applied to the membrane potential [Fig. 7*A*, $V_m(t)$], moving it further away from the spiking threshold. Note that, while biophysically different, in our model this shift is equivalent to increasing the spiking threshold (V_{thresh}) of the spiking nonlinearity. We found that this shift could account for the observed changes in gain, the additive changes (Fig. 7*D*), as well as the small increase in latency (Fig. 7*B*,*E*). A simple subtractive change of a threshold-linear spiking nonlinearity can therefore capture the serotonin-induced modulation of the visual responses.

Serotonin has no systematic effect on response variability or covariability

Neuromodulators, such as acetylcholine, have been implicated in affecting not only the magnitude (Disney et al., 2007) but also the variability of sensory responses (Pinto et al., 2013), and it has been hypothesized that serotonin mediates an additional, acetyl-

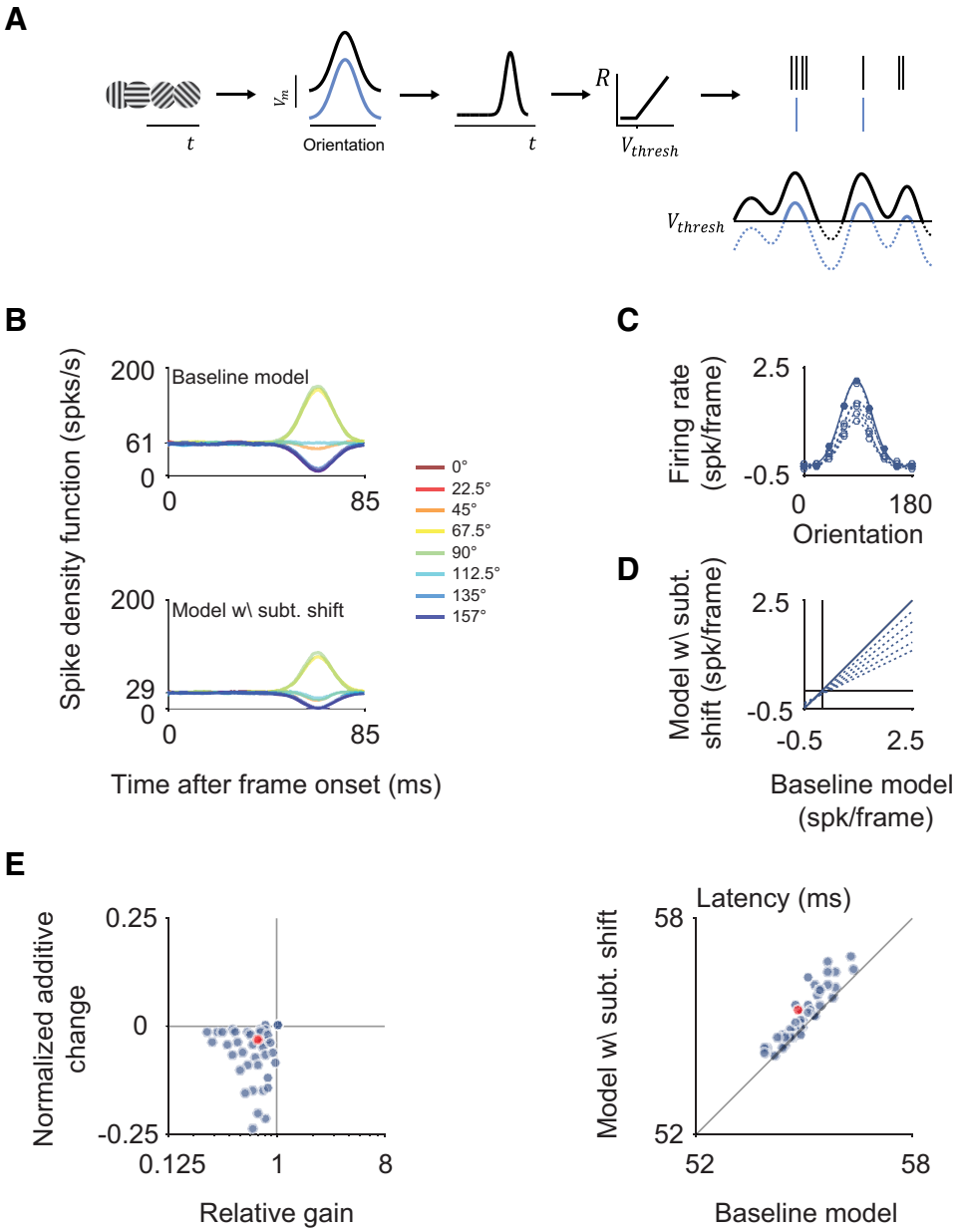

Figure 7. A simple threshold-linear model can account for the observed effects. ***A***, Schematic of the model: the orientation-selective response of the membrane potential to the stimulus sequence is temporally low-pass filtered before being passed through a threshold-linear nonlinearity and a Poisson process to generate spikes. The only effect by serotonin is a subtractive shift to the membrane potential (blue lines) that is equivalent to a higher value of the threshold (V_{thresh}). ***B***, Example SDFs for the modeled baseline condition (top) and after a subtractive shift to the membrane potential aimed at mimicking the serotonin condition (bottom). ***C***, Tuning curves for the baseline condition (solid) and for subtractive shifts of different sizes (dotted) are shown. ***D***, Best fitting regression lines to quantify additive and subtractive changes are shown for different models. ***E***, The subtractive change in the model leads to gain changes, additive changes (left), as well as latency shifts (right) in the range (blue data points) observed in our data (red circles).

choline-independent, mechanism of response desynchronization (Harris and Thiele, 2011). To test for this possibility, we measured the stimulus-independent response covariability ["noise-correlation" (Bair et al., 2001; Cohen and Kohn, 2011)] between the single-unit and the multiunit activity recorded on the same electrode. We note that measuring this correlation between single-unit and multiunit activity recorded on the same electrode has been shown to overestimate the absolute size of this correlation (Ecker et al., 2010). Nonetheless, this approach allows us to infer relative changes in noise correlation between the baseline and the serotonin condition. To reduce the effect of nonstationarities resulting from the onset of the serotonin application on noise correlations, we excluded the first 20 stimulus presentations of each experimental block for this analysis. Since fixational eye movements can affect the variability and covariability of visual neurons, we explored whether these differed systematically between the serotonin application and the saline controls. To this end, we compared the fixation precision (Cherici et al., 2012) as well as the frequency and amplitude of microsaccades within the fixation window (Fig. 8). For none of these metrics differed the modulation systematically between the serotonin and the saline application. Finally, we corrected noise correlation by that predicted from the change in firing rate (see Materials and Methods). In contrast to the hypothesis, we found no significant change in noise correlations for the serotonin condition (Fig. 9*B*; for orientation: $p = 0.74$, $n_{5\text{-HT}} = 63$ for serotonin; for spatial frequency:

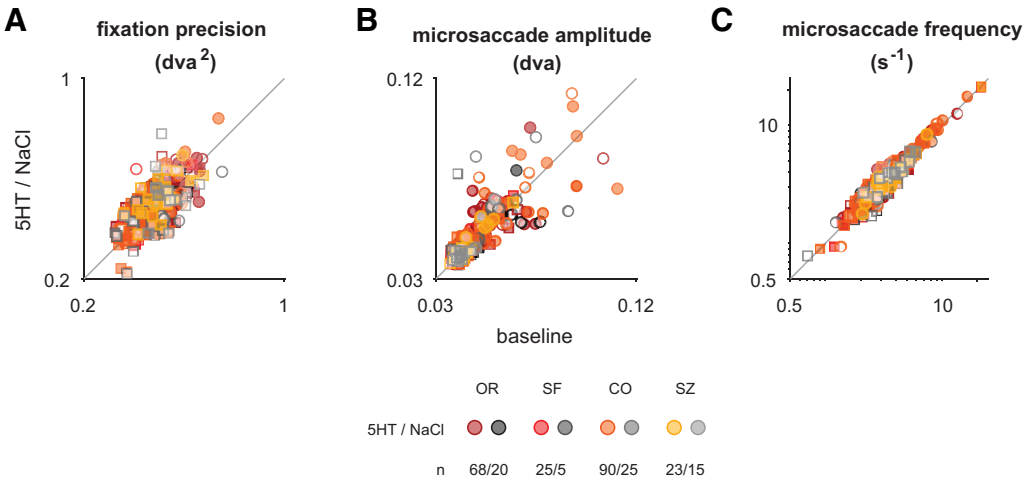

Figure 8. No systematic difference in eye movements between drug and baseline conditions. ***A***, Fixation precision (see Materials and Methods) did not differ between conditions [median 0.49 degrees of visual angle squared (dva ^{2}) for both baseline and 5-HT application, respectively; median 0.49 dva ^{2} and 0.50 dva ^{2} for baseline and saline application, respectively; the change with drug application did not differ significantly between the saline and 5-HT experiments, $p = 0.68$]. ***B***, Microsaccade amplitudes were similar between conditions (median 0.04 dva for baseline and serotonin application, respectively, $n_{5\text{-HT}} = 206$; median 0.04 dva for baseline and saline application, respectively, $n_{\text{NaCl}} = 65$) and their changes did not differ significantly for serotonin versus saline application ($p = 0.43$). **C**, Similarly, the frequency of microsaccades did not change between conditions (median, 3.4 s $^{-1}$ for baseline and serotonin application, respectively, $n_{5\text{-HT}} = 206$; median, 3.2 and 3.3 s $^{-1}$ for baseline and saline application, respectively), and the changes did not differ between conditions ($p = 0.96$; $n_{5\text{-HT}} = 206$, $n_{\text{NaCl}} = 65$, Wilcoxon rank-sum test for all comparisons). Note that for units for which several experiments were performed, only the first experiment was included. Symbols are the same as in Figure 1. Shading represents the type of experiment for which the modulation by drug application [serotonin (5HT) or saline (NaCl)] was quantified.

$n_{5\text{-HT}} = 2$ for serotonin; for contrast: $p = 0.07$, $n_{5\text{-HT}} = 45$ for serotonin; for size: $p = 0.59$, $n_{5\text{-HT}} = 15$ for serotonin; all Wilcoxon paired signed-rank test). We also did not observe a systematic relationship between the size of effect on firing rate and noise correlation (Fig. 9*D*; for orientation: $r = 0.07$, $p = 0.57$, $n_{5\text{-HT}} = 63$; for spatial frequency: $n_{5\text{-HT}} = 2$; for contrast: $r = -0.02$, $p = 0.88$, $n_{5\text{-HT}} = 45$; for size: $r = -0.13$, $p = 0.66$, $n_{5\text{-HT}} = 15$; all Spearman's rank correlation). Finally, we also explored the effect of serotonin on the variability of the sensory response, quantified as Fano factor, and observed no systematic change in the two conditions (Fig. 9*A*; for orientation: $p = 0.77$, $n_{5\text{-HT}} = 61$; for spatial frequency: $n_{5\text{-HT}} = 1$; for contrast: $p = 0.81$, $n_{5\text{-HT}} = 42$; for size: $p = 0.17$, $n_{5\text{-HT}} = 11$; all Wilcoxon paired signed-rank tests). Moreover, the change in mean firing rate was not associated with a systematic change in Fano factor (Fig. 9*C*; for orientation: $r = -0.22$, $p = 0.08$, $n_{5\text{-HT}} = 61$; for spatial frequency: $n_{5\text{-HT}} = 1$; for contrast: $r = -0.14$, $p = 0.38$, $n_{5\text{-HT}} = 42$; for size: $r = 0.19$, $p = 0.58$, $n_{5\text{-HT}} = 11$; all Spearman's rank correlation). Additionally, there was no systematic change in the difference in Fano factor in response to a neuron's preferred stimulus compared with that to a blank stimulus (Fig. 9*E*). Together, these analyses indicate that the application of serotonin leaves the response variability and covariability in macaque V1 largely unchanged.

Discussion

Here we combined extracellular recordings and iontophoresis in V1 of awake macaques to explore the modulatory effects of serotonin on visual processing. We found that across a variety of visual stimulus dimensions, the modulation by serotonin across the neuronal population was surprisingly uniform and (1) was dominated by a decrease in the neurons' response gain, (2) showed a slight slowing of the dynamics of the response, and (3) resulted in no systematic change of the neuronal variability, covariability, or stimulus selectivity. Our observed effects could be captured by a descriptive model in which serotonin caused a simple additive change at the level of the threshold-linear spiking nonlinearity.

A surprisingly uniform effect despite receptor and cellular diversity

In this study, we focused on the serotonergic modulation in the awake macaque of functional tuning properties along four well characterized visual dimensions (orientation, spatial frequency, contrast, and size) that are encoded by neurons in V1. We focused on awake animals using the endogenous ligand while previous work examined the modulation to receptor-specific ligands in the striate cortex of anesthetized macaques and, in contrast with the predominantly suppressive effect we found, observed variable modulation (Watakabe et al., 2009). This apparent discrepancy may in part reflect a net effect between facilitation and suppression mediated by different receptor classes all activated by serotonin. Additionally, our recordings in the awake animal likely mimimized fluctuations in brain state found under anesthesia (Ecker et al., 2014) and avoided effects of anesthesia on serotonergic neurons (Johansen et al., 2015). Moreover, the focus on parametrized functional properties may have contributed to our ability to identify an effect—a gain decrease—that is surprisingly functionally uniform across the population and stimulus dimensions. This effect dominated despite variability on a neuron-by-neuron basis, which was also observed previously in anesthetized animals (Waterhouse et al., 1990; Watakabe et al., 2009). In light of the known diversity of receptor expression on different cell types in the macaque V1 (Watakabe et al., 2009), this main observed effect is likely mediated by different cellular or network mechanisms. For example, in the input layers of V1, receptors 5-HT$_{1B}$ and 5-HT$_{2A}$ are expressed by the majority of excitatory neurons, but not by GABAergic neurons, and are typically coexpressed by the same neurons in layer IVC (Watakabe et al., 2009). The predominantly divisive effect of serotonin may therefore result from an interaction of the receptor activation in excitatory neurons. A previous study applied a 5-HT$_{1A}$ agonist to layers IV and V in V1 of anesthetized macaques and also observed a decrease of multiunit activity (Rauch et al., 2008). Given the lack of 5-HT$_{1A}$-receptor expression in these layers in macaque V1

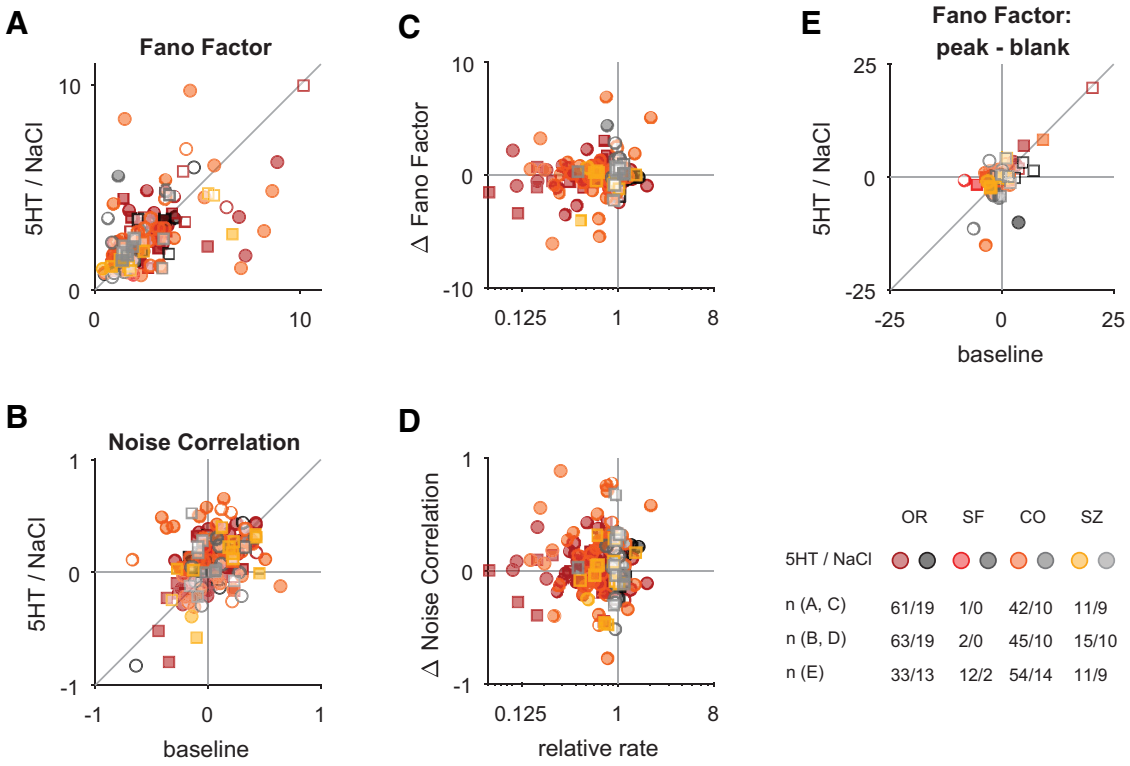

Figure 9. Serotonin application does not systematically change the Fano factor or noise correlation. Warm and gray colors depict experiments with serotonin (5HT) and saline (NaCl) application, respectively, as indicated. The number of units per experiment and condition included are specified. Filled symbols depict units with significant modulation (compare Fig. 1*E*). Circles and squares correspond to data from monkey M and K, respectively. ***A***, The variability of the neuronal response quantified by the Fano factor does not change systematically for the application of serotonin orientation: $p = 0.77, n = 61$ for serotonin; $p = 0.55, n = 19$ for saline; spatial frequency: $n = 1$ for serotonin; $n = 0$ for saline; contrast: $p = 0.81, n = 42$ for serotonin; $p = 0.13, n = 10$ for saline; size: $p = 0.17, n = 11$ for serotonin; $p = 0.57, n = 9$ for saline; all Wilcoxon paired signed-rank test). Note the similar distribution for serotonin and saline application in ***A–D***. ***B***, The single-unit multiunit noise correlation (corrected for changes in firing rate; see Materials and Methods) is compared for the baseline condition (abscissa) and the application of serotonin or saline (ordinate). The serotonin application did not result in a significant change of noise correlation across the population (orientation: $p = 0.74, n = 63$ for serotonin; $p = 0.15, n = 19$ for saline; spatial frequency: $n = 2$ for serotonin; $n = 0$ for saline; contrast: $p = 0.07, n = 45$ for serotonin; $p = 0.38, n = 10$ for saline; size: $p = 0.59, n = 15$ for serotonin; $p = 0.43, n = 10$ for saline; all Wilcoxon paired signed-rank test). The change in noise correlation (***D***) and Fano factor (***C***), respectively, are not systematically associated with the serotonergic modulation of a neuron's mean response ($p >$ 0.20 for all Spearman's rank correlations for serotonin and $p > 0.06$ for all equivalent comparisons for saline application). ***E***, Serotonin also did not result in a significantly different change in the difference in Fano factor for the peak versus blank response compared with the saline application ($p = 0.15, n_{5\text{-HT}} = 110, n_{\text{NaCl}} = 38$). Note that for this analysis the preferred and blank stimuli had to be presented ≥4 times each for each unit.

(Watakabe et al., 2009), this decrease in activity may at least partially reflect a cross-activation of the densely expressed 5-HT_{1B} receptors. This modulation was thought to be mediated by a hyperpolarization of the membrane potential, analogous to the membrane potential-based model we present here. Serotonin-mediated hyperpolarization of the membrane potential was also recently identified at the axon initial segment in auditory neurons in gerbils (Ko et al., 2016). Conversely, in layer II, where the receptors are expressed on a subset of both excitatory and inhibitory neurons, but typically not coexpressed (Watakabe et al., 2009), the decrease in gain may reflect network interactions between inhibition and excitation. Different circuit elements may also include vasoactive intestinal peptide-positive (VIP+) interneurons that express the 5-HT_{3A} receptor (Rudy et al., 2011), although in the macaque V1 5-HT_{3A}-receptor expression has only been observed for layers 5/6 (Watakabe et al., 2009), while VIP+ interneurons are most pronounced in layers 2/3 (Gabbott and Bacon, 1997). The same functional computation—gain control—may therefore be implemented by different components of the neuronal hardware within the same neuromodulator system serotonin, at least on the time scale we examined.

Indeed, since we applied serotonin in blocks in the minute time scale, the modulation likely mimics changes in the tonic level of discharge of serotonergic neurons, implicated in signaling the contextual valence on such slow time scales, and providing different signals from the phasic responses (Cohen et al., 2015). Interestingly, for short (<1 s) phasic serotonergic stimulation, a divisive modulation was previously observed only for the spontaneous response, not the sensory-driven response, in the olfactory bulb in anesthetized mice (Lottem et al., 2016), in contrast with our findings. Conversely, a decrease in gain of the sensory response in the mouse olfactory bulb was observed for sustained (>30 s) serotonergic activation (Petzold et al., 2009), similar to the modulation observed in this study.

Behaviorally, decreasing the gain of a sensory response can contribute to a delay or reduction in the response to sensory stimulation, as has been previously observed for a reduced startle response in rats (Davis et al., 1980; Sipes and Geyer, 1994), or reduced mechanosensory responsivity in mice (Dugué et al., 2014). Although these behavioral findings have typically been interpreted in the context of a serotonergic role for motor or emotional processing (Crockett et al., 2009; Cools et al., 2011; Correia et al., 2017), the observed decreased sensory gain suggests at least partially a sensory involvement. It may also reflect a sensory signature of how serotonin promotes waiting (Miyazaki et al., 2014;

Ranade et al., 2014; Fonseca et al., 2015) by lowering the salience of sensory input.

On this slow (minute) time scale, serotonin may be complementary to the action of cholinergic neuromodulation, which has been found to increase the gain of the visual input in macaque V1 (Disney et al., 2007), and has been linked to mediating spatial attention (Herrero et al., 2008). Notably, acetylcholine in macaque V1 was found to substantially modulate the gain but not the variability of the response (Herrero et al., 2008), a dissociation that is mirrored by our results here. It suggests that distinct mechanisms are available to modulate the variability and level of the sensory responses, although cognitive states, such as spatial attention, typically affect both (Cohen and Maunsell, 2009; Mitchell et al., 2009).

Potential implications for the serotonergic role in visual hallucinations

An influential perspective of perception is that it reflects an inference process (Helmholtz, 1867; Gregory, 1980; Lee and Mumford, 2003; Yuille and Kersten, 2006), in which internal beliefs about the world are combined with the incoming sensory evidence (Lee and Mumford, 2003; Yuille and Kersten, 2006). Mounting physiological evidence suggests that some of this combination of internal ("top-down") and external sensory signals occur already at the level of sensory neurons (Fiser et al., 2010; Nienborg and Roelfsema, 2015; Cumming and Nienborg, 2016). In this framework, psychiatric diseases such as schizophrenia (Friston, 2005) are associated with an imbalance between internally generated (top-down) and externally driven feed-forward signals. Hallucinations, for example, have been suggested to arise from an imbalance toward internally generated over externally driven sensory signals (Friston, 2005; Notredame et al., 2014; Jardri et al., 2016; Schmack et al., 2017). Such an imbalance may also explain, for example, visual hallucinations during visual impairment (Charles Bonnet syndrome; Gold and Rabins, 1989), when the feed-forward visual input is degraded. Similarly, decreasing the gain of the visual input could shift the balance toward the internally generated signals, and thus result in visual hallucinations. The decrease in gain by serotonin we found here may therefore shed light onto the mechanism by which the visual cortex is involved in hallucinations caused by serotonergic hallucinogens (Bressloff et al., 2002; de Araujo et al., 2012; Kometer et al., 2013; Carhart-Harris et al., 2016; Kometer and Vollenweider, 2016).

Conclusion

To our knowledge this is the first study to explore the role of serotonergic modulation of neuronal activity in the sensory cortex of awake animals. The modulatory effect we observed across the population was surprisingly homogeneous—a simple decrease in the response gain of the neural activity. Such gain modulation is an important component of the cortical computation (Salinas and Thier, 2000) that controls the responses without changing the receptive field properties. It is therefore well suited to modulate the responses according to the animal's internal state, e.g. influenced by the valence of the contextual environment (Cohen et al., 2015).

References

Albrecht DG, Hamilton DB (1982) Striate cortex of monkey and cat: contrast response function. J Neurophysiol 48:217–237. Medline

Atallah BV, Bruns W, Carandini M, Scanziani M (2012) Parvalbumin-expressing interneurons linearly transform cortical responses to visual stimuli. Neuron 73:159–170. CrossRef Medline

Bachatene L, Bharmauria V, Cattan S, Molotchnikoff S (2013) Fluoxetine and serotonin facilitate attractive-adaptation-induced orientation plasticity in adult cat visual cortex. Eur J Neurosci 38:2065–2077. CrossRef Medline

Bair W, Zohary E, Newsome WT (2001) Correlated firing in macaque visual area MT: time scales and relationship to behavior. J Neurosci 21:1676–1697. Medline

Bracewell RN (1986) The Fourier transform and its applications. Singapore: McGraw-Hill.

Brainard DH (1997) The psychophysics toolbox. Spat Vis 10:433–436. Medline

Bressloff PC, Cowan JD, Golubitsky M, Thomas PJ, Wiener MC (2002) What geometric visual hallucinations tell us about the visual cortex. Neural Comput 14:473–491. Medline

Carandini M (2004) Amplification of trial-to-trial response variability by neurons in visual cortex. PLoS Biol 2:E264. CrossRef Medline

Carandini M, Ferster D (2000) Membrane potential and firing rate in cat primary visual cortex. J Neurosci 20:470–484. Medline

Carandini M, Heeger DJ, Movshon JA (1997) Linearity and normalization in simple cells of the macaque primary visual cortex. J Neurosci 17:8621–8644. Medline

Carhart-Harris RL, Muthukumaraswamy S, Roseman L, Kaelen M, Droog W, Murphy K, Tagliazucchi E, Schenberg EE, Nest T, Orban C, Leech R, Williams LT, Williams TM, Bolstridge M, Sessa B, McGonigle J, Sereno MI, Nichols D, Hellyer PJ, Hobden P, et al. (2016) Neural correlates of the LSD experience revealed by multimodal neuroimaging. Proc Natl Acad Sci U S A 113:4853–4858. CrossRef Medline

Cavanaugh JR, Bair W, Movshon JA (2002) Nature and interaction of signals from the receptive field center and surround in macaque V1 neurons. J Neurophysiol 88:2530–2546. CrossRef Medline

Cherici C, Kuang X, Poletti M, Rucci M (2012) Precision of sustained fixation in trained and untrained observers. J Vis 12(6):pii:31. CrossRef Medline

Clery S, Cumming BG, Nienborg H (2017) Decision-related activity in macaque V2 for fine disparity discrimination is not compatible with optimal linear read-out. J Neurosci 37:715–725. CrossRef Medline

Cohen JY, Amoroso MW, Uchida N (2015) Serotonergic neurons signal reward and punishment on multiple timescales. Elife 4. CrossRef Medline

Cohen MR, Kohn A (2011) Measuring and interpreting neuronal correlations. Nat Neurosci 14:811–819. CrossRef Medline

Cohen MR, Maunsell JH (2009) Attention improves performance primarily by reducing interneuronal correlations. Nat Neurosci 12:1594–1600. CrossRef Medline

Cools R, Nakamura K, Daw ND (2011) Serotonin and dopamine: unifying affective, activational, and decision functions. Neuropsychopharmacology 36:98–113. CrossRef Medline

Correia PA, Lottem E, Banerjee D, Machado AS, Carey MR, Mainen ZF (2017) Transient inhibition and long-term facilitation of locomotion by phasic optogenetic activation of serotonin neurons. Elife 6:pii:e20975. CrossRef Medline

Crockett MJ, Clark L, Robbins TW (2009) Reconciling the role of serotonin in behavioral inhibition and aversion: acute tryptophan depletion abolishes punishment-induced inhibition in humans. J Neurosci 29:11993–11999. CrossRef Medline

Cumming BG, Nienborg H (2016) Feedforward and feedback sources of choice probability in neural population responses. Curr Opin Neurobiol 37:126–132. CrossRef Medline

Davis M, Strachan DI, Kass E (1980) Excitatory and inhibitory effects of serotonin on sensorimotor reactivity measured with acoustic startle. Science 209:521–523. CrossRef Medline

Dayan P (2012) Twenty-five lessons from computational neuromodulation. Neuron 76:240–256. CrossRef Medline

Dayan P, Huys Q (2015) Serotonin's many meanings elude simple theories. Elife 4. CrossRef Medline

de Araujo DB, Ribeiro S, Cecchi GA, Carvalho FM, Sanchez TA, Pinto JP, de Martinis BS, Crippa JA, Hallak JE, Santos AC (2012) Seeing with the eyes shut: neural basis of enhanced imagery following Ayahuasca ingestion. Hum Brain Mapp 33: 2550–2560. CrossRef Medline

de Lima AD, Bloom FE, Morrison JH (1988) Synaptic organization of

serotonin-immunoreactive fibers in primary visual cortex of the macaque monkey. J Comp Neurol 274:280–294. CrossRef Medline
Disney AA, Aoki C, Hawken MJ (2007) Gain modulation by nicotine in macaque V1. Neuron 56:701–713. CrossRef Medline
Dugué GP, Lörincz ML, Lottem E, Audero E, Matias S, Correia PA, Léna C, Mainen ZF (2014) Optogenetic recruitment of dorsal raphe serotonergic neurons acutely decreases mechanosensory responsivity in behaving mice. PLoS One 9:e105941. CrossRef Medline
Eastman KM, Huk AC (2012) PLDAPS: a hardware architecture and software toolbox for neurophysiology requiring complex visual stimuli and online behavioral control. Front Neuroinform 6:1. CrossRef Medline
Ecker AS, Berens P, Keliris GA, Bethge M, Logothetis NK, Tolias AS (2010) Decorrelated neuronal firing in cortical microcircuits. Science 327:584–587. CrossRef Medline
Ecker AS, Berens P, Cotton RJ, Subramaniyan M, Denfield GH, Cadwell CR, Smirnakis SM, Bethge M, Tolias AS (2014) State dependence of noise correlations in macaque primary visual cortex. Neuron 82:235–248. CrossRef Medline
Fiser J, Berkes P, Orbán G, Lengyel M (2010) Statistically optimal perception and learning: from behavior to neural representations. Trends Cogn Sci 14:119–130. CrossRef Medline
Fonseca MS, Murakami M, Mainen ZF (2015) Activation of dorsal raphe serotonergic neurons promotes waiting but is not reinforcing. Curr Biol 25:306–315. CrossRef Medline
Friedman HS, Priebe CE (1998) Estimating stimulus response latency. J Neurosci Methods 83:185–194. CrossRef Medline
Friston K (2005) Disconnection and cognitive dysmetria in schizophrenia. Am J Psychiatry 162:429–432. CrossRef Medline
Gabbott PL, Bacon SJ (1997) Vasoactive intestinal polypeptide containing neurones in monkey medial prefrontal cortex (mPFC): colocalisation with calretinin. Brain Res 744:179–184. CrossRef Medline
Gold K, Rabins PV (1989) Isolated visual hallucinations and the Charles Bonnet syndrome: a review of the literature and presentation of six cases. Compr Psychiatry 30:90–98. CrossRef Medline
Goris RL, Movshon JA, Simoncelli EP (2014) Partitioning neuronal variability. Nat Neurosci 17:858–865. CrossRef Medline
Gregory RL (1980) Perceptions as hypotheses. Philos Trans R Soc Lond B Biol Sci 290:181–197. CrossRef Medline
Gur M, Kagan I, Snodderly DM (2005) Orientation and direction selectivity of neurons in V1 of alert monkeys: functional relationships and laminar distributions. Cereb Cortex 15:1207–1221. CrossRef Medline
Harris KD, Thiele A (2011) Cortical state and attention. Nat Rev Neurosci 12:509–523. CrossRef Medline
Hayashi K, Nakao K, Nakamura K (2015) Appetitive and aversive information coding in the primate dorsal raphé nucleus. J Neurosci 35:6195–6208. CrossRef Medline
Heeger DJ (1992) Normalization of cell responses in cat striate cortex. Vis Neurosci 9:181–197. CrossRef Medline
Helmholtz H (1867) Handbuch der physiologischen optik. Leipzig: Voss.
Herrero JL, Roberts MJ, Delicato LS, Gieselmann MA, Dayan P, Thiele A (2008) Acetylcholine contributes through muscarinic receptors to attentional modulation in V1. Nature 454:1110–1114. CrossRef Medline
Hurley LM, Pollak GD (2005) Serotonin shifts first-spike latencies of inferior colliculus neurons. J Neurosci 25:7876–7886. CrossRef Medline
Hurley LM, Devilbiss DM, Waterhouse BD (2004) A matter of focus: monoaminergic modulation of stimulus coding in mammalian sensory networks. Curr Opin Neurobiol 14:488–495. CrossRef Medline
Jacob SN, Ott T, Nieder A (2013) Dopamine regulates two classes of primate prefrontal neurons that represent sensory signals. J Neurosci 33:13724–13734. CrossRef Medline
Jacobs BL, Azmitia EC (1992) Structure and function of the brain serotonin system. Physiol Rev 72:165–229. Medline
Jardri R, Hugdahl K, Hughes M, Brunelin J, Waters F, Alderson-Day B, Smailes D, Sterzer P, Corlett PR, Leptourgos P, Debbané M, Cachia A, Denève S (2016) Are hallucinations due to an imbalance between excitatory and inhibitory influences on the brain. Schizophr Bull 42:1124–1134. CrossRef Medline
Johansen, SL, Iceman KE, Iceman CR, Taylor BE, Harris MB (2015) Isoflurane causes concentration-dependent inhibition of medullary raphé 5-HT neurons *in situ*. Auton Neurosci 193:51–56. CrossRef Medline
Kleiner M, Brainard DH, Pelli DG (2007) What's new in Psychtoolbox-3? Perception 36, ECVP Abstract Supplement.
Ko KW, Rasband MN, Meseguer V, Kramer RH, Golding NL (2016) Serotonin modulates spike probability in the axon initial segment through HCN channels. Nat Neurosci 19:826–834. CrossRef Medline
Kometer M, Vollenweider FX (2016) Serotonergic hallucinogen-induced visual perceptual alterations. Curr Top Behav Neurosci. Advance online publication. Retrieved October 19, 2017. CrossRef Medline
Kometer M, Schmidt A, Jäncke L, Vollenweider FX (2013) Activation of serotonin 2A receptors underlies the psilocybin-induced effects on α oscillations, N170 visual-evoked potentials, and visual hallucinations. J Neurosci 33:10544–10551. CrossRef Medline
Lee J, Williford T, Maunsell JH (2007) Spatial attention and the latency of neuronal responses in macaque area V4. J Neurosci 27:9632–9637. CrossRef Medline
Lee TS, Mumford D (2003) Hierarchical Bayesian inference in the visual cortex. J Opt Soc Am A Opt Image Sci Vis 20:1434–1448. CrossRef Medline
Lottem E, Lörincz ML, Mainen ZF (2016) Optogenetic activation of dorsal raphe serotonin neurons rapidly inhibits spontaneous but not odor-evoked activity in olfactory cortex. J Neurosci 36:7–18. CrossRef Medline
Maya Vetencourt JF, Sale A, Viegi A, Baroncelli L, De Pasquale R, O'Leary OF, Castrén E, Maffei L (2008) The antidepressant fluoxetine restores plasticity in the adult visual cortex. Science 320:385–388. CrossRef Medline
McAdams CJ, Maunsell JH (1999) Effects of attention on orientation-tuning functions of single neurons in macaque cortical area V4. J Neurosci 19:431–441. Medline
Mitchell JF, Sundberg KA, Reynolds JH (2009) Spatial attention decorrelates intrinsic activity fluctuations in macaque area V4. Neuron 63:879–888. CrossRef Medline
Miyazaki KW, Miyazaki K, Tanaka KF, Yamanaka A, Takahashi A, Tabuchi S, Doya K (2014) Optogenetic activation of dorsal raphe serotonin neurons enhances patience for future rewards. Curr Biol 24:2033–2040. CrossRef Medline
Nienborg H, Cumming BG (2006) Macaque V2 neurons, but not V1 neurons, show choice-related activity. J Neurosci 26:9567–9578. CrossRef Medline
Nienborg H, Cumming BG (2009) Decision-related activity in sensory neurons reflects more than a neuron's causal effect. Nature 459:89–92. CrossRef Medline
Nienborg H, Cumming BG (2014) Decision-related activity in sensory neurons may depend on the columnar architecture of cerebral cortex. J Neurosci 34:3579–3585. CrossRef Medline
Nienborg H, Roelfsema PR (2015) Belief states as a framework to explain extra-retinal influences in visual cortex. Curr Opin Neurobiol 32:45–52. CrossRef Medline
Nienborg H, Bridge H, Parker AJ, Cumming BG (2004) Receptive field size in V1 neurons limits acuity for perceiving disparity modulation. J Neurosci 24:2065–2076. CrossRef Medline
Nienborg H, Hasenstaub A, Nauhaus I, Taniguchi H, Huang ZJ, Callaway EM (2013) Contrast dependence and differential contributions from somatostatin- and parvalbumin-expressing neurons to spatial integration in mouse V1. J Neurosci 33:11145–11154. CrossRef Medline
Notredame CE, Pins D, Deneve S, Jardri R (2014) What visual illusions teach us about schizophrenia. Front Integr Neurosci 8:63. CrossRef Medline
Ott T, Jacob SN, Nieder A (2014) Dopamine receptors differentially enhance rule coding in primate prefrontal cortex neurons. Neuron 84:1317–1328. CrossRef Medline
Pelli DG (1997) The VideoToolbox software for visual psychophysics: transforming numbers into movies. Spat Vis 10:437–442. CrossRef Medline
Petzold GC, Hagiwara A, Murthy VN (2009) Serotonergic modulation of odor input to the mammalian olfactory bulb. Nat Neurosci 12:784–791. CrossRef Medline
Pinto L, Goard MJ, Estandian D, Xu M, Kwan AC, Lee SH, Harrison TC, Feng G, Dan Y (2013) Fast modulation of visual perception by basal forebrain cholinergic neurons. Nat Neurosci 16:1857–1863. CrossRef Medline
Priebe NJ, Ferster D (2008) Inhibition, spike threshold, and stimulus selectivity in primary visual cortex. Neuron 57:482–497. CrossRef Medline
Rabinowitz NC, Goris RL, Cohen M, Simoncelli E (2015) Attention stabilizes the shared gain of V4 populations. Elife 4:e08998. CrossRef Medline
Ranade S, Pi HJ, Kepecs A (2014) Neuroscience: waiting for serotonin. Curr Biol 24:R803–R805. CrossRef Medline
Ranade SP, Mainen ZF (2009) Transient firing of dorsal raphe neurons en-

codes diverse and specific sensory, motor, and reward events. J Neurophysiol 102:3026–3037. CrossRef Medline

Rauch A, Rainer G, Logothetis NK (2008) The effect of a serotonin-induced dissociation between spiking and perisynaptic activity on BOLD functional MRI. Proc Natl Acad Sci U S A 105:6759–6764. CrossRef Medline

Ringach DL, Hawken MJ, Shapley R (1997) Dynamics of orientation tuning in macaque primary visual cortex. Nature 387:281–284. CrossRef Medline

Ringach DL, Shapley RM, Hawken MJ (2002) Orientation selectivity in macaque V1: diversity and laminar dependence. J Neurosci 22:5639–5651. Medline

Rudy B, Fishell G, Lee S, Hjerling-Leffler J (2011) Three groups of interneurons account for nearly 100% of neocortical GABAergic neurons. Dev Neurobiol 71:45–61. CrossRef Medline

Salinas E, Thier P (2000) Gain modulation: a major computational principle of the central nervous system. Neuron 27:15–21. CrossRef Medline

Schmack K, Rothkirch M, Priller J, Sterzer P (2017) Enhanced predictive signalling in schizophrenia. Hum Brain Mapp 38:1767–1779. CrossRef Medline

Schmitzer-Torbert N, Jackson J, Henze D, Harris K, Redish AD (2005) Quantitative measures of cluster quality for use in extracellular recordings. Neuroscience 131:1–11. CrossRef Medline

Sipes TA, Geyer MA (1994) Multiple serotonin receptor subtypes modulate prepulse inhibition of the startle response in rats. Neuropharmacology 33:441–448. CrossRef Medline

Skottun BC, De Valois RL, Grosof DH, Movshon JA, Albrecht DG, Bonds AB (1991) Classifying simple and complex cells on the basis of response modulation. Vision Res 31:1079–1086. Medline

Thiele A, Delicato LS, Roberts MJ, Gieselmann MA (2006) A novel electrode-pipette design for simultaneous recording of extracellular spikes and iontophoretic drug application in awake behaving monkeys. J Neurosci Methods 158:207–211. CrossRef Medline

Watakabe A, Komatsu Y, Sadakane O, Shimegi S, Takahata T, Higo N, Tochitani S, Hashikawa T, Naito T, Osaki H, Sakamoto H, Okamoto M, Ishikawa A, Hara S, Akasaki T, Sato H, Yamamori T (2009) Enriched expression of serotonin 1B and 2A receptor genes in macaque visual cortex and their bidirectional modulatory effects on neuronal responses. Cereb Cortex 19:1915–1928. CrossRef Medline

Waterhouse BD, Azizi SA, Burne RA, Woodward DJ (1990) Modulation of rat cortical area 17 neuronal responses to moving visual stimuli during norepinephrine and serotonin microiontophoresis. Brain Res 514:276–292. CrossRef Medline

Williams GV, Rao SG, Goldman-Rakic PS (2002) The physiological role of 5-HT_{2A} receptors in working memory. J Neurosci 22:2843–2854. Medline

Williford T, Maunsell JH (2006) Effects of spatial attention on contrast response functions in macaque area V4. J Neurophysiol 96:40–54. CrossRef Medline

Yuille A, Kersten D (2006) Vision as Bayesian inference: analysis by synthesis? Trends Cogn Sci 10:301–308. CrossRef Medline

Serotonergic modulation of functional connectivity in awake macaque V1

Katsuhisa Kawaguchi*[1,2], Lenka Seillier*[1], Hendrikje Nienborg[1,+]

[1] University of Tuebingen, Werner Reichardt Centre for Integrative Neuroscience, 72076 Tuebingen, Germany

[2] Graduate School of Neural and Behavioural Sciences, International Max Planck Research School, 72074 Tuebingen, Germany

*these authors contributed equally to this work

+correspondence should be addressed to: hendrikje.nienborg@cin.uni-tuebingen.de

Abstract

The responses of neurons in the primary visual cortex (V1) to identical stimuli depend on an animal's cognitive or behavioral state. Such state-dependence has been shown to involve neuromodulators such as acetylcholine or noradrenaline. In contrast, the involvement of the neuromodulator serotonin (5HT), which has pronounced projections to the primary visual cortex, is remarkably understudied. We recently reported that iontophoretically applied serotonin decreases the spiking activity in V1 of awake macaques predominantly by lowering the response gain (Seillier et al., 2017). Here, we explore the role of serotonin on local network state in awake macaque V1 by examining the relationships between extracellular spiking activity and the membrane potential of the local population as inferred by the local field potential (LFP). To examine the extent to which a neuron's response was coupled with the local ongoing activity we computed spike-triggered LFPs (stLFP). We found that during the 5HT application but not for pH-matched NaCl the amplitude of the stLFP was significantly decreased, resulting in a corresponding decrease in the power of the stLFP. The decrease in the stLFP amplitude was opposite to what is expected for decreasing firing rate by 5HT. It suggests that serotonin decouples responses of a neuron from the ongoing local network activity and thereby decreases the functional connectivity of the local population. Interestingly, this serotonergic effect is reminiscent of the decrease in the stLFP amplitude with spatial attention, raising the possibility of a serotonergic involvement in attentional modulation in visual responses.

Significance statement

Neural responses in the primary visual cortex are state-dependent and shown to be affected by neuromodulators such as acetylcholine. Although serotonin is involved in diverse cognitive and behavioral state in the brain, its role in visual processing is relatively unknown. We previously reported that serotonin decreases the gain of visual responses (Seillier et al., 2017). Here we analyzed local field potentials to study the role of 5HT in local network state and found evidence that serotonin decouples a neuron's visual responses from the local ongoing network activity, thereby decreasing functional connectivity within V1. That serotonergic modulation resembled attentional modulation in visual cortices, suggesting a potential serotonergic involvement in attention.

Introduction

Neurons in the primary visual cortex (V1) sensitively respond to several visual features such as orientation, motion direction, size, and binocular disparity of visual stimulus contours (Hubel & Wiesel, 1962; Priebe, 2016). Although V1 neurons are sensitive enough to exhibit a tuning curve, the tuning property is also influenced by internal state including arousal and attention (Fischer & Whitney, 2009; McAdams & Maunsell, 1999; Reimer et al., 2014; Sanayei et al., 2015; Vinck et al., 2015). Neuromodulators such as acetylcholine (ACh) and serotonin (5HT) have been also shown to alter the tuning curve of V1 neurons (Disney et al., 2007; Seillier et al., 2017; Watakabe et al., 2009; Zinke et al., 2006), raising the possibility that these neuromodulators are linked to state-dependent visual processes. In fact, acetylcholine was shown to affect attentional modulation in macaque V1 (Herrero et al., 2008). Despite pronounced serotonergic projections to V1 (Jacobs & Nienborg, 2018), a role of 5HT in state-dependent visual processes in V1 is relatively unknown.

State-dependent visual processes are not only accompanied by change in sensory coding but change in local network state inferred by the local field potential (LFP). For example, spatial attention was shown to decrease the LFP power especially in low-frequency range (Chalk et al., 2010; Das & Ray, 2018; Spyropoulos et al., 2018). Stimulation of the basal forebrain, the primary source of cholinergic inputs to cortex, has been also shown to decrease in low-frequency LFP power in mouse V1 (De Luna et al., 2017; Goard & Dan, 2009; Pinto et al., 2013). Although the computational role in the LFP power in sensory areas is under debate, the decrease in low-frequency LFP power is thought of a signature of desynchronized cortical state (Harris & Thiele, 2011), which is claimed to improve sensory coding and perceptual performance (Beaman et al., 2017; Pinto et al., 2013). Therefore, the brain may benefit from the local network state associated with spatial attention and basal brain stimulation. Although 5HT was also shown to decrease low-frequency LFP power in the prefrontal cortex of rodents (Kjaerby et al., 2016; Puig et al., 2010), whether this serotonergic modulation in LFPs is similar in macaque V1 was not demonstrated.

To examine the role of 5HT on local network state in macaque V1, we recorded both single unit activity and LFPs in V1 while two macaque monkeys performed a fixation task and were presented with dynamic visual stimuli during blockwise iontophoretic application of 5HT or pH-matched saline as control. Consistently with previous rodent studies, we found that serotonin decreased LFP power especially in low-frequency range also in awake macaque V1. To see whether serotonin affects spike-LFP relationships, we computed spike-triggered average LFP

(stLFP) and found that the amplitude of the stLFP was smaller in 5HT conditions than baseline. It suggests that 5HT decreases local functional connectivity (Nauhaus et al., 2009; Okun et al., 2015). The observed serotonergic modulations in V1 resemble the results from macaque studies of spatial attention (Chalk et al., 2010) and mice studies with basal forebrain stimulation (De Luna et al., 2017; Goard & Dan, 2009; Pinto et al., 2013), suggesting that 5HT in addition to ACh contributes to state-dependent visual processes in V1.

Materials & Methods

Animals. Two adult male rhesus monkeys *(Macaca mulatta)*; m (8 kg; 11 years) and k (12 kg; 7 years), participated in the experiments. All experimental procedures were in accordance with the guidelines for animal experimentation and approved by the local authorities, the Regierungspräsidium Tübingen, Germany.

Electrophysiological recordings and iontophoresis. Details in recordings with iontophoresis were previously reported (Seillier et al., 2017). Briefly, we recorded extracellular single-unit activity in V1 while the animals performed a 2 sec fixation task while we presented flash-grating stimuli in the receptive field of the recorded unit. For each unit we initially quantified the center of the receptive field from receptive field profiles along a horizontal and vertical axis as described previously (Nienborg et al., 2004) by presenting an elongated rectangular grating (height 3°-5°; width 0.2°) at different horizontal or vertical positions across the receptive field and its immediate surround. Subsequent stimuli were centered on the receptive field at a median eccentricity of 3.6° [range 1.6 to 6.4°].

The positions of both eyes were recorded at 500 Hz using an infrared optical recording system (Eyelink 1000, SR Research Ltd). Experimental control and stimulus presentation were achieved using custom written software in MATLAB modified after (Eastman and Huk, 2012) using the psychophysics toolbox (Brainard, 1997; Pelli, 1997; Kleiner et al., 2007).

Recordings with iontophoresis were performed using custom-made tungsten-in-glass electrodes flanked by two pipettes as described previously (Thiele et al., 2006; Jacob et al., 2013). One barrel of the electrode-pipette was filled with serotonin hydrochloride (5HT; Sigma-Aldrich; 10mM in double distilled water; pH=3.5-3.8), the other with pH-matched saline (NaCl; 0.9%). The electrodes typically had impedances between 0.3-1.6 MΩ (measured at 1 kHz) and tip sizes of 10-15 µm. The ejection current for serotonin (5HT) ranged between 2-50 nA (median = 10nA) and 5-20nA (median = 11nA) for saline. The retention current was -8 nA to prevent

leakage from the drug barrels during the control conditions. The pipette resistance ranged from 10-150 MΩ, as used previously (Ott et al., 2014). To minimize long-term effects of serotonin (Vetencourt et al., 2008; Correia et al., 2017) we avoided recording from nearby locations in V1 in consecutive recording sessions.

This electrode-pipette was mounted inside a guide tube and inserted transdurally without a dura-piercing guide tube using a custom-made electric microdrive. Iontophoretic application was controlled by an MVCS iontophoresis system (NPI electronics). To obtain multi-unit activity, neuronal signals were amplified, digitized and filtered (250 Hz to 5kHz) with the Ripple Grapevine System (Ripple LLC). Spike sorting was performed offline using the Plexon Offline Sorter. The local field potentials (LFPs) were recorded simultaneously on the same electrodes as the spikes. The LFP signals were digitized and sampled at 1 kHz after removing the 50Hz line noise with a notch filter and subsequent band-pass filtering (an eight-order high-pass Butterworth filter with a cutoff of 3Hz and a tenth-order low-pass Butterworth filter with a cutoff at 90Hz, same as Nauhaus et al., 2009). We observed that this bandpass filtering effectively removed spike-related-transients in LFPs, which have been known to bias phase estimation of the spike-LFP coherence and often observed when spikes and LFPs are recorded from the same electrode (Das & Ray, 2018; Ray & Maunsell, 2011b; Ray, 2015). Lastly, LFPs were z-scored within the same units.

Stimuli. Visual stimuli were back-projected on a screen using DLP LED Propixx projector (1920 × 1080 pixels resolution; 30 cd/m^2 mean luminance; linearized gray values; run at 100Hz/eye, combined with an active circular polarizer, DepthQ, run at 200Hz) at a distance of 98 cm in front of the animals. The animals viewed the screen through passive circular polarizing filters monocularly or binocularly. Visual stimuli were generated in MATLAB (Mathworks, USA) using the Psychophysics toolbox (Brainard, 1997; Pelli, 1997; Kleiner et al., 2007).

For this study, we focused on analyzing data from the experiments with flash gratings to ensure stable LFP signals lasting over 1 sec in each trial. Stimuli were circular drifting sinusoidal luminance gratings centered on and slightly exceeding a neuron's receptive field and presented for 2000ms (temporal frequency typically 7 Hz). We briefly flashed sinusoidal luminance gratings (flash duration typically 10ms; 100% contrast; preferred spatial frequency; presented binocularly or monocularly to the preferred eye) that randomly varied in orientation (8 equally spaced values) and spatial phase (4 values), randomly interleaved by blank stimuli (also 10ms duration, presented with equal probability as each orientation).

Data analysis. All analyses were performed in MATLAB (Mathworks, USA). All the analysis described below used the analysis window of 800 – 2,000 ms after stimulus onset to ensure stable LFP signals in each trial. For the LFP analysis in the frequency domain, we limited our analysis to the frequency range below 48 Hz to minimize the effect of the notch filter (for 50Hz line noise removal) and widely reported contamination of firing rate on LFPs above 50 Hz (Ray & Maunsell, 2011a; Ray, 2015).

Control for difference in the mean firing rates. We reported previously that 5HT decreased the firing rate of V1 neurons (Seillier et al., 2017). Therefore, it is conceivable that our findings in LFPs could be explained simply by the difference in the mean firing rate between baseline and 5HT conditions. To account for the difference, we resampled and split trials in the baseline condition into the low firing rate (low FR) and the high firing rate (high FR) conditions until the ratio of the mean firing rate between conditions were smaller across populations in low FR/high FR (0.63) than 5HT/baseline (0.65). This procedure enabled us to identify the generic accounts of firing rate on LFPs within the same single-units. For the analysis to see the relationship between spikes and LFPs, we performed a so-called 'thinning' procedure; we randomly removed spikes from baseline conditions such that the difference in the mean firing rate between baseline and 5HT becomes near-zero (Gregoriou et al., 2009; Mitchell et al., 2009).

Power spectral densities (PSDs). The multi-taper method was used to estimate the PSDs of LFPs during the analysis window ('mtspecgramc.m' in the Chronux toolbox with three tapers). This was done in every trial, and the estimated power spectrum was subsequently averaged across trials to yield a single PSD in each session.

Spike-triggered average LFP. The LFP signal during the analysis window in each trial was subtracted from its mean such that the mean becomes zero. Next, ±100ms segments of the LFP centered at the timing of every spike were obtained. The spike-triggered average LFP (stLFP) was computed as the average of these LFP segments. The amplitude of the stLFP was computed as the difference between the maximum and the minimum of the stLFP (Fig. 3A). The short-time Fourier transform ('spectrogram.m' function) was used to obtain the power spectral densities (PSDs) of the stLFP.

Spike-LFP coherence. Coherence between spike trains of the single-unit and the LFP signal and its phase were computed using the multi-taper method implemented in the Chronux toolbox with three tapers ('coherencycpt.m' function). This function computes the cross-spectrum

between LFPs and timing of spikes ($S_{LFP,\ spikes}$) and the spectrum for LFPs (S_{LFP}) and timing of spikes (S_{spikes}) such that the spike-LFP coherence *c* is computed in the following:

$$c = |\frac{S_{LFP,\ spikes}}{\sqrt{S_{LFP}S_{spikes}}}|$$

Since the spike-field coherence is inevitably biased by the firing rate (Lepage et al., 2011), we randomly removed spikes from the baseline condition such that difference in the mean firing rate between baseline and 5HT conditions becomes near-zero and non-significant ('thinning'). We did not perform the thinning for the firing-rate control condition (low FR vs high FR) to observe generic accounts of firing rate for coherence estimation.

Generalized linear regression model. We used a generalized linear regression model (GLM) to explain trial-by-trial low-frequency LFP power (< 10Hz) during the analysis window by linear combination of trial-by-trial pupil size, pupil derivative, drug, and interactions between pupil metrics and drug (pupil size x drug and pupil derivative x drug). The low-frequency LFP power was converted into the decibel scale by taking ten times its logarithm to base 10. The recorded raw pupil data were bandpass-filtered using a 0.01-10 Hz second-order Butterworth filter (Urai et al., 2017), down-sampled to match the monitor's refresh rate, and z-scored within session (Kawaguchi et al., 2018). The included pupil size was the mean pupil size during the 1 sec towards the stimulus offset in each trial. The pupil derivative was the maximum value of *PS(t+1)-PS(t)* during the 1 sec towards the stimulus offset in each trial, where *PS* is pupil size time-course in each trial and *t* is time. The included predictor "drug" was binary (0: baseline, 1: drug application). The 3-fold cross-validation was used to train the model and test its performance using the Pearson correlation coefficient. Each predictor was included stepwise in the above order to quantify to which extent the predictor improves model performance (similar to Lueckmann et al., 2018).

Statistical test. Wilcoxson signed-rank test was used to test the null hypothesis that two paired groups have the same mean-rank. Spearman rank correlation was used to compute a correlation coefficient r, which quantifies a monotonic relationship between two variables.

Inclusion criteria. In total we recorded 70 single-units (monkey K: 13 with NaCl, 16 with 5HT; monkey M: 4 with NaCl, 37 with 5HT) from the flash-grating experiments. All the units were included for the analysis.

Results

Two macaque monkeys performed a standard fixation task while we recorded the spiking activity of single units and LFPs simultaneously in V1 during blockwise iontophoretic application of NaCl or 5HT (Fig. 1A). Previously we showed that 5HT predominantly decreased the spiking activity of single units in V1 (Seillier et al., 2017; Fig. 1B; both monkeys: $p_{5HT} < 10^{-7}$, $n_{5HT} = 53$, $p_{NaCl} = 0.21$, $n_{NaCl} = 17$; monkey K: $p_{5HT} < 10^{-3}$, $n_{5HT} = 16$, $p_{NaCl} = 0.5$, $n_{NaCl} = 13$; monkey M: $p_{5HT} < 10^{-4}$, $n_{5HT} = 37$, $p_{NaCl} = 0.25$, $n_{NaCl} = 4$). We reasoned that 5HT is well-suited to control the visual activity of V1 neurons depending on a behavioral or motivational context of animals, likely complementing the role of other neuromodulators such as acetylcholine (ACh). Here we investigated the role of 5HT in V1's local network state which was shown to be altered by basal forebrain stimulation (De Luna et al., 2017; Goard & Dan, 2009; Pinto et al., 2013) and cognitive state including attention (Chalk et al., 2010; Das & Ray, 2018) and arousal (Reimer et al., 2014; Vinck et al., 2015). To ensure the stable LFP signal over 1 sec in each trial, we only used the data from the flash-grating experiments where a gabor grating was flashed for typically 10ms and repeated with different orientations for 2sec. The LFPs were first notch-filtered to remove 50Hz line noise and subsequently band-pass filtered (3-90Hz; same as Nauhaus et al., 2009). Lastly the LFPs were z-scored within the same units for comparison across recording sessions. We analyzed the preprocessed LFPs between 0.8 sec after stimulus onset and stimulus offset (2 sec after stimulus onset). Since 5HT decreases firing rate of V1 neurons, there is inevitably a difference in the firing rate between baseline and 5HT conditions. To show that our findings on LFPs are not simply explained by the difference in firing rate, we performed two control analysis. First, we randomly removed spikes from baseline condition such that the difference becomes near 0 and non-significant ('thinning'; Gregoriou et al., 2009; Mitchell et al., 2009). Second, we prepared low firing rate (low FR) and high firing rate (high FR) conditions by resampling and splitting trials from baseline condition until the ratio of the mean firing rate between the low FR and high FR conditions became smaller than that between baseline and 5HT conditions (5HT/baseline = 0.65, low FR/high FR = 0.63). We recorded total of 70 single units in macaque V1 (monkey K: 13 with NaCl, 16 with 5HT; monkey M: 4 with NaCl, 37 with 5HT). All the statistical tests used in this study were non-parametric.

Serotonin decreases LFP power, especially in low-frequency range

We used the multi-taper method implemented in the Chronux toolbox (Bokil et al., 2010) to compute the power of LFPs. To visually observe the effect of a drug on the power spectrum, the difference in average power spectrum densities (PSDs) between baseline and drug conditions

were computed across sessions (Fig. 2A, E). Compared to NaCl condition (Fig. 2A), 5HT seemed to decrease especially low-frequency LFP power (Fig. 2E). This observation is confirmed by the power spectrum analysis using the LFPs during the analysis window (0.8 – 2 sec after the stimulus onset). We used this analysis window to ensure the LFP signals were stable without a stimulus-driven component (two examples shown in Fig. 1A right). As expected, no difference in LFP power was observed when NaCl was applied compared to baseline (Fig. 2B, C; both monkeys: $p = 0.94$, $n = 17$; monkey K: $p = 1$, $n = 13$; monkey M: $p = 1$, $n = 4$). In contrast, application of 5HT decreased the LFP power especially in low-frequency range (Fig. 2F, G; both monkeys: $p < 10^{-7}$, $n = 53$; monkey K: $p < 10^{-3}$, $n = 16$; monkey M: $p < 10^{-4}$, $n = 37$). Although the effect size was small, the gamma LFP power was also significantly smaller in 5HT condition than baseline (Fig. 2H, NaCl: both monkeys: $p < 10^{-5}$, $n = 53$; monkey K: $p < 10^{-2}$, $n = 16$; monkey M: $p < 10^{-3}$, $n = 37$). Such modulation was not observed in baseline vs NaCl (Fig. 2D, NaCl: both monkeys: $p = 0.36$, $n = 17$; monkey K: $p = 0.11$, $n = 13$; monkey M: $p = 0.63$, $n = 4$).

Our finding of the decrease in low-frequency LFP power is consistent with rodent studies showing that 5HT decreases low-frequency LFP power in the prefrontal cortex (Kjaerby et al., 2016; Puig et al., 2010). Interestingly, in awake macaque V1, such decrease in the low-frequency LFP power was observed when monkeys pay attention to the location within the receptive field (RF) of the recorded units (Chalk et al., 2010; Das & Ray, 2018; Spyropoulos et al., 2018). Therefore, it is conceivable that 5HT plays a role for attentional modulation in macaque V1. However, it is also possible that the decrease in the low-frequency LFP power by 5HT is simply a byproduct of the decrease in the firing rate by 5HT (Fig. 1B), because change in broadband LFP power is positively correlated with spiking activity (Henrie & Shapley, 2005; Manning et al., 2009). To elucidate this possibility, we split baseline condition into low firing-rate (low FR) and high firing-rate (high FR) conditions such that the rate of the mean firing rate (low FR/high FR = 0.63) became slightly smaller than that between baseline and 5HT conditions (5HT/baseline = 0.65). This procedure mimics the effect of 5HT on spiking activity in the baseline condition to account for the generic effect of change in firing rate on LFPs within the same units. We then computed the LFP power in low and high FR conditions separately. The observed difference in PSD (Fig. 2I) and power spectrum (Fig. 2J) between low and high FR conditions were qualitatively different from those from baseline vs 5HT conditions. Indeed, we did not find significant difference in low-frequency LFP power (Fig. 2K; both monkeys: $p = 0.56$, $n = 70$; monkey K: $p = 0.06$, $n = 29$; monkey M: $p = 0.27$, $n = 41$), suggesting that the decrease in low-frequency LFP power by 5HT was not accounted for the decrease in firing rate by 5HT. In

contrast, we found that the gamma LFP power was significantly larger in high FR than small FR conditions (Fig. 2L; both monkeys: $p < 10^{-3}$, n = 70; monkey K: $p < 10^{-2}$, n = 29; monkey M: $p < 10^{-2}$, n = 41). This small yet significant positive correlation between the gamma LFP power and firing rate was consistent with previous studies (Ray et al., 2008; Ray & Maunsell, 2011a). Therefore, contrary to the decrease in low-frequency LFP power, the decrease in gamma LFP power by 5HT (Fig. 2H) could be accounted for by the decrease in firing rate by 5HT. we conclude that 5HT decreases the LFP power especially in low-frequency range, which might not be explained by the decrease in firing rate by 5HT.

Serotonin decreases functional connectivity of V1 neurons

To see if 5HT alters the relationship between spikes and LFPs, we computed the spike-triggered average LFP (stLFP). The stLFP is thought to effectively exhibit spike locked components of LFPs, since LFPs are averaged across a number of spikes and thus non-spike locked components of LFPs are subject to be cancelled out (Ray, 2015). Especially, the stLFP has been used to estimate the degree to which the activity of the recorded neuron is correlated with the local network activity, termed as functional connectivity or population coupling (Nauhaus et al., 2009; Okun et al., 2015). Indeed, an intracellular recording using awake rats showed that the stLFP represents the cross-correlation between the membrane potential of the neuron and the LFP (Okun et al., 2010). To quantify the functional connectivity, we computed the stLFP amplitude as the maximum – minimum of the stLFP within -0.05 to 0.05 sec time window around spikes (example in Fig. 3A). We found that 5HT, not NaCl, significantly decreased the stLFP amplitude compared to baseline (Fig. 3B; both monkeys: $p_{5HT} < 10^{-2}$, n_{5HT} = 53, p_{NaCl} = 0.98, n_{NaCl} = 17; monkey K: $p_{5HT} < 0.05$, n_{5HT} = 16, p_{NaCl} = 0.68, n_{NaCl} = 13; monkey M: $p_{5HT} < 0.05$, n_{5HT} = 37, p_{NaCl} = 0.38, n_{NaCl} = 4), suggesting that functional connectivity is decreased by 5HT. Another measure of functional connectivity is spike-LFP coherence (Bastos & Schoffelen, 2015). Since this measure is shown to be affected by firing rate, we performed 'thinning' to match firing rate between baseline and drug and then computed spike-LFP coherence (Gregoriou et al., 2009; Mitchell et al., 2009). We found that the rate-adjusted spike-LFP coherence in low-frequency range (< 10Hz) was smaller in 5HT but not NaCl condition than baseline (Fig. 3C; both monkeys: $p_{5HT} < 0.05$, n_{5HT} = 53, p_{NaCl} = 0.69, n_{NaCl} = 17; monkey K: $p_{5HT} < 0.05$, n_{5HT} = 16, p_{NaCl} = 1, n_{NaCl} = 13; monkey M: p_{5HT} = 0.13, n_{5HT} = 37, p_{NaCl} = 0.88, n_{NaCl} = 4). These two measures of functional connectivity were positively correlated in 5HT condition (both monkeys: r_{5HT} = 0.66, $p_{5HT} < 10^{-6}$, n_{5HT} = 53, r_{NaCl} = 0.29, p_{NaCl} = 0.25, n_{NaCl} = 17; monkey K: r_{5HT} = 0.76, $p_{5HT} < 10^{-2}$, n_{5HT} = 16, r_{NaCl} = 04, p_{NaCl} = 0.18, n_{NaCl} = 13; monkey M: r_{5HT} = 0.63, p_{5HT} <

10^{-4}, n_{5HT} = 35, r_{NaCl} = -0.2, p_{NaCl} = 0.92, n_{NaCl} = 4). It suggests that these two measures reflect the common mechanism: likely serotonergic modulation in functional connectivity.

Previous studies pointed out that the stLFP was influenced by the low-frequency oscillatory signals (Ray & Maunsell, 2011b; Ray, 2015). To address this issue, we computed correlation between change in the stLFP amplitude and the observed change in the low-frequency LFP power (Fig. 2G). In fact, we found significant positive correlation (Fig. 3D; both monkeys; r_{5HT} = 0.63, $p_{5HT} < 10^{-6}$, n_{5HT} = 51, r_{NaCl} = 0.29, p_{NaCl} = 0.26, n_{NaCl} = 17). This was driven by monkey M (r_{5HT} = 0.82, $p_{5HT} < 10^{-9}$, n_{5HT} = 37, r_{NaCl} = 0.6, p_{NaCl} = 0.42, n_{NaCl} = 4) and not by monkey K (r_{5HT} = 0.03, p_{5HT} = 0.89, n_{5HT} = 16, r_{NaCl} = 0.28, p_{NaCl} = 0.35, n_{NaCl} = 13). This suggests that at least for monkey M, the stLFP amplitude might be influenced by low-frequency rhythm. Fig. 3E-J shows the mean stLFP across units and its difference in PSD in each condition. We found little difference in the stLFP amplitude and its difference in PSD when NaCl was applied (Fig. 3E, F). In contrast, 5HT decreased the stLFP amplitude (Fig. 3G, H), which was accompanied by decrease in the stLFP power especially in low-frequency range after spike. Such modulation was not accounted for simply by the difference in firing rate. Rather, low FR was associated with larger stLFP amplitude than high FR (Fig. 5I, J). This is consistent with previous studies showing that stLFP amplitude is larger in spontaneous (no stimulus) period or when low-intensity sensory stimulus is presented (Nauhaus et al., 2009; Ray et al., 2008; Ray & Maunsell, 2011b). Therefore, the decrease in the stLFP amplitude by 5HT was opposite to what is expected based on the role of serotonin to decrease the spiking activity. This observation also supports our previous finding that the serotonergic modulation in V1 cannot be accounted for by a contrast-gain model (Seillier et al., 2017). Together, we conclude that 5HT decreases functional connectivity in awake macaque V1.

Serotonergic modulation in low-frequency LFP power shows no interactions with the modulation by pupil-linked neuromodulators

5HT is one of the neuromodulators reported to decrease low-frequency LFP power in cortex. Other neuromodulators including acetylcholine also desynchronize cortical state (Harris & Thiele, 2011; Lee & Dan, 2012). Whether 5HT decreases low-frequency activity in cortex in tandem with ACh or not is an important question to elucidate the role of neuromodulators in cortical processes. Here we tried to test the hypothesis that 5HT and ACh independently decrease low-frequency rhythmic activity in cortical areas (Harris & Thiele, 2011; Vanderwolf & Baker, 1986). To this end we leveraged the finding that pupil diameter is correlated with the cholinergic activity (Reimer et al., 2016). This finding allowed us to formulate the hypothesis; if 5HT and ACh acts

on low-frequency LFP power independently of each other, the decrease in low-frequency LFP power by 5HT must have no interactions with effects of pupil size. We used a generalized linear regression model to see whether including interaction terms (pupil size x drug) in the model improves the prediction of trial-by-trial low-frequency LFP power. If the hypothesis is true, we should not see significant interaction. We found that including pupil size improved model predictions in experiments with both NaCl and 5HT compared to when only mean low-frequency LFP power was used as the predictor (Fig. 4; $p_{NaCl} < 0.05$, $p_{5HT} < 0.05$), suggesting the modulatory role of pupil-linked neuromodulators including ACh. Consistent with our findings, including drug terms (0: baseline trials, 1: trials with drug application) also significantly improved model predictions only in experiments with 5HT ($p_{NaCl} = 0.17$, $p_{5HT} < 10^{-7}$). However, we failed to find significant interaction between pupil size and drug (Fig. 4; $p_{\text{pupil size x 5HT}} = 0.56$, $p_{\text{pupil derivative x 5HT}} = 1$). This result supports the hypothesis that the action of 5HT on low-frequency LFP power is independent of that of pupil-linked neuromodulators including ACh.

Discussion

We found that 5HT decreased LFP power especially in low-frequency range. To see whether 5HT alters a relationship between spikes and LFPs, we computed the spike-triggered average LFP. We found that 5HT decreased the stLFP amplitude and spike-LFP coherence, suggesting that 5HT de-correlates response of a single neuron with local network activity and thereby decreases functional connectivity locally in V1. Our control analysis confirmed that all the above results were not simply accounted for by the decrease in firing rate by 5HT.

Roles of neuromodulators on local network state

Stimulation of the basal forebrain or cholinergic brainstem nuclei decreases low-frequency LFP power in cortex and is thought to desynchronize cortical state (Buzsaki et al., 1988; De Luna et al., 2017; Goard & Dan, 2009; Pinto et al., 2013). However, ACh may not be the only neuromodulator to do so. Other neuromodulators such as monoamines (5HT, noradrenaline, and dopamine) are also linked to cortical desynchronization (Harris & Thiele, 2011; Lee & Dan, 2012), presumably counteracting cortical synchronization caused by shared inputs (Harris & Thiele, 2011). Indeed, stimulation to the dorsal raphe, which is the primary source of serotonergic innervation to the cortex, also decreases low-frequency LFP power in rats' prefrontal cortex (Puig et al., 2010). We showed that the decrease in low-frequency LFP power by 5HT was also found in awake macaque V1. Our previous study (Seillier et al., 2017) argued that 5HT may control the response gain of V1 neurons potentially complementing the effect of

ACh. Complementary roles of these two neuromodulators may involve in each effect on local network state, too. One hypothesis is that 5HT and ACh decrease low-frequency LFP power independently (Vanderwolf et al., 1986). This is intuitive given that 5HT and ACh in cortex come from different sources and do not share receptors. Testing this hypothesis requires a future research examining the interaction between these two neuromodulators in cortex.

Mechanisms of serotonergic modulations in spiking activity and local network state

Do the serotonergic modulations in spiking activity and local network state stem from the same mechanism? We have to admit that our current research is not able to address this question, as we applied neither serotonergic agonist nor antagonist. Previous studies showed mixed results of the type of 5HT receptors decreasing the low-frequency LFP power. For example, a mice study showed that the decrease was mediated by the 5HT1B receptor (Kjaerby et al., 2016), whereas a rat study showed that it was mediated by the 5HT2A receptor (Puig et al., 2010). These two types of serotonergic receptors indeed exist in primate V1 (Watakabe et al., 2009; Shukla et al., 2014) and likely contribute to our observation in the LFPs. Since LFP can be used to predict subthreshold synaptic input to single neurons in visual cortex (Haider et al., 2016), the observed decrease in low-frequency LFP power by 5HT in macaque V1 may be mediated by the 5HT1B receptor that is preferentially expressed in pre-synapse (Boschert et al., 1994), whereas the decrease in spiking activity by 5HT may be mediated by the 5HT2A receptor that is shown to suppress the gain of visual response in a divisive manner (Azimi et al., 2018). Depending on the type of serotonergic receptors, hyperpolarization-activated cyclic nucleotide–gated (HCN) channels may also play a role in the serotonergic modulations in spiking activity and LFP (Ko et al., 2017; Sinha & Narayanan, 2015). Although speculative, distinct cellular mechanisms may explain the similarity and difference between the observed serotonergic modulations and previously reported attentional modulations. Spatial attention is typically accompanied by increase in firing rate of V1 neurons responding to the attended stimuli (Motter et al., 1993; Roelfsema et al., 1998) and decrease in response latency (Sundberg et al., 2012), whereas 5HT decreases V1 responses (Seillier et al., 2017; Azimi et al., 2018) and increases response latency (Seillier et al., 2017). In contrast, similar to 5HT, spatial attention decreases low-frequency LFP power (Chalk et al., 2010; Das & Ray, 2018; Spyropoulos et al., 2018) and stLFP amplitude (Chalk et al., 2010). Like ACh, in which the muscarinic receptor but not the nicotinic receptor is involved in attentional modulation (Herrero et al., 2008), 5HT may contribute to state-dependent visual processes through different types of serotonergic receptors.

Serotonergic modulation on global and local functional connectivity

We observed decrease in functional connectivity by 5HT within V1. Although whether such serotonergic modulation in functional connectivity holds true in other cortical areas cannot be elucidated from the current study, studies using resting-state functional magnetic resonance imaging (rs-fMRI) demonstrated that the increase level of 5HT by serotonin reuptake inhibitors (SSRIs) generally decreased functional connectivity throughout the whole brain (Klaassens et al., 2015; Schaefer et al., 2014). Therefore, it is predicted that the serotonergic modulation in functional connectivity within V1 may be generalized at least in other cortical areas that belong to networks where functional connectivity was shown to decrease by SSRIs (Klaassens et al., 2015). This is conceivable given the widespread projections of serotonergic neurons (Jacobs & Azmitia, 1992). Whether the serotonergic modulation in global and local functional connectivity shares the same mechanism is potentially an important question to get better insight into the serotonergic system in the brain and its link to psychiatric disorders including depression.

References

Azimi, Z., Spoida, K., Barzan, R., Wollenweber, P., Mark, M. D., Herlitze, S., & Jancke, D. (2018). Subtraction and division of visual cortical population responses by the serotonergic system. *bioRxiv*, 444943.

Bastos, A. M., & Schoffelen, J. M. (2016). A tutorial review of functional connectivity analysis methods and their interpretational pitfalls. *Frontiers in systems neuroscience*, *9*, 175.

Beaman, C. B., Eagleman, S. L., & Dragoi, V. (2017). Sensory coding accuracy and perceptual performance are improved during the desynchronized cortical state. *Nature communications*, *8*(1), 1308.

Bokil, H., Andrews, P., Kulkarni, J. E., Mehta, S., & Mitra, P. P. (2010). Chronux: a platform for analyzing neural signals. *Journal of neuroscience methods*, *192*(1), 146-151.

Boschert, U., Amara, D. A., Segu, L., & Hen, R. (1994). The mouse 5-hydroxytryptamine 1B receptor is localized predominantly on axon terminals. *Neuroscience*, *58*(1), 167-182.

Brainard, D. H., & Vision, S. (1997). The psychophysics toolbox. *Spatial vision*, *10*, 433-436.

Buzsaki, G. Y., Bickford, R. G., Ponomareff, G., Thal, L. J., Mandel, R., & Gage, F. H. (1988). Nucleus basalis and thalamic control of neocortical activity in the freely moving rat. *Journal of neuroscience*, *8*(11), 4007-4026.

Chalk, M., Herrero, J. L., Gieselmann, M. A., Delicato, L. S., Gotthardt, S., & Thiele, A. (2010). Attention reduces stimulus-driven gamma frequency oscillations and spike field coherence in V1. *Neuron*, *66*(1), 114-125.

Correia, P. A., Lottem, E., Banerjee, D., Machado, A. S., Carey, M. R., & Mainen, Z. F. (2017). Transient inhibition and long-term facilitation of locomotion by phasic optogenetic activation of serotonin neurons. *Elife*, *6*, e20975.

Das, A., & Ray, S. (2018). Effect of stimulus contrast and visual attention on spike-gamma phase relationship in macaque primary visual cortex. *Frontiers in computational neuroscience*, *12*.

De Luna, P., Veit, J., & Rainer, G. (2017). Basal forebrain activation enhances between-trial reliability of low-frequency local field potentials (LFP) and spiking activity in tree shrew primary visual cortex (V1). *Brain Structure and Function*, *222*(9), 4239-4252.

Disney, A. A., Aoki, C., & Hawken, M. J. (2007). Gain modulation by nicotine in macaque v1. *Neuron*, *56*(4), 701-713.

Eastman, K. M., & Huk, A. C. (2012). PLDAPS: a hardware architecture and software toolbox for neurophysiology requiring complex visual stimuli and online behavioral control. *Frontiers in neuroinformatics*, *6*, 1.

Fries, P., Reynolds, J. H., Rorie, A. E., & Desimone, R. (2001). Modulation of oscillatory neuronal synchronization by selective visual attention. *Science*, *291*(5508), 1560-1563.

Fischer, J., & Whitney, D. (2009). Attention narrows position tuning of population responses in V1. *Current biology*, *19*(16), 1356-1361.

Goard, M., & Dan, Y. (2009). Basal forebrain activation enhances cortical coding of natural scenes. *Nature neuroscience*, *12*(11), 1444.

Gregoriou, G. G., Gotts, S. J., Zhou, H., & Desimone, R. (2009). High-frequency, long-range coupling between prefrontal and visual cortex during attention. *science*, *324*(5931), 1207-1210.

Haider, B., Schulz, D. P., Häusser, M., & Carandini, M. (2016). Millisecond coupling of local field potentials to synaptic currents in the awake visual cortex. *Neuron*, *90*(1), 35-42.

Henrie, J. A., & Shapley, R. (2005). LFP power spectra in V1 cortex: the graded effect of stimulus contrast. *Journal of neurophysiology*, *94*(1), 479-490.

Herrero, J. L., Roberts, M. J., Delicato, L. S., Gieselmann, M. A., Dayan, P., & Thiele, A. (2008). Acetylcholine contributes through muscarinic receptors to attentional modulation in V1. *Nature*, *454*(7208), 1110.

Hubel, D. H., & Wiesel, T. N. (1968). Receptive fields and functional architecture of monkey striate cortex. *The Journal of physiology*, *195*(1), 215-243.

Jacobs, B. L., & Azmitia, E. C. (1992). Structure and function of the brain serotonin system. *Physiological reviews*, *72*(1), 165-229.

Jacob, S. N., Ott, T., & Nieder, A. (2013). Dopamine regulates two classes of primate prefrontal neurons that represent sensory signals. *Journal of Neuroscience*, *33*(34), 13724-13734.

Nienborg, H., & Jacob, S. (2018). Monoaminergic neuromodulation of sensory processing. *Frontiers in neural circuits*, *12*, 51.

Kawaguchi, K., Clery, S., Pourriahi, P., Seillier, L., Haefner, R. M., & Nienborg, H. (2018). Differentiating between models of perceptual decision making using pupil size inferred confidence. *Journal of Neuroscience*, *38*(41), 8874-8888.

Kjaerby, C., Athilingam, J., Robinson, S. E., Iafrati, J., & Sohal, V. S. (2016). Serotonin 1B receptors regulate prefrontal function by gating callosal and hippocampal inputs. *Cell reports*, *17*(11), 2882-2890.

Klaassens, B. L., van Gorsel, H. C., Khalili-Mahani, N., van der Grond, J., Wyman, B. T., Whitcher, B., ... & van Gerven, J. M. (2015). Single-dose serotonergic stimulation shows widespread effects on functional brain connectivity. *Neuroimage*, *122*, 440-450.

Kleiner, M., Brainard, D. H., & Pelli, D. G. (2007). What is new in Psychophysics Toolbox. *Perception*, *36*.

Ko, K. W., Rasband, M. N., Meseguer, V., Kramer, R. H., & Golding, N. L. (2016). Serotonin modulates spike probability in the axon initial segment through HCN channels. *Nature neuroscience*, *19*(6), 826.

Lee, S. H., & Dan, Y. (2012). Neuromodulation of brain states. *Neuron*, *76*(1), 209-222.

Lepage, K. Q., Kramer, M. A., & Eden, U. T. (2011). The dependence of spike field coherence on expected intensity. *Neural Computation*, *23*(9), 2209-2241.

Lueckmann, J. M., Macke, J. H., & Nienborg, H. (2018). Can serial dependencies in choices and neural activity explain choice probabilities?. *Journal of Neuroscience*, 2225-17.

Manning, J. R., Jacobs, J., Fried, I., & Kahana, M. J. (2009). Broadband shifts in local field potential power spectra are correlated with single-neuron spiking in humans. *Journal of Neuroscience*, *29*(43), 13613-13620.

McAdams, C. J., & Maunsell, J. H. (1999). Effects of attention on orientation-tuning functions of single neurons in macaque cortical area V4. *Journal of Neuroscience*, *19*(1), 431-441.

Mitchell, J. F., Sundberg, K. A., & Reynolds, J. H. (2009). Spatial attention decorrelates intrinsic activity fluctuations in macaque area V4. *Neuron*, *63*(6), 879-888.

Motter, B. C. (1993). Focal attention produces spatially selective processing in visual cortical areas V1, V2, and V4 in the presence of competing stimuli. *Journal of neurophysiology*, *70*(3), 909-919.

Nauhaus, I., Busse, L., Carandini, M., & Ringach, D. L. (2009). Stimulus contrast modulates functional connectivity in visual cortex. *Nature neuroscience*, *12*(1), 70.

Nienborg, H., Bridge, H., Parker, A. J., & Cumming, B. G. (2004). Receptive field size in V1 neurons limits acuity for perceiving disparity modulation. *Journal of Neuroscience*, *24*(9), 2065-2076.

Okun, M., Naim, A., & Lampl, I. (2010). The subthreshold relation between cortical local field potential and neuronal firing unveiled by intracellular recordings in awake rats. *Journal of neuroscience*, *30*(12), 4440-4448.

Okun, M., Steinmetz, N. A., Cossell, L., Iacaruso, M. F., Ko, H., Barthó, P., ... & Harris, K. D. (2015). Diverse coupling of neurons to populations in sensory cortex. *Nature*, *521*(7553), 511.

Ott, T., Jacob, S. N., & Nieder, A. (2014). Dopamine receptors differentially enhance rule coding in primate prefrontal cortex neurons. *Neuron*, *84*(6), 1317-1328.

Pelli, D. G. (1997). The VideoToolbox software for visual psychophysics: Transforming numbers into movies. *Spatial vision*, *10*(4), 437-442.

Pinto, L., Goard, M. J., Estandian, D., Xu, M., Kwan, A. C., Lee, S. H., ... & Dan, Y. (2013). Fast modulation of visual perception by basal forebrain cholinergic neurons. *Nature neuroscience*, *16*(12), 1857.

Priebe, N. J. (2016). Mechanisms of orientation selectivity in the primary visual cortex. *Annual review of vision science*, *2*, 85-107.

Puig, M. V., Watakabe, A., Ushimaru, M., Yamamori, T., & Kawaguchi, Y. (2010). Serotonin modulates fast-spiking interneuron and synchronous activity in the rat prefrontal cortex through 5-HT1A and 5-HT2A receptors. *Journal of neuroscience*, *30*(6), 2211-2222.

Ray, S. (2015). Challenges in the quantification and interpretation of spike-LFP relationships. *Current opinion in neurobiology*, *31*, 111-118.

Ray, S., Hsiao, S. S., Crone, N. E., Franaszczuk, P. J., & Niebur, E. (2008). Effect of stimulus intensity on the spike–local field potential relationship in the secondary somatosensory cortex. *Journal of Neuroscience*, *28*(29), 7334-7343.

Ray, S., & Maunsell, J. H. (2011a). Different origins of gamma rhythm and high-gamma activity in macaque visual cortex. *PLoS biology*, *9*(4), e1000610.

Ray, S., & Maunsell, J. H. (2011). Network rhythms influence the relationship between spike-triggered local field potential and functional connectivity. *Journal of Neuroscience*, *31*(35), 12674-12682.

Reimer, J., Froudarakis, E., Cadwell, C. R., Yatsenko, D., Denfield, G. H., & Tolias, A. S. (2014). Pupil fluctuations track fast switching of cortical states during quiet wakefulness. *Neuron*, *84*(2), 355-362.

Roelfsema, P. R., Lamme, V. A., & Spekreijse, H. (1998). Object-based attention in the primary visual cortex of the macaque monkey. *Nature*, *395*(6700), 376.

Sanayei, M., Herrero, J. L., Distler, C., & Thiele, A. (2015). Attention and normalization circuits in macaque V1. *European Journal of Neuroscience*, *41*(7), 949-964.
Schaefer, A., Burmann, I., Regenthal, R., Arélin, K., Barth, C., Pampel, A., ... & Sacher, J. (2014). Serotonergic modulation of intrinsic functional connectivity. *Current Biology*, *24*(19), 2314-2318.

Seillier, L., Lorenz, C., Kawaguchi, K., Ott, T., Nieder, A., Pourriahi, P., & Nienborg, H. (2017). Serotonin decreases the gain of visual responses in awake macaque V1. *Journal of Neuroscience*, 1339-17.

Shukla, R., Watakabe, A., & Yamamori, T. (2014). mRNA expression profile of serotonin receptor subtypes and distribution of serotonergic terminations in marmoset brain. *Frontiers in neural circuits*, *8*, 52.

Sinha, M., & Narayanan, R. (2015). HCN channels enhance spike phase coherence and regulate the phase of spikes and LFPs in the theta-frequency range. *Proceedings of the National Academy of Sciences*, *112*(17), E2207-E2216.

Spyropoulos, G., Bosman, C. A., & Fries, P. (2018). A theta rhythm in macaque visual cortex and its attentional modulation. *Proceedings of the National Academy of Sciences*, 201719433.

Sundberg, K. A., Mitchell, J. F., Gawne, T. J., & Reynolds, J. H. (2012). Attention influences single unit and local field potential response latencies in visual cortical area V4. *Journal of Neuroscience*, *32*(45), 16040-16050.

Thiele, A., Delicato, L. S., Roberts, M. J., & Gieselmann, M. A. (2006). A novel electrode–pipette design for simultaneous recording of extracellular spikes and iontophoretic drug application in awake behaving monkeys. *Journal of neuroscience methods*, *158*(2), 207-211.

Urai, A. E., Braun, A., & Donner, T. H. (2017). Pupil-linked arousal is driven by decision uncertainty and alters serial choice bias. *Nature communications*, *8*, 14637.

Vanderwolf, C. H., & Baker, G. B. (1986). Evidence that serotonin mediates non-cholinergic neocortical low voltage fast activity, non-cholinergic hippocampal rhythmical slow activity and contributes to intelligent behavior. *Brain research*, *374*(2), 342-356.

Vetencourt, J. F. M., Sale, A., Viegi, A., Baroncelli, L., De Pasquale, R., O'leary, O. F., ... & Maffei, L. (2008). The antidepressant fluoxetine restores plasticity in the adult visual cortex. *Science*, *320*(5874), 385-388.

595 Vinck, M., Batista-Brito, R., Knoblich, U., & Cardin, J. A. (2015). Arousal and locomotion make
596 distinct contributions to cortical activity patterns and visual encoding. *Neuron*, *86*(3), 740-754.

597 Watakabe, A., Komatsu, Y., Sadakane, O., Shimegi, S., Takahata, T., Higo, N., ... & Sakamoto,
598 H. (2008). Enriched expression of serotonin 1B and 2A receptor genes in macaque visual cortex
599 and their bidirectional modulatory effects on neuronal responses. *Cerebral cortex*, *19*(8), 1915-
600 1928.

601 Zinke, W., Roberts, M. J., Guo, K., McDonald, J. S., Robertson, R., & Thiele, A. (2006).
602 Cholinergic modulation of response properties and orientation tuning of neurons in primary
603 visual cortex of anaesthetized Marmoset monkeys. *European Journal of Neuroscience*, *24*(1),
604 314-328.

605

606

607

608

609

610

611

612

613

614

615

616

617

618

619

620

621

622

623

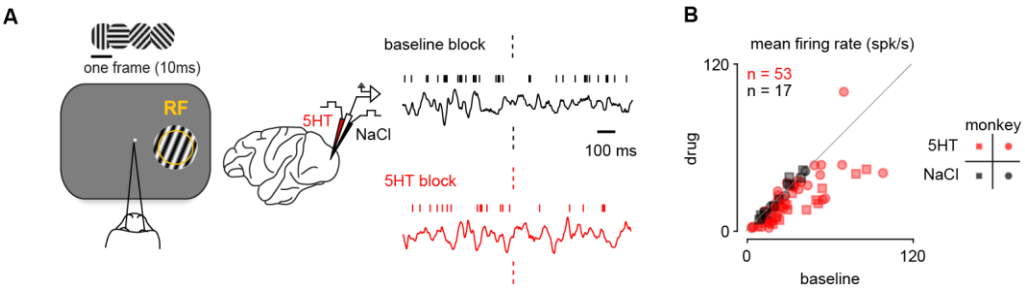

Figure 1. Serotonin decreases firing rate in awake macaque V1. A, Schematic of the experimental setup. While the monkeys performed a fixation task for 2 sec per trial, random sequences of briefly (typically 10 ms) flashed gratings of different orientations were presented on the receptive field of recorded single-unit. There are two conditions: baseline (no drug application) and subsequent iontophoretic application of drug: serotonin (5HT) or pH-matched saline (NaCl). Spikes and LFPs were recorded simultaneously (right). **B,** 5HT predominantly decreases firing rate of V1 single-units ($p_{5HT} < 10^{-7}$, $p_{NaCl} = 0.21$).

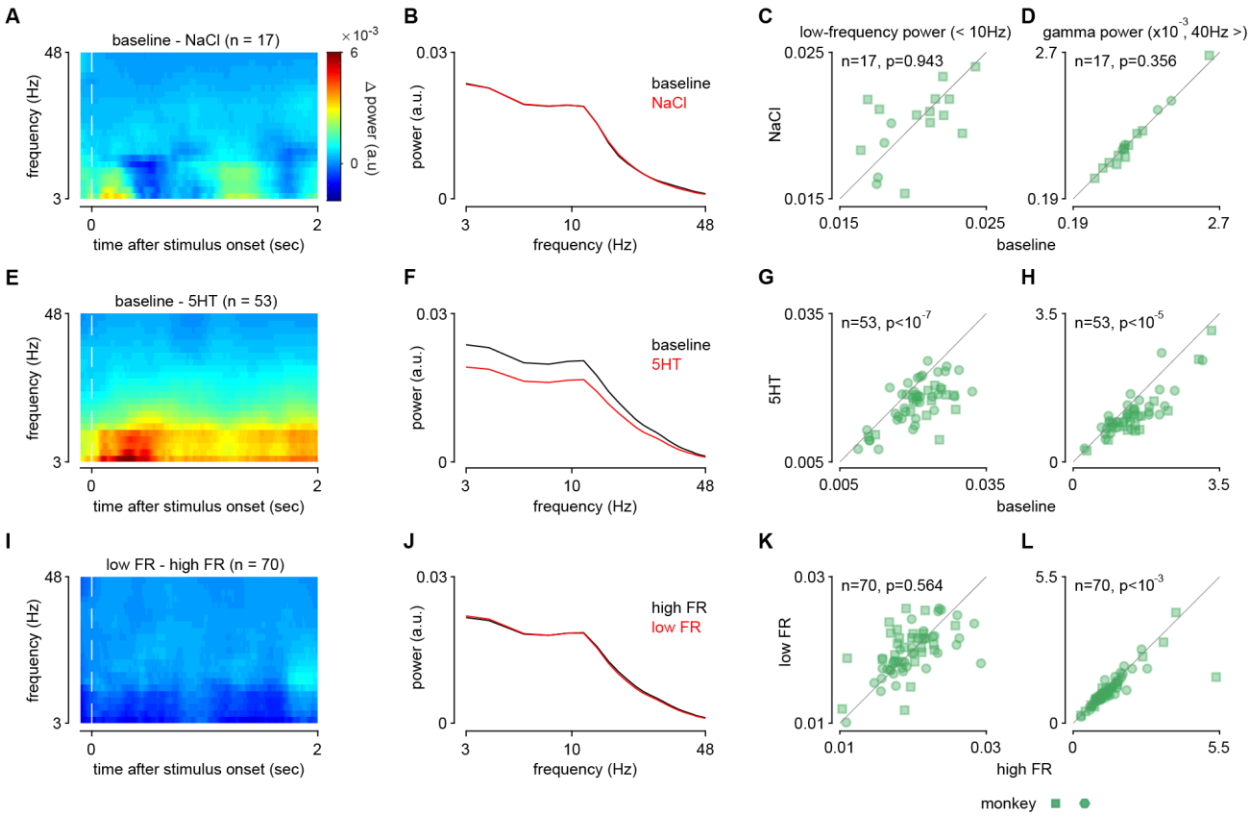

644

645 **Figure 2. Serotonin decreases LFP power, especially in low-frequency range.** ***A,*** Difference
646 in spectrogram between baseline and NaCl across sessions (17 units). ***B,*** Average power spectrum of
647 LFP power (log-log scale) in baseline (black) and NaCl (red) conditions. LFP signals between 0.8 and 2
648 sec after stimulus onset are used to avoid non-stationary component in the signal driven by stimulus
649 onset. LFPs are z-scored across baseline and drug conditions, which yielded arbitrary unit. ***C, D,*** No
650 significant difference in low-frequency LFP power (< 10Hz) and gamma LFP power (> 40Hz) between
651 baseline and NaCl conditions (Wilcoxson signed-rank test). ***E, F, G, H,*** Same as A, B, C, D but comparing
652 baseline and 5HT conditions (53 units). One outlier was omitted from *G, H* for visualization purpose. ***I, J,***
653 ***K, L,*** Same as A, B, C, D but comparing low firing rate and high firing rate conditions split from baseline
654 (see methods; 70 units). Small yet significant increase in gamma LFP power by high firing rate is found as
655 expected for known positive correlation between firing rate and gamma power (Ray et al., 2009). One
656 outlier was omitted from *K, L* for visualization purpose. Shaded area represents SEM across sessions.
657

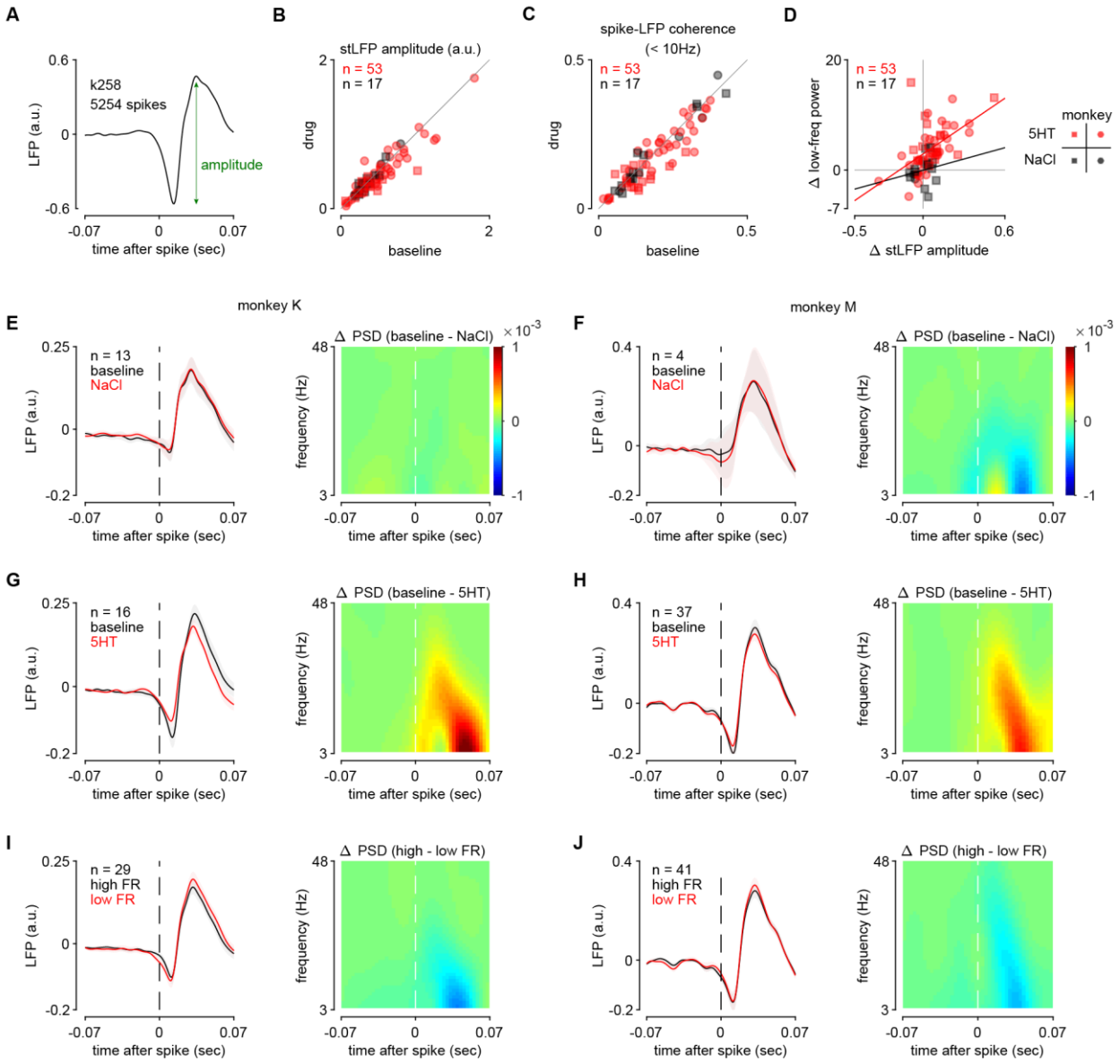

Figure 3. Serotonin decreases functional connectivity of V1 neurons. ***A,*** Example spike-triggered average LFP (stLFP) from monkey K. The stLFP amplitude is defined as the maximum – minimum of the stLFP between -0.05 and 0.05 sec relative to the timing of spikes. ***B,*** 5HT decreased the stLFP amplitude ($p_{5HT} < 10^{-3}$, $p_{NaCl} = 0.91$), suggesting that 5HT decreases functional connectivity or population coupling (Nauhaus et al., 2009; Okun et al., 2015). ***C,*** Spike-LFP coherence, another measure of functional connectivity, is smaller in low-frequency range (<10Hz) with 5HT than baseline ($p_{5HT} < 0.05$, $p_{NaCl} = 0.69$). ***D,*** Difference in the stLFP amplitude between baseline and 5HT is significantly correlated with difference in the low-frequency LFP power (<10Hz; $r_{5HT} = 0.65$, $p_{5HT} < 10^{-6}$, $r_{NaCl} = 0.19$, $p_{NaCl} = 0.46$). ***E,*** NaCl did not change the stLFP amplitude (left, p = 0.79) and power spectrogram (right). ***F,*** Same result as *E* was found in monkey M (p = 0.625). ***G,*** 5HT decreases the stLFP amplitude (left, p < 0.05) and LFP power after spikes, especially in a low-frequency range (right). ***H,*** Same result as *G* was found in monkey

M ($p < 0.05$). ***I,*** Low FR condition was associated with larger stLFP amplitude than high FR condition (left, $p < 0.01$), consistent with previous studies showing that spontaneous period or low-intensity sensory stimuli led to smaller stLFP amplitude (Nauhaus et al., 2009; Ray et al., 2008; Ray & Maunsell, 2011b). Around spikes especially low-frequency LFP power was larger in low FR than high FR (right). ***J,*** same result as *I* was found in monkey M ($p < 0.01$).

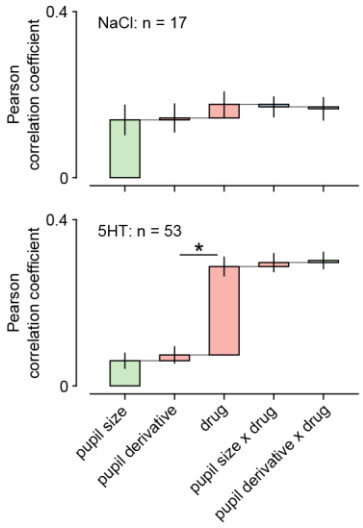

Figure 4. Serotonergic modulation in low-frequency LFP power shows no interactions with the modulation by pupil-linked neuromodulators. Stepwise generalized linear regression models to analyze the contributing factors to low-frequency LFP. Pearson correlation coefficient was used to quantify how the inclusion of each predictor improved model performance. (Top) Pupil size significantly contributed to explaining low-frequency LFP power ($p < 0.05$), whereas NaCl did not ($p = 0.17$). (Bottom) Both pupil size and 5HT significantly contributed to explaining low-frequency LFP power (pupil size: $p < 0.05$; 5HT: $p < 10^{-7}$). Interactions between pupil metrics and 5HT did not significantly improve the prediction of low-frequency LFP power (pupil size x 5HT: $p = 0.56$; pupil derivative x 5HT; $p = 1$), suggesting that the effect of pupil metrics and 5HT were independent. Wilcoxon signed rank test was used. P-values were corrected (Bonferroni). Error bars were ± 1 SE.